Novel Supramolecular Design Strategies for Mixed-Stack Charge Transfer Nanostructures

A Thesis

Submitted in partial fulfillment for the degree of
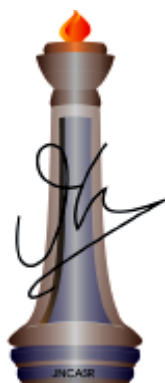
Master of Science

as a part of

Integrated Ph.D Programme (NCU)

By

Krishnendu Jalani

New Chemistry Unit

Jawaharlal Nehru Centre for Advanced Scientific Research

(A Deemed University)

Bangalore - 560064 (INDIA)

MARCH-2014

Novel Supramolecular Design Strategies for Mixed-Stack Charge Transfer Nanostructures

A Thesis

Submitted in partial fulfillment for the degree of
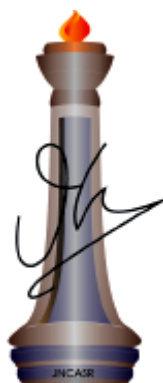
Master of Science

as a part of

Integrated Ph.D Programme (NCU)

By

Krishnendu Jalani

New Chemistry Unit

Jawaharlal Nehru Centre for Advanced Scientific Research

(A Deemed University)

Bangalore - 560064 (INDIA)

MARCH-2014

DECLARATION

I hereby declare that the matter embodied in the thesis entitled "**Novel Supramolecular Design Strategies for Mixed-Stack Charge Transfer Nanostructures**" is the result of investigations carried out by me at the New Chemistry Unit, Jawaharlal Nehru Centre for Advanced Scientific Research, Bangalore, India under the supervision of Dr. Subi J. George and that it has not been submitted elsewhere for any degree or diploma.

In keeping with the general practice in reporting scientific observations, due acknowledgement has been made whenever the work described is based on the findings of other investigators. Any omission that might have occurred by oversight or error of judgment is regretted.

Krishnendu Jalani

Jawaharlal Nehru Centre for Advanced Scientific Research

Dr. Subi J. George
New Chemistry Unit
Jawaharlal Nehru Centre for Advanced
Scientific Research (JNCASR)
Bangalore-560064,India
Phone : +91 80 2208 2964
Fax: + 91 80 22082627
E-mail: george@jncasr.ac.in

Date

March 29, 2014

CERTIFICATE

I hereby certify that the work described in this thesis titled "**Novel Supramolecular Design Strategies for Mixed-Stack Charge Transfer Nanostructures**" has been carried out by Mr. Krishnendu Jalani at the New Chemistry Unit, Jawaharlal Nehru Centre for Advanced Scientific Research, Bangalore, India under my supervision and it has not been submitted elsewhere for the award of any degree or diploma.

Dr. Subi J. George

(Research Supervisor)

iii

Dedicated to my Parents

ACKNOWLEDGEMENTS

Firstly I would like to thank my research supervisor Dr. Subi J. George for his constant guidance and support throughout the course of my research. I am very grateful to him for suggesting such an interesting project and encouraging me towards new explorations. He always inspired me in my research work and also taught how to become a good researcher and successful person in life. I also acknowledge the academic freedom that I enjoyed in the lab.

I would also like to thank the Chairman of New Chemistry Unit, Prof. C. N. R. Rao, F.R.S., for being a source of constant inspiration. I am also thankful to him for providing necessary facilities to carry out this work.

I express my sincere thanks to my senior lab mates Dr. K. Venkata Rao and Mohit Kumar for their excellent training in synthesis and photophysical studies. I also thank them for many fruitful discussions and guidance during the course of this work and manuscript writing.

I would like to thank prof. H. Ila, Dr. Sridhar Rajaram, Dr. Subi J. George, Dr. M. Eswarmoorthy, Dr. T. Govindaraju, Dr. Ranjani Viswanatha, Dr. Jayanta Haldar, Dr. Sebastian C. Peter, Dr. Tapas K. Maji, Dr. Ujjal Gautam, Dr. Kanishka Biswas, Dr. A Sundaresan, Prof. Chandrabhas Narayana for the various courses which were extremely helpful to me.

It is my great pleasure to thank my other lab mates Chidambar Kulkarni, Ankit Jain, Bhawani Narayan and Ananya Mishra for many fruitful discussions that we had all through my research.

TABLE OF CONTENTS

CHAPTER-1

Introduction

CHAPTER-2

Mixed Charge Transfer Nanostructures

PART-2 *Alternate Tetrathiafulvalene-Naphthalene Diimide D-A Arrays by an Amphiphilic Co-Assembly*

CHAPTER-3

Non-covalent Amphiphilic Foldameric Design for Mixed CT Nanostructures

CHAPTER-1

Introduction

1.1. Mixed-Stack Charge Transfer Complexes

Mixed-Stack charge transfer (MS-CT) interaction refers to the interaction between the electron rich (donor, D) and electron deficient (acceptor, A) π-conjugated chromophores which are arranged in an alternative co-facial fashion along the π-stacked arrays (Figure 1.1a). Here the electronic coupling between the highest occupied molecular orbital (HOMO) of the D and the lowest unoccupied molecular orbital (LUMO) of the A leads to a partial degree of charge transfer between the two, which results in a ground state CT formation (Figure 1.1b),[1] characterized by a partial ionicity, $D^{\delta+}A^{\delta-}$, where δ is the degree of charge transfer.[2] The resulting CT complex would have a different band structure, but related to those of parent compounds. Several recent reports have caused a renewal of interest in MS-CT complexes by highlighting a variety of properties arising at the interface between the D and A molecules that are not present in either of the parent compounds, such as charge transport and ferroelectric properties.[3] In addition MS-CT complex have also been used in the design of "smart" macromolecular materials.[4] Apart from the mixed stack arrangement, the D and A can also be organised in segregated-stack geometry where they are individually π-stacked as …A-A-A-A…and …D-D-D-D… CT assemblies with orthogonal D and A organization, which is very important for photoconductivity and ambipolar charge transport property.[5]
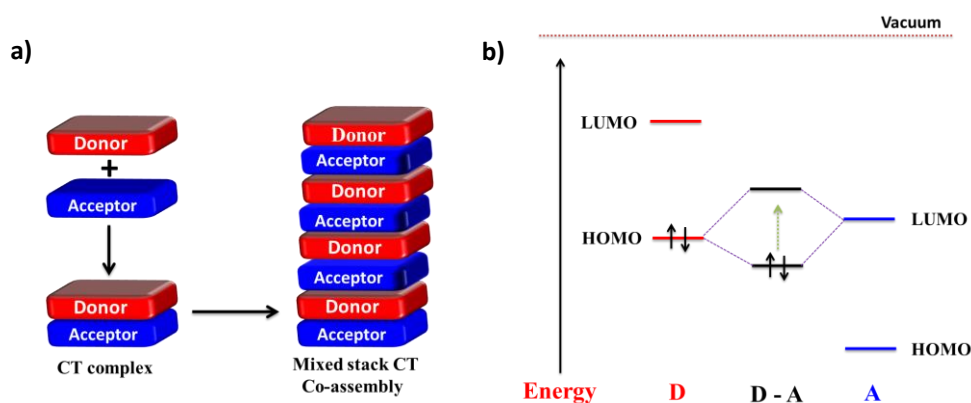
Figure 1.1: *a) Schematic representation of mixed-stack donor and acceptor molecules in a MS-CT assembly. b) Molecular orbital interaction in D and A moieties leading to D-A CT complex.*

The well-known D-A pairs which have been extensively explored in literature to form mixed-stack CT complexes are shown in Figure 1.2. Among these molecules TTF-TCNQ **(1, 4)** is the well-studied D-A CT pair and also the first organic metal discovered in 1973.[6] From then on various chemically modified TTF and TCNQ derivatives were synthesised which have vivid application in organic electronics.[7,8] The aromatic donors with larger π surfaces such as dialkoxy naphthalene **(2)** , pyrene **(3)** are also shown to form efficient CT complexes with the acceptors naphthalene diimide **(5)** and viologen **(6),** respectively.
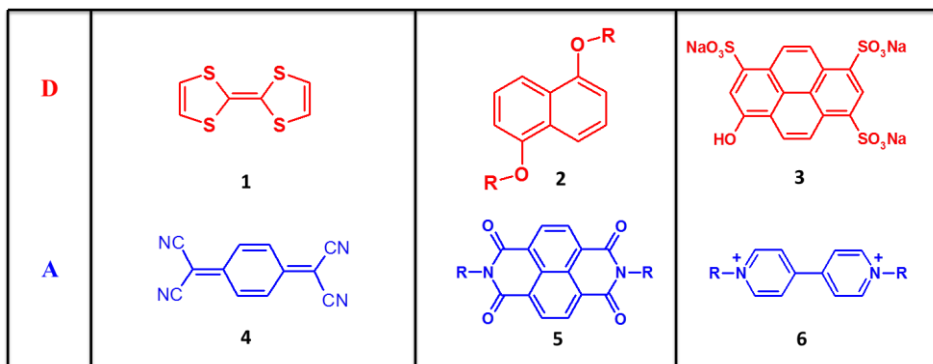
Figure 1.2: *Well-known D (marked in red ink) and A (marked in blue ink) pairs for MS-CT formation.*

1.2. MS-CT as a Supramolecular Motif

The strength and potential of D-A CT-interactions between different π-systems have been exploited extensively as a supramolecular motif in the design and synthesis of various self-organising systems in solution (Figure 1.3). One of the important classes of supramolecular system based on MS-CT are mechanically interlocked compounds such as rotaxanes and catenanes, thoroughly studied by Stoddart *et al*. and others for the design of molecular machines and switches (Figure 1.3a).[9] Apart from this the CT interactions can also be used for the elegant design of various host-guest supramolecular systems and novel macromolecules with folded structures, called "foldamers". It can also be used in the construction of smart reversible supramolecular polymers and liquid crystals.

Mechanically interlocked molecules (MIMs), such as rotaxanes and catenanes have been the subject of great interest over the past few decades because of their interesting topologies and potential applications as switches and machines in nano-mechanical systems. Bistable [2]rotaxanes (**7**) and [2]catenanes (**8**), generally contains the cyclobis(paraquat-p-phenylene) cyclophane $CBPQT^{4+}$ as a π-electron-accepting ring component which recognizes a dumbbell or macrocycle containing complementary π-electron-rich recognition units such as 1,5-dioxynaphthalene (DNP), hydroquinone (HQ), Tetrathiafulvalene (TTF), embedded in the polyether chain (Figure 1.3a). Here CT interactions between various donor-acceptor pairs with a wide range of association constants (10^2 to 10^5 M^{-1}), plays a crucial role for the switching reaction. Redox stimuli have been used to switch the movable molecular components across various available sites, bringing in a reversible switching or rotary action in these systems.
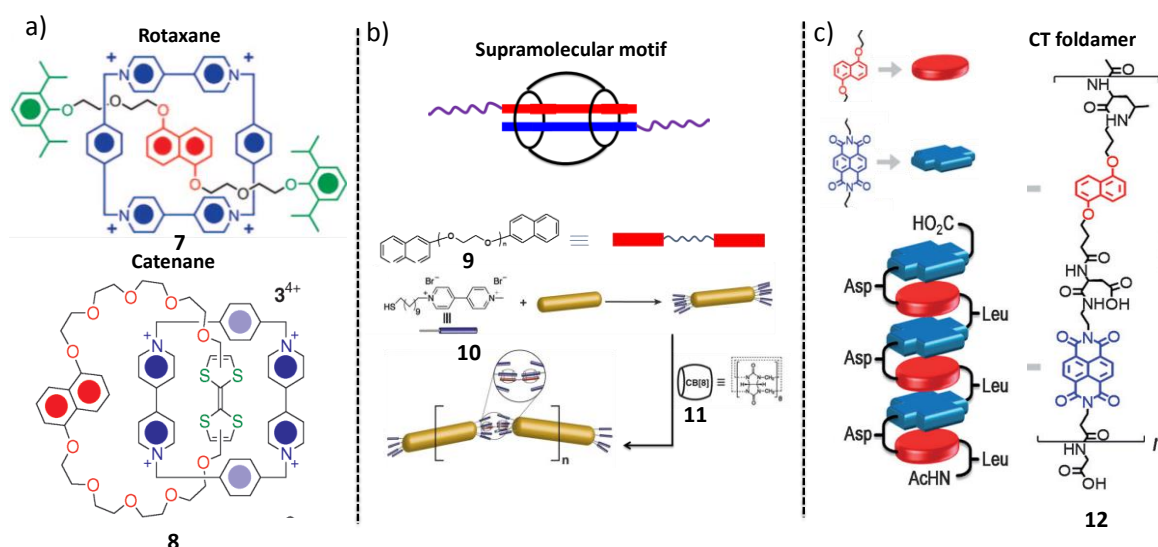
Figure 1.3: *a) Molecular structures of rotaxane **7,** (top) and catenane **8** (bottom), b) longitudinal (end to end) alignment of gold nanorods by CB[8](**11**), D and A (1:1:1) ternary complex and c) Structure of amphiphilic CT foldamer containing alternatively arranged naphthalene diimide and naphthalene dihydroxide moieties.*

The D-A CT-interaction has also been explored in host-guest chemistry as a supramolecular motif. In order to increase the association constant of the CT complexes host-stabilized ternary complexes of CT pairs have emerged recently as a novel design of macromolecular assemblies.[10] In this respect cucurbit[n]uril (CB[n], n = 5–10), comprising 'n' glycoluril units have been studied in an extensive way to investigate CT interaction between various D and A molecules. CB[n]s have received considerable attention due to their abilities to bind selectively to a wide variety of substrates over an exceptionally large range of affinities, with equilibrium association constants (K_a) as high as 10^{16} M^{-1} in aqueous media.[11] It has a hydrophobic cavity and two identical carbonyl-laced portals which allows them to form stable inclusion complexes with a wide variety of guest molecules. Compared to smaller and higher homologues, CB[8] exhibits remarkable host–guest properties which can stabilize otherwise unstable species in its cavity such as methyl viologen cation radicals or tetrathiafulvalene cation radicals which

form stable π-dimers in the cavity. Donor molecule, 2, 6-dihydroxynaphthalene or 1, 4-dihydroxybenzene (HB) can form CT with methyl viologen dication in presence of CB[8] resulting instantaneous and quantitative formation of (1:1:1) stable ternary complex of CT with guests. It has been shown that the stronger CT interaction between the D and A aromatic molecules in presence of CB[8] are the major driving force behind the formation of such 1:1:1 ternary complexes inside the host cavity. Recently, Scherman *et al.* have shown for the first time that this 1:1:1 ternary complexes can align gold nanorods (AuNRs) through supramolecular host-guest interactions leading to control over AuNR end-to-end assembly (Figure 1.3b).[12] In order to achieve the one-dimensional alignment of AuNRs, they have used **9,** a telechelic, ditopic linker molecules (n = 3, ethylene glycol repeat unit, Figure 1.3b) with naphthol moieties at each end and the functional moieties (methyl viologen, MV^{+2}, **10**) in presence of **11**. First they have attached **10** only at the end sides of the AuNRs by using cetyltrimethylammonium bromide (CTAB) as a stabilising ligand which has preferential binding affinity to the {100} side facets of the long face of AuNRs. Once the end-functionalization of the AuNRs were achieved it was mixed with **9** which can align the AuNRs through the formation of CB[8] 1:1:1 ternary complex between the MV^{2+} termini of two adjacent AuNRs and ditopic Naphthol moieties. The 1:1:1 ternary complex of CB[8] with D and A as guest pair acting as a supramolecular motif have been used for the formation of supramolecular polymers and block copolymers by a so called 'non-covalent handcuff' strategy.[13]

Iverson *et al*. and Ramakrishnan *et al*. have described various interesting design of foldamers based on CT interactions.[14] Here the term "foldamer" refers to the synthetic oligomers or macromolecules that can fold in a well-defined conformation in solution by inclusion of a specific intra-chain interaction such as D−A CT interaction, hydrogen

bonding and solvophobic interactions. Iverson and co-workers demonstrated the folding of a series of D–A oligomers with varying chain length where an electron-rich 1, 5-dialkoxynaphthalene (**DAN**) and relatively electron deficient 1,4,5,8-naphthalenetetracarboxylic diimide (**NDI**) chromophores were alternatingly linked by flexible amino acid linkers containing a pendant carboxylic acid functional group (**12**) (Figure 1.3c).[15] The intra-chain folding induced by D−A interaction was confirmed by the appearance of a red-shifted CT band with higher oligomers and a change in the chemical shift values of the aromatic ring protons in ^{1}H NMR. Such chain folding driven by D−A interactions can also be achieved between two structurally similar homo oligomers composed of either DAN or NDI units thereby demonstrating the potential of D−A CT interaction as a powerful supramolecular motif.[16]

1.3. Functionality

In addition to the use as a supramolecular motif, more importantly MS-CT complexes offer various functionalities for electronic and ferroelectric application. One of the most interesting concepts related to the choice of D and A molecules is the potential for band engineering in the resulting complexes. The CT complexes vary in band gap from insulators to metals, and can even be superconductors which are determined by the degree of charge transfer from donor to acceptor in the CT complexes. Recently Park and co-workers have reported 1:1 D-A co-crystal system of two isometric distyrylbenzene (**15**) and dicyanodistyrylbenzene-based molecules (**16**), containing regular 1D mixed stacks which exhibit strongly red-shifted, bright photoluminescence in combination with high ambipolar p-/n-type field-effect mobility[17] (Figure 1.4b). In support of these experimental results, the theoretical explanation of Brédas *et al*. predicted high ambipolar mobility in mixed-stack CT crystals using density functional theory calculations and

mixed quantum/classical dynamics simulations.[18] They suggested that the electronic coupling in the CT complex has a superexchange nature which describes mixing of frontier orbitals of the donor with two neighbouring acceptors and vice versa with large transfer integrals where similar charge transport of hole and electron along D−A stacking directions can takes place which is responsible for their ambipolar charge transport property making them as a potential candidate in organic electronics. On the other hand, one-dimensional (1D) mixed-stack CT crystals because of their alternate D−A arrangement, undergoes spontaneous electric polarisation and provides a long range ordering of electrical dipoles through the collective CT processes, thereby proposed as potential candidates for ferroelectric applications. Though 1D ferroelectricity was already observed in mixed-stack CT complexes of tetrathiafulvalene (TTF) with *p*-bromanil or *p*-chloranil, the ferroelectric Curie temperature (T_c) was well below the ambient temperature thereby limiting their device application.[19] Recently Stupp *et al*. have shown room temperature ferroelectricity in mixed CT crystal based on pyrene, naphthalene, TTF as donors and pyromellitic diimide as acceptor in which 1D D-A stacks are interconnected by H-bonding interactions (Figure 1.4a).[20]
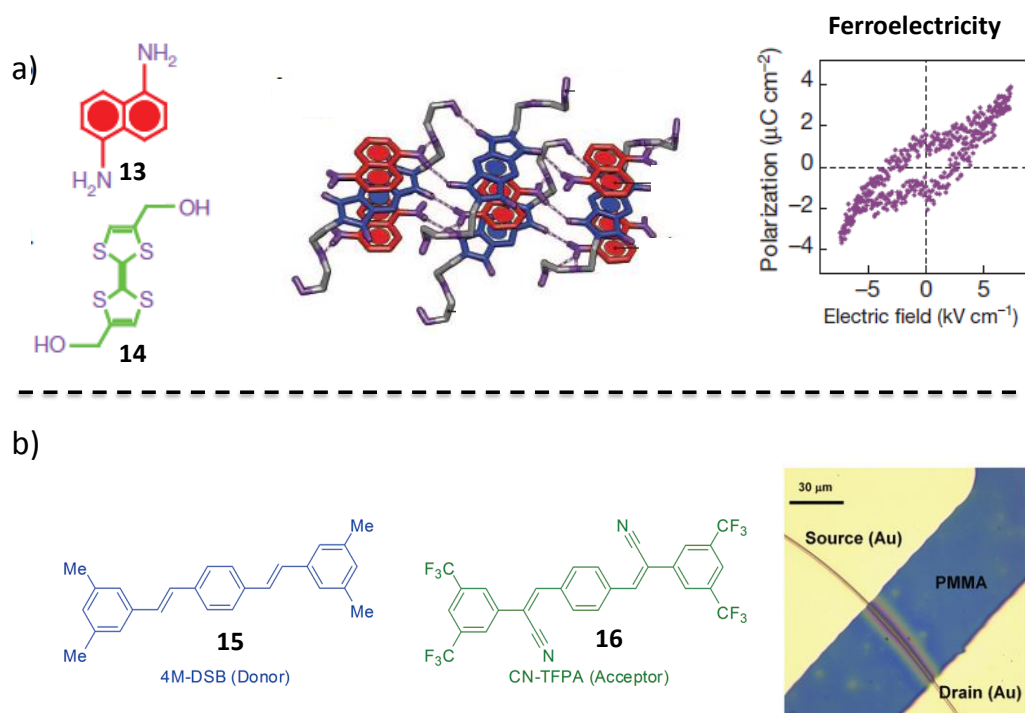
Figure 1.4: *a) Room temperature ferroelectricity exhibited by* ***13–14*** *CT co-crystal. Molecular organization in the co-crystal is also shown. (b) Optical photograph of the MS-CT co-crystal of* ***15–16***.

1.4. Supramolecular CT-nanostructures

One-dimensional supramolecular analogue of MS-CT systems constructed via the bottom-up supramolecular approach can lead to organic MS-CT nanostructures. They can facilitate the directional movement of charge carriers and forms conducting nanowires. However attempts to co-assemble the D and A molecules in solution to extended mixed stacks, often resulted in phase-separation and hence requires better design for the construction of corresponding supramolecular analogues. Hence to achieve better organisation in supramolecular assemblies various approaches have been utilized such as by forming supramolecular admixture, H-bonding and non-covalent amphiphilic design which are discussed below.

1.4.1. Supramolecular Admixture

Earlier supramolecular host-guest designs were utilised to construct CT nanostructure by mixing the A chromophores to the pre-assembled D molecules. This approach of making supramolecular nanostructure deals with a simple design where the donor assemblies are created by attaching well-known self-assembling motifs to the chromophores and the A molecules get encapsulated into the assemblies because of D−A CT interaction.[21] The well-known D and A chromophores forming supramolecular admixture are listed in figure 1.4, which sometimes undergoes gelation forming two component low molecular weight gelators.[22] Maitra *et al.* presented the first report on donor-acceptor interactions in organogels, by doping gels of donor-substituted derivatives with trinitrofluorenone (TNF, **19**), a well-known acceptor molecule. As a donor counterpart they have synthesised a bile acid derivative (**17**) attached with pyrene chromophore via carbamate or ester linkage.[23]
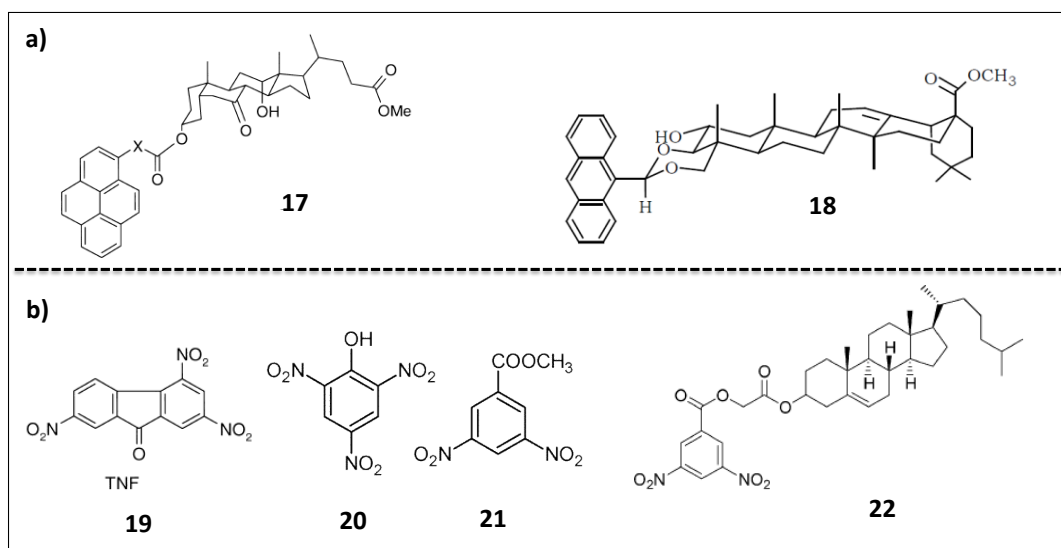
Figure 1.5: *a), b) are the various D and A building blocks respectively for gelation promoted by CT complexation.*

Interestingly an anthrylidene derivative of arjunolic acid (**18**) undergoes excellent gelation in variety of organic solvents in the presence of electron-deficient guests such as picric acid (**20**) or methyl-3, 5-dinitrobenzoate (**21**).[24] In most of the cases it was observed that the critical gelator concentration (CGC) of gels decreased significantly (less than 1% in suitable solvents) along with improved mechanical strength indicating the crucial role of CT interaction. However this type of CT complexes can be simply considered as a inclusion type of complex as they don't have any long range directional ordering.

1.4.2. Hydrogen Bonding

Alternate D−A CT interaction has been extensively used in the design of supramolecular assemblies. There are few examples of CT complexes having very high association constants which limit their long range ordering to extended D-A arrays of CT assemblies. Thus considerable stability could be achieved by reinforcing the CT complexes by using other non-covalent forces such as solvophobic forces, electrostatic interaction and metal-ligand interactions. H-bonding has also been utilised to construct mixed-stack assembly along with D−A CT interaction. There are mainly two basic designs of hydrogen bonded D–A pairs; (1) where only one of the two components (either donor or acceptor) is functionalized or (2) where both the components are functionalized with the hydrogen bonding motif. Recently Kimura and co-workers have reported an amphiphilic TTF derivative (**23**) as the D, attached to four chiral amides end group as hydrogen bonding units.[25] These were shown to form helical nanofibers in the presence of simple 2, 3, 5, 6-tetrafluoro-7, 7′, 8, 8′-tetracyano p-quinodimethane (F_4TCNQ, **24**) as the acceptor. The existence of hydrogen bonding in the CT assembly was established by FTIR measurements in the 1:1 D–A gel state. In another example Ghosh et al. have shown that H-bonding can still be retained in aqueous media playing a distinct role in the

Hydrogen Bonding
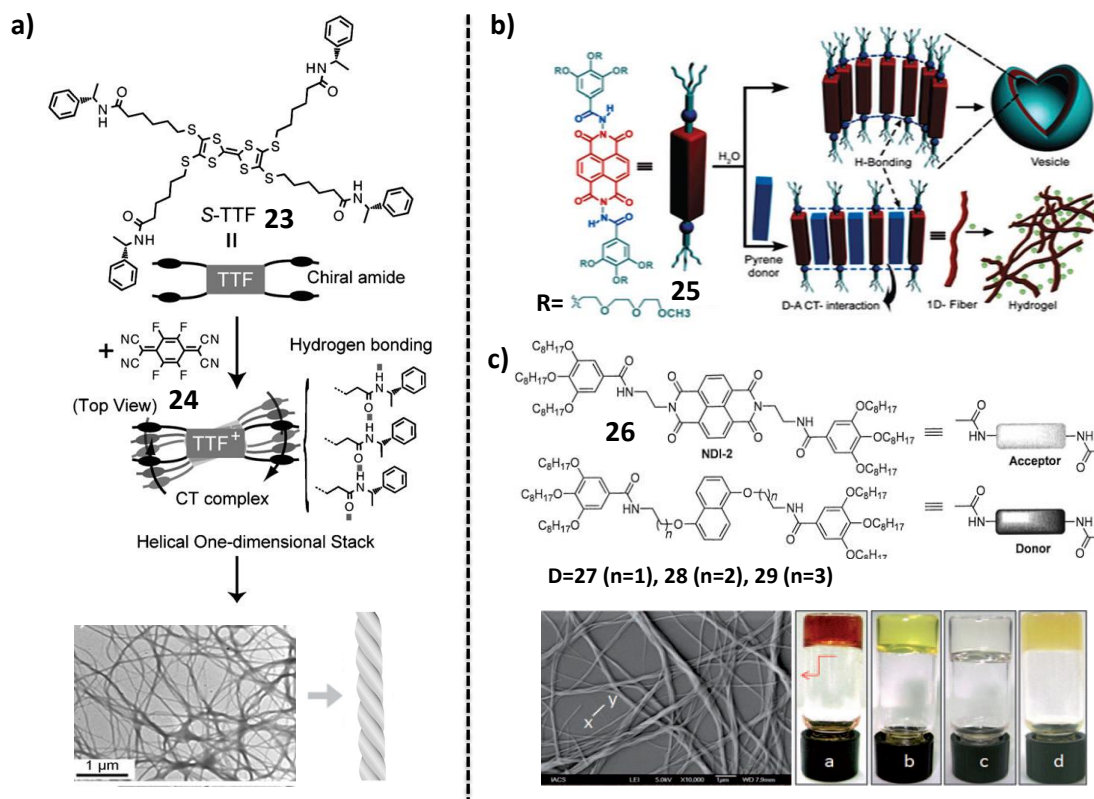
Figure 1.6: *a) Molecular structure of TTF based donor (**23**) attached to four chiral amide groups and the schematic representation of its 1:1 MS CT assembly with a F₄TCNQ (**24**) leading to the formation of one dimensional helical fiber as seen in the TEM image. b) Chemical structure of NDI based acceptor (**25**) and a schematic showing inclusion of pyrene donor into the NDI self-assembled matrix, leading to a morphology transition from vesicles to fibers. (c) Molecular structure of NDI (**26**) and DAN (**27-29**) derivatives functionalized with the gallic amide derived gelator motif, along with the SEM image and the photograph of the MS-CT gel (a) formed between **26** and **29** (1:1). b, c and d corresponds to the gel of **26, 29** and (**26+27**).*

self-assembly of hydrazide-functionalized NDI building blocks (**25**) forming vesicular aggregates which further could intercalate the pyrene donor through alternating D−A based CT interactions.[26] The pyrene incorporation led to a sandwiched structure between two NDIs (Figure 1.6b), retaining the hydrogen bonding between the two NDI-linked hydrazide groups.

11

Incorporation of pyrene showed an increase in radius of curvature and a gradual morphology transition from vesicle to 1D nano-fibers mediated by strong CT interaction. In another report they have shown the mixed-stack CT formation between bis-(trialkoxybenzamide)-functionalized dialkoxy naphthalene (DAN) donors (**27-29**) and naphthalene diimide (NDI) acceptor (**26**) due to the co-operative effects of π-π, charge-transfer (CT) interactions, hydrogen bonding and solvophobic effects leading to gel formation (Figure 1.6c). Through systematic study they have shown the important role of spacer length for appropriate positioning of the hydrogen bonding moiety for efficient CT formation. The 1:1 pair of **26:29** showed the formation of deep red colour gel (a) through alternate co-stacking of D and A. The individual D (**29**) and A (**26**) chromophores also showed gelation under identical condition. However the pair **26:27** forms gel but does not give any CT band suggesting the lack of alternate co-assembly because of the mismatch in the spacer length.

1.5. Supramolecular Amphiphile and Mixed-Stack CT Nanostructures
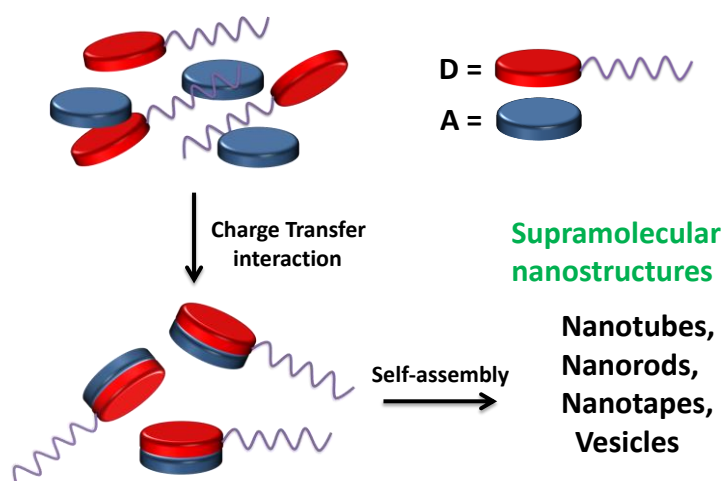
Figure 1.7: *Schematic representation of the non-covalent amphiphilic design for the construction of CT pair from appropriately designed D and A molecules.*

Supramolecular amphiphiles refer to amphiphiles that are synthesized on the basis of non-covalent interactions. Incorporation of amphiphilicity in the D and or A molecules would help in achieving more diversity in their aggregation properties by virtue of directional non-covalent interactions. Recently 1D nanostructures such as nanotubes and nanowires of semiconducting materials have attracted a lot of interest because of their vivid application in optical and electronic nano-devices which requires a long range ordering of D-A chromophores with strong intermolecular interactions.[27] In this respect mixed-stack amphiphilic approach would be useful for construction of 1D nanostructure with improved electronic properties because of their less dynamicity and inherent and uniform doping throughout the stack. Zhang and co-workers showed the fabrication of 1D CT nanofiber in water utilising CT interaction between viologen derivative (**32**) as an acceptor and 8- hydroxypyrene-1, 3, 6-trisulfonic acid trisodium salt (**31**) as a donor.[28] Self-assembly of this supramolecular amphiphile in water resulted in the formation of wormlike micelles whose stiffness can be modulated with pH (Figure 1.8). The amphiphilic viologen acceptor (**32**) itself aggregates into vesicles which transformed into wormlike micelles with the addition of equivalent amount of **31** in solution at pH 9. With increasing pH the worm like nanofibers were straightened as a result of extra charge repulsion, caused due to deprotonation of the hydroxyl group of **31**. Thus, these CT based nanostructures can be exploited as pH responsive smart materials as its pH dependent morphology change is shown to be completely reversible.
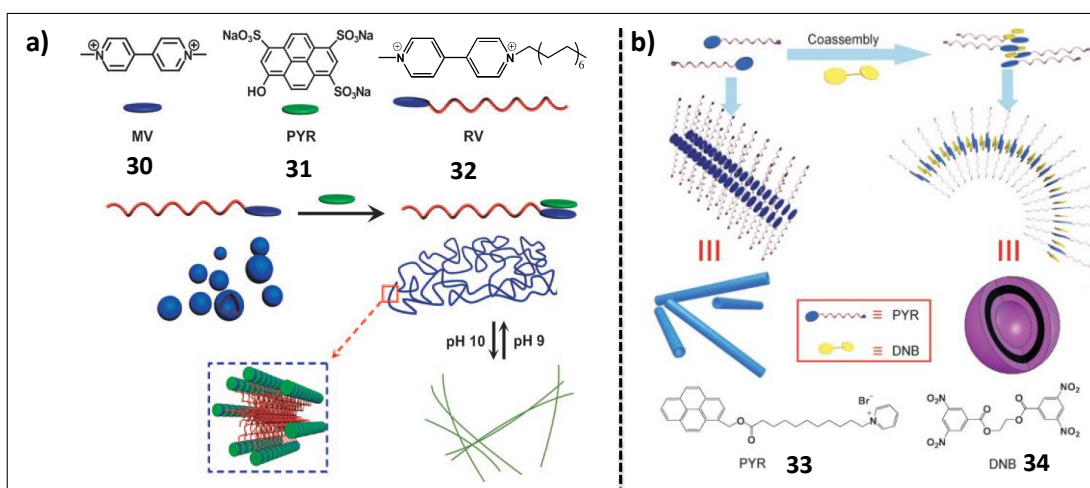
Figure 1.8: *a) Molecular structures of anionic pyrene D (**31**) and cationic A (**32**) and schematic representation of the preparation of the pH-responsive nanofibers through self-assembly of supramolecular amphiphile. b) Molecular structures of pyrene derived D (**33**) and nitro derived A (**34**) and schematic representation of the transformation of **33** from tubes to vesicles due to CT interactions.*

In another report the authors have demonstrated the structural regulation of self-assembling nanostructures from fluorescent tubes to vesicles in aqueous media, manipulated by CT-interactions. Here they have used amphiphilic electron rich pyrene (**31**) derivative as donor which self-assembled to form nanotubes. The co-assembly of pyrene donor with the electron deficient nitro (**32**) derivative resulted in the formation of supramolecular mixed-stack CT-amphiphiles which further self-assemble into vesicles via extended amphiphilic CT-interactions (Figure 1.8b).[29] This clearly indicates the more dominant nature of amphiphilic CT interaction compared to their individual π-π interactions.

1.6. Conclusion

1D mixed-stack CT-nanostructures with extended D-A stacking are important for their potential use in advanced nanoelectronic devices which requires further control over its function and structure for the application as a conducting nanowire. In recent years the conducting properties of the self-assembled 1D nanostructures has been improved by either the modification of molecular structure or by external doping. The former strategy would require tedious synthetic efforts on the other hand it is very difficult to get uniform doping throughout the assemblies preserving their morphology. In this respect mixed-stack CT crystals obtained from amphiphilic D and A molecules have attracted much attention because of their inherent conducting properties and ambipolar charge transport property.

In this thesis, we have extended the non-covalent amphiphilic design strategy to construct 1D Mixed-stack D-A CT-nanostructure with better iconicity which can find potential application in organic ferroelectrics and multiferroics which will be discussed in the following chapters.

1.7. References

[1]   K. P. Goetz, D. Vermeulen, M. E. Payne, C. Kloc, L. E. McNeil and O. D. Jurchescu, *J. Mater. Chem. C.*, DOI: 10.1039/c3tc32062f; H. Mendez, G. Heimel, A. Opitz, K. Sauer, P. Barkowski, M. Oehzelt, J. Soeda, T. Okamoto, J. Takeya, J.-B. Arlin, J.-Y. Balandier, Y. Geerts, N. Koch, and I. Salzmann, *Angew. Chem. Int. Ed.*, 2013, **52**, 1.

[2]   Z. G. Soos, H. J. Keller, W. Moroni and D. Nothe, *Ann. N. Y. Acad. Sci.*, 1978, **313**, 442.

[3]   V. Coropceanu, J. Cornil, D. A. da S. Filho, Y. Olivier, R. Silbey and J.-L. Brédas, *Chem. Rev.,* 2007, **107**, 926; L. Zhu, Y. Yi, Y. Li, E.-G. Kim, V. Coropceanu and

J.-L. Brédas, *J. Am. Chem. Soc.* 2012, **134**, 2340; G. Giovannetti, S. Kumar, A. Stroppa, J. van den Brink and S. Picozzi, *Phys. Rev. Lett*., 2009, **103**, 266401; M. Masino and A. Girlando, *Phys. Rev. B.,* 2007, **76**, 064114; P. Ranzieri, M. Masino, A. Girlando and M.-H. Lemée-Cailleau, *Phys. Rev. B.,* 2007, **76**, 134115.

[4]   E. A. Appel, F. Biedermann, U. Rauwald, S. T. Jones, J. M. Zayed and O. A. Scherman, *J. Am. Chem. Soc.*, 2010, **132**, 14251; E. A. Appel, X. J. Loh, S. T. Jones, F. Biedermann, C. A. Dreiss and O. A. Scherman, *J. Am. Chem. Soc.,* 2012, **134**, 11767; S. De and S. Ramakrishnan*, Macromolecules,* 2009, **42**, 8599; C. Wang, D. Zhang, D. Zhu, *J. Am. Chem. Soc*., 2005, **127**, 16372.

[5]   E. H. A. Beckers, S. C. J. Meskers, A. P. H. J. Schenning, Z. Chen, F. Würthner, P. Marsal, D. Beljonne, J. Cornil and R. A. J. Janssen, *J. Am. Chem. Soc*., 2006, **128**, 649; A. P. H. J. Schenning, J. van Herrikhuyzen, P. Jonkheijm, Z. Chen, F. Würthner and E. W. Meijer, *J. Am. Chem. Soc.* 2002, **124**, 10252.

[6]   J. Ferraris, D. O. Cowan, V. Walatka, Jr. and J. H. Perlstein, *J. Am. Chem. Soc.,* 1973, **95**, 948.

[7]   M. Sakai, H. Sakuma, Y. Ito, A. Saito, M. Nakamura and K. Kudo, *Phys. Rev. B: Condens. Matter Mater. Phys.*, 2007, **76**, 045111.

[8]   S. Horiuchi and Y. Tokura, *Nat. Mat.* 2008, **7**, 357; A. Girlando, A. Painelli, C. Pecile, G. Calestani, C. Rizzoli and R. M. Metzger, *J. Chem. Phys*. 1993, **98**, 7692.

[9]   A. R. Pease, J. O. Jeppesen, Y. Luo, C. P. Collier, J. R. Heath and J. F. Stoddert, *Acc. Chem. Res***.,** 2001, **34**, 433; J. M. Spruell, W. F. Paxton, J.-C. Olsen, D. Benı́tez, E. Tkatchouk, C. L. Stern, A. Trabolsi, D. C. Friedman, W. A. Goddard III and J. F. Stoddart. *J. Am. Chem. Soc*., 2009, **131**, 11571; K. B. Simonsen, K. Zong, R. D. Rogers and M. P. Cava*, J. Org. Chem*., 1997, **62**, 679; D. B. Amabilino and J. F. Stoddart*, Chem. Rev*., 1995, **95**, 2725; C. O. D-Buchecker and J. P. Sauvage, *Chem. Rev.,* 1987, **87**, 795; L. Raehm, D. G. Hamilton and J. K. M. Sanders, *Synlett,* 2002, 1743; S. A. Vignon, T. Jarrosson, T. Iijima, H.-R. Tseng, J. K. M. Sanders and J. F. Stoddart, *J. Am. Chem. Soc*., 2004, **126**, 9884; M. A. Olson, A. Coskun, L. Fang, A. N. Basuray and J. F. Stoddart, *Angew. Chem., Int. Ed.,* 2010, **49**, 3151; G. Koshkakaryan, L. M. Klivansky, D. Cao, M. Snauko, S. J. Teat, J. O. Struppe and Y. Liu, *J. Am. Chem. Soc.,* 2009, **131**, 2078; H. M. Colquhoun and Z. Zhu, *Angew. Chem., Int. Ed*., 2004, **43**, 5040; E. A. Appel, F. Biedermann,

U. Rauwald, S. T. Jones, J. M. Zayed and O. A. Scherman, *J. Am. Chem. Soc.*, 2010, **132**, 14251; D. Jiao, J. Geng, X. J. Loh, D. Das, T.-C. Lee and O. A. Scherman, *Angew. Chem., Int. Ed.,* 2012, **51**, 9633; B. V. V. S. P. Kumar, K. V. Rao, T. Soumya, S. J. George and M. Eswaramoorthy, *J. Am. Chem. Soc.*, 2013, **135**, 10902.

[10] E. A. Appel, X. Jun Loh, S. T. Jones, F. Biedermann, C. A. Dreiss and O. A. Scherman*, J. Am. Chem. Soc.,* 2012, **134,** 11767; D. Jiao, J. Geng, X. J. Loh, D. Das, T-C. Lee and O. A. Scherman, *Angew. Chem. Int. Ed.,* 2012**, 51**, 9633; E. A. Appel, F. Biedermann, U. Rauwald, S. T. Jones, J. M. Zayed and O. A. Scherman, *J. Am. Chem. Soc.,* 2010, **132**, 14251; Y. H. Ko, E. Kim, I. Hwang and K. Kim, *Chem. Commun.*, 2007, 1305.

[11] J. Lagona, P. Mukhopadhyay, S. Chakrabarti and L. Isaacs, *Angew. Chem., Int. Ed.,* 2005, **44**, 4844. b) J. Kim, I. S. Jung, S. Y. Kim, E. Lee, J. K. Kang, S. Sakamoto, K. Yamaguchi and K. Kim, *J. Am. Chem. Soc.,* 2000, *122*, 540.

[12] S. T. Jones, J. M. Zayed and O. A. Scherman, *Nanoscale*, 2013, **5**, 5299.

[13] U. Rauwald and O. A. Scherman, *Angew. Chem., Int. Ed.,* 2008, **47**, 3950; X. J. Loh, J. del Barrio, P. P. C. Toh, T.-C. Lee, D. Jiao, U. Rauwald, E. A. Appel and O. A. Scherman, *Biomacromolecules,* 2012, **13**, 84; Y. Liu, Y. Yu, J. Gao, Z. Wang and X. Zhang, *Angew. Chem., Int. Ed.,* 2010, **49**, 6576.

[14] S. Ghosh and S. Ramakrishnan, *Angew. Chem., Int. Ed.,* 2004, **43**, 3264; S. G. Ramkumar and S. Ramakrishnan, *Macromolecules,* 2010**, 43**, 2307; S. Ghosh and S. Ramakrishnan, *Angew. Chem., Int. Ed.,* 2005, **44**, 5441; S. De and S. Ramakrishnan, *Chem. Asian J.,* 2011, **6**, 149; G. J. Gabriel and B. L. Iverson, *J. Am. Chem. Soc.,* 2002, 124, 15174

[15] R. S. Lokey and B. L. Iverson, *Nature*, 1995, **375**, 303.

[16] G. J. Gabriel and B. L. Iverson*, J. Am. Chem. Soc.* 2002**, 124**, 15174.

[17] S. K. Park, S. Varghese, J. H. Kim, S.-J Yoon, O.-K. Kwon, B. An, J. Gierschner and S. Y. Park, *J. Am. Chem. Soc.* 2013, **135**, 4757.

[18] L. Zhu, Y. Yi, Y. Li, E. Kim, V. Coropceanu, J. L. Brédas, *J. Am. Chem. Soc.* 2012, **134**, 2340; b) W. Yu, X.-Y. Wang, J. Li, Z.-T. Li, Y.-K. Yan, W. Wang and J. Pei, *Chem. Commun.*, 2013, 54.

[19] Y. Tokura, S. Koshihara, *Phys. Rev. Lett.,* 1989, **63**, 2405; H. Okamoto and T. Mitani, *Phys. Rev. B.,* 1991, 43, 8224.

[20] A. S. Tayi, A. K. Shveyd, A. C.-H. Sue, J. M. Szarko, B. S. Rolczynski, D. Cao, T. J. Kennedy, A. Sarjeant, C. L. Stern, W. F. Paxton, W. Wu, S. K. Dey, A. C. Fahrenbach, J. R. Guest, H. Mohseni, L. X. Chen, K. L. Wang, J. F. Stoddart and S. I. Stupp, *Nature*, 2012, **488**, 485; b) S. Horiuchi and Y. Tokura, *Nature Mater*., 2008, **7**, 357; A. Girlando, A. Painelli, C. Pecile, G. Calestani, C. Rizzoli, R. M. Metzger, *J. Chem. Phys*., 1993, **98**, 7692.

[21] S. S. Babu, S. Prasanthkumar and A. Ajayaghosh, *Angew. Chem., Int. Ed.*, 2012, **51**, 1766; A. Friggeri, O. Gronwald, K. J. C. v. Bommel, S. Shinkai and D. N. Reinhoudt, *J. Am. Chem. Soc*., 2002, **124**, 10754.

[22] L. E. Buerkle and S. J. Rowan, *Chem. Soc. Rev.,* 2012, **41**, 6089; A. Ajayaghosh, V. K. Praveen and C. Vijayakumar, *Chem. Soc. Rev.,* 2008, **37**, 109.

[23] U. Maitra, P. V. Kumar, N. Chandra, L. J. D'Souza, M. D. Prasanna and A. R. Raju, *Chem.Commun.,* 1999, 595.

[24] B. G. Bag, G. C. Maity and S. K. Dinda, *Org. Lett*., 2006, **8**, 5457.

[25] Y. Tatewaki, T. Hatanaka, R. Tsunashima, T. Nakamura, M. Kimura and H. Shirai, *Chem. Asian J.* 2009, **4**, 1474.

[26] M. R. Molla and S. Ghosh, *Chem. −Eur. J.,* 2012, **18**, 9860; A. Das, M. R. Molla, A. Banerjee, A. Paul and S. Ghosh, *Chem. −Eur. J.,* 2011, 17, 6061.

[27] K. V. Rao, K. Jayaramulu, T. K. Maji and S. J. George, *Angew. Chem.* 2010, **122,** 4314; *Angew. Chem. Int. Ed.,* 2010, **49**, 4218; K. V. Rao, S. J. George, *Chem. −Eur. J.* 2012, **18**, 14286; A. A. Sagade, K. V. Rao, S. J. George, A. Datta and G. U. Kulkarni, *Chem. Commun.* 2013, **49,** 5847; A. A. Sagade, K. V. Rao, U. Mogera, S. J. George, A. Datta and G. U. Kulkarni, *Adv. Mater.* 2013, **25**, 559; K. Jalani, M. Kumar, S. J. George, *Chem. Commun.* 2013**, 49**, 5174.

[28] C. Wang, Y. Guo, Y. Wang, H. Xu, R. Wang and X. Zhang, *Angew. Chem. Int. Ed*., 2009, **48**, 8962.

[29] C. Wang, S. Yin, S. Chen, H. Xu, Z. Wang and X. Zhang, *Angew. Chem., Int. Ed.,* 2008, **47**, 9049.

CHAPTER - 2

Mixed-Stack Charge Transfer Nanostructures

PART-1: Tetrathiafulvalene-Viologen derived Mixed-Stack

Donor-Acceptor Array via Non-covalent Amphiphilic

Design

PART-2: Alternate Tetrathiafulvalene-Naphthalene Diimide D-A

Arrays by an Amphiphilic Co-Assembly

Chapter-2, Part-1

Tetrathiafulvalene-Viologen derived Mixed-Stack Donor-Acceptor Arrays via Non-covalent Amphiphilic Design*

Abstract

An extended alternate array of tetrathiafulvalene (TTF) donor and Viologen acceptor are constructed via a non-covalent amphiphilic design. The resulting charge transfer (CT) pair has a strong red shifted absorption band at 725 nm. The two-probe electrical measurement on the resulting CT nanostructures revealed that they are semiconducting in nature and can be a viable candidate for organic electronics.
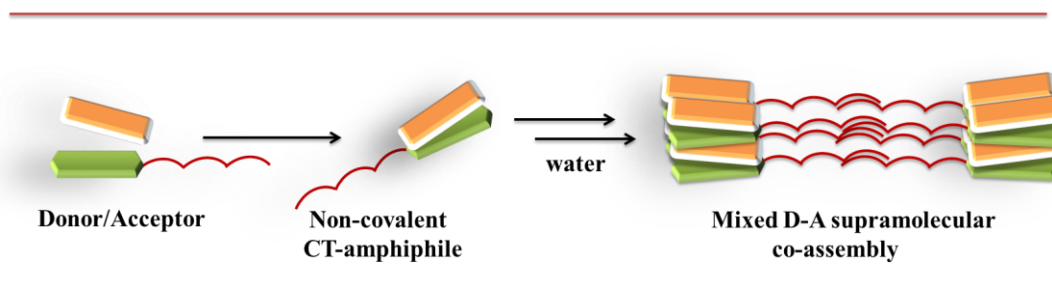
2.1.1. Introduction

Organic mixed-stack (MS), donor-acceptor (D-A) charge transfer crystals formed via face-to-face organization of aromatic electron D and electron A molecules attracted much research interest because of their interesting electronic properties.[1] Interestingly, recent research provides a theoretical prediction of high ambipolar charge transport characteristics in mixed-stack CT crystals.[2] One-dimensional supramolecular analogues of the MS-CT crystals would facilitate the directional movement of charge carriers and are extremely important for the formation of conducting organic nanowires for nanosized electronics. In addition, a long range ordering of electrical dipoles in this mixed CT co-assembly can also lead to ferroelectricity.[3]

Tetrathiafulvalene (**TTF**) and its derivatives are well known electro-active aromatic π-conjugated donor molecules which form efficient charge transfer complexes with various acceptors and are thoroughly exploited in the field of organic electronics.[4] In literature TTF-viologen pairs are well known to form efficient CT complexes and are extensively used for the construction of molecular machines such as catenanes, rotaxanes and molecular switches.[5,6,7] However supramolecular assemblies of this CT pair has not been explored. Recently, we have reported on MS-CT nanostructures of Coronene tetracarboxylate salt (**CS**) and viologen (**DMV**) D-A pair following a non-covalent amphiphilic design (Figure 2.1.1a).[8,9] Detailed microscopic analysis revealed the cylindrical micellar type molecular arrangement of the **CS-DMV** CT amphiphile in which the hydrophilic chromophoric part acts as the polar head and the dodecyl chain as the nonpolar tail (Figure 2.1.1b). Single fiber transistor made from these supramolecular systems have shown excellent charge transport properties.[9]
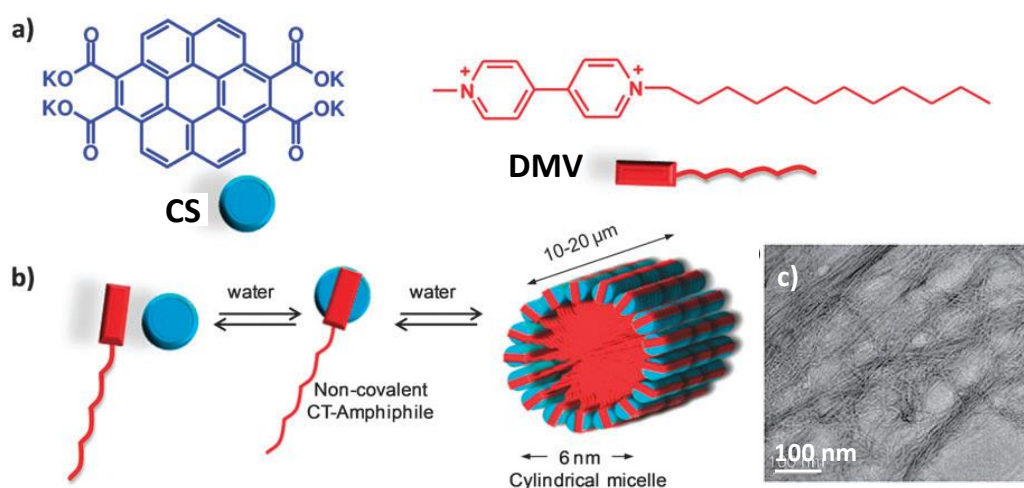
Figure 2.1.1: *a) Molecular structure of donor, coronene tetracarboxylate salt (CS) and acceptor, dodecyl methyl viologen acceptor (DMV). b) Schematic representation of the non-covalent design of the CT co-assembly and its self-assembly into high aspect ratio cylindrical micelles. c) TEM image of the self-assembled cylindrical micelles.*

On the other hand, in order to observe ferroelectricity in CT crystals, a neutral to ionic phase transition of electrical dipoles should be present and this can be predicted from Raman spectroscopic experiments.[10] In order to investigate the ionicity of this CT pair, detailed Raman spectroscopic measurements on the **CS-DMV** nanostructures were performed. Figure 2.1.2 compares the Raman spectra of **CS** and **DMV** (lower part of the Figure, green and red lines, respectively) with the spectrum of the **CS-DMV** fiber (upper part of the figure). The latter has been obtained from a bunch of fibers left once the CT complex solution was evaporated. The spectrum is essentially the superposition of the spectra of the component molecules, which indicates that the degree of charge transfer in the fiber is close to zero and CT crystals are neutral. This fact indicates the lower ionicity of **CS-DMV** CT nanostructures.
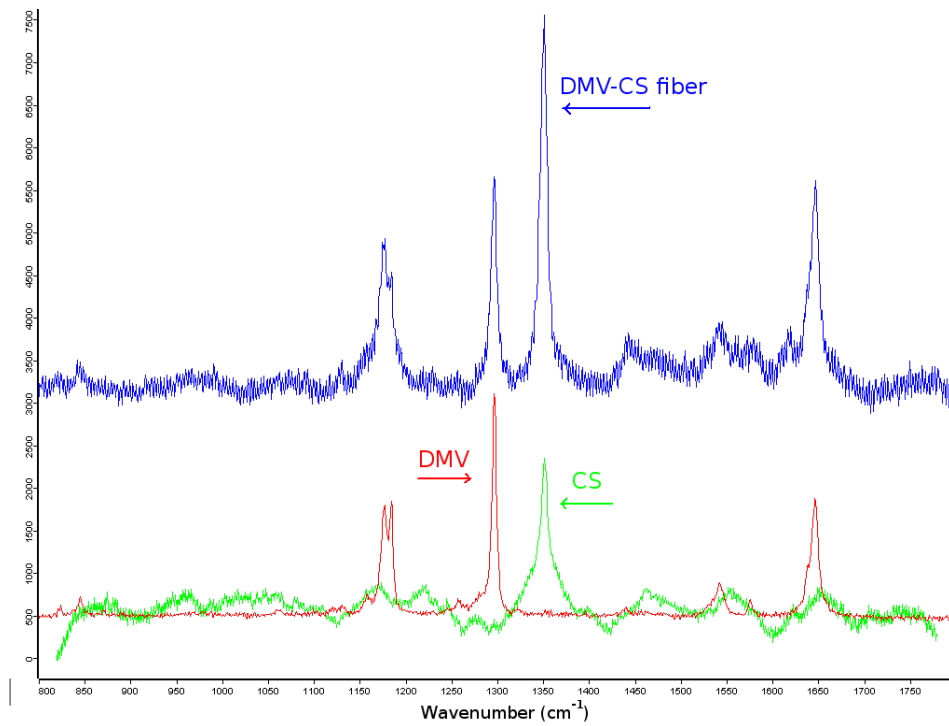
Figure 2.1.2: *Raman spectra of **CS, DMV** (bottom) and of the **CS-DMV** fiber (top), λ_{exc} = 676 nm. The spectra of **CS** and **CS-DMV** have been manipulated to subtract the background and reduce the noise (Unpublished results. This experiment is done by prof. A. Girlando and Dr. M. Masino, University of Parma, Italy)*

Hence, in this chapter, we target a strong CT pair with better ionicity using a non-covalent amphiphilic design which can form CT nanostructures with better ferroelectric property. Therefore, we have used a stronger donor **TTFS** instead of coronene to construct the CT nanostructures.

2.1.2. Design Strategy and Molecular Structures
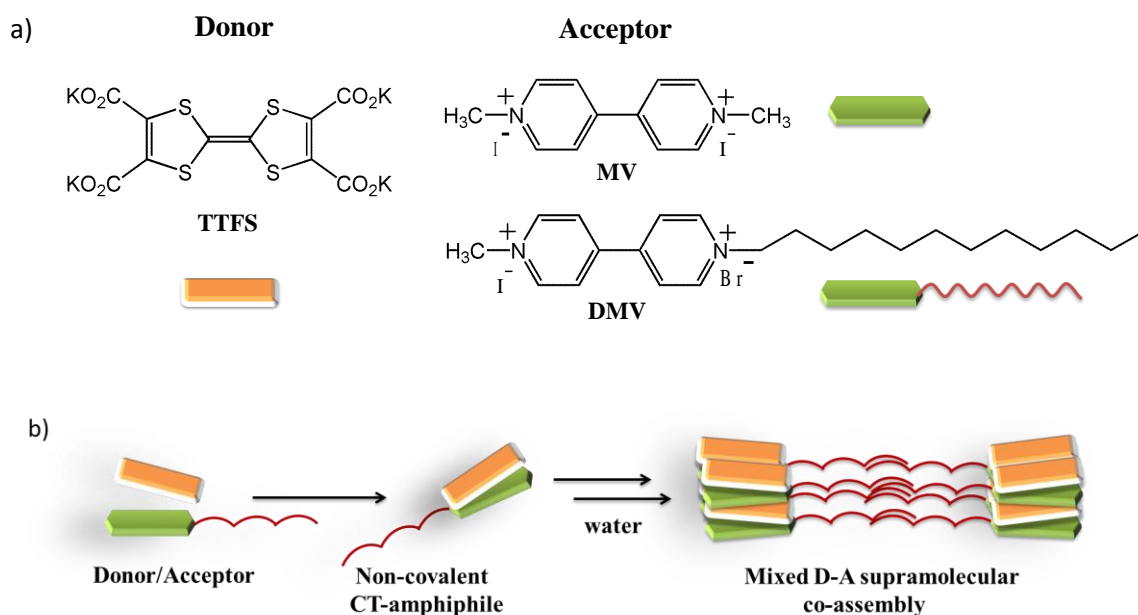
Figure 2.1.3: *a) Molecular structures of D and A molecules used in this section. b) Non-covalent amphiphilic design strategy.*

In this study, we have designed the molecules in such a way that the D-A co-assembly would structurally resemble a non-covalent amphiphile in their CT state, so that they can assemble further to extended arrays upon higher order aggregation. Here we have synthesised hydrophilic TTF-donor (**TTFS**) having four polar carboxylate groups and amphiphilic viologen acceptor (**DMV**) having long dodecyl chain. The extended π-conjugated nature of the D and A bearing opposite charges, would promote their efficient face-to-face co-assembly through synergistic π-π stacking, CT and electrostatic interactions in a mixed-stack organisation. The ionic nature of the D and A molecules would further help them to be soluble in water which is an environmentally friendly solvent. Here we have used **MV**, without any long alkyl side chains, as a model compound for the NMR study which would give a better insight into the molecular arrangement of the chromophores in the D-A pair.

2.1.3. Synthetic Scheme for Donor and Acceptor

Synthetic schemes for **TTFS** and **DMV** are shown in the Scheme 2.1.1 and Scheme 2.1.2, respectively.
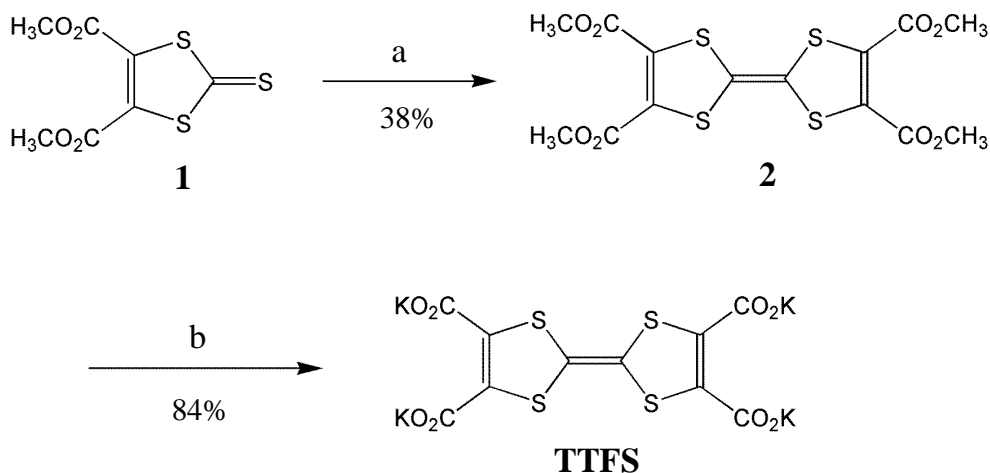
Scheme 2.1.1: *Synthesis of **TTFS**: a) P(OEt)$_3$, benzene, reflux, 85°C, 12 hr. b) 3.5 % aq KOH, EtOH, reflux, 95°C, 12 h.*
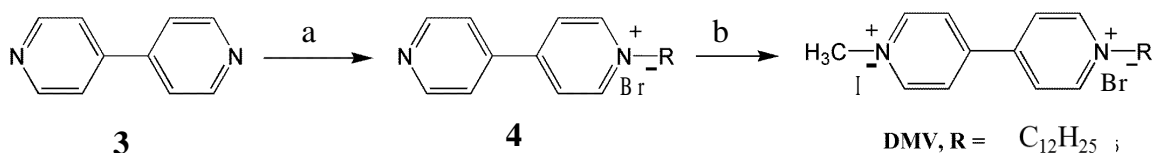
Scheme 2.1.2: *Synthetic routes for **DMV**, a) C$_{12}$H$_{25}$Br, CH$_3$CN, reflux, 16 h. b) CH$_3$I, CH$_3$CN, reflux, 12 h.*

The donor **TTFS** derivative was synthesised by the hydrolysis of the TTF tetraester (**2**) which was obtained from the homocoupling of the corresponding diester (**1**) in presence of P(OEt)$_3$ (Scheme 2.1.1). **DMV** was synthesised in two steps starting from 4, 4'-bipyridine (Scheme 2.1.2) following the literature procedure.[11] The model compound **MV** was purchased from Acros Organics.

2.1.4. Co-Assembly of TTFS and DMV/MV in solution

Formation of MS-CT complex between **TTFS** and viologens were studied in detail using optical spectroscopic measurements. **TTFS** is molecularly dissolved in water at 5 x 10^{-4} M concentration whereas **DMV** being amphiphilic in nature self-assemble in water forming vesicular morphology.[8] The D-A mixtures for optical studies were prepared by injecting the aqueous solution of **DMV** into an aqueous solution of **TTFS** in appropriate ratio. Though **DMV** aggregates in water, this sample preparation doesn't affect the CT absorption features as it was observed that **DMV** self-assembly in water is dynamic enough to reorganize and form CT complex with donor molecules.[12] Addition of varying amounts of **DMV** (upto 1 equiv.) to **TTFS** (c = 5 x 10^{-4} M) in water resulted in the appearance of a broad, red shifted absorption band in the with a maximum at 725 nm, characteristic of the ground state CT interaction between **TTFS** and **DMV** chromophores (*vide infra*).[12] This was further evident from visible color changes observed when the mixture of yellow colored **TTFS** and colorless **DMV** solutions showed the formation of dark green colored solution as a result of CT-interactions (Figure 2.1.4b). In order to investigate the stoichiometry of the CT co-assembly, spectroscopic properties of **TTFS** were probed against the molar concentration of **DMV** using Job method. Job plot at 5 x 10^{-4} M concentrations clearly showed the saturation of absorbance corresponding to the CT maxima at mole fractions of 0.5 confirming the 1:1 binding stoichiometry of D and A molecules (Figure 2.1.4c). In addition, high resolution mass-spectrometry (HRMS) analysis of **TTFS-DMV** co-assembly showed a mass of (*m/z)* 716.5460 corresponding to 1:1 complex [**TTFS+DMV**]$^+$ ion, which reiterates 1:1 molar ratio of binding between D and A (Figure 2.1.5). Similar observations were made when **TTFS** was co-assembled with the model compound **MV**. To use **MV** as model compounds for NMR studies we

have performed absorption spectroscopic measurement which shows that it interacts in a similar way as **DMV** to form efficient CT complex with **TTFS** (Figure 2.1.4d). When **TTFS** was titrated with increasing equivalents of **MV**, gradual changes in the absorption features of **TTFS** with concomitant appearance of new broad band centred at 725 nm clearly indicates the formation ground state CT-complex between **TTFS** and **MV**. Inset in Figure 2.1.4d shows the absorbance vs. equivalent plot for **TTFS-MV** CT complex which shows the saturation of CT absorption at one equivalent of **MV**, indicating 1:1 stoichiometry.
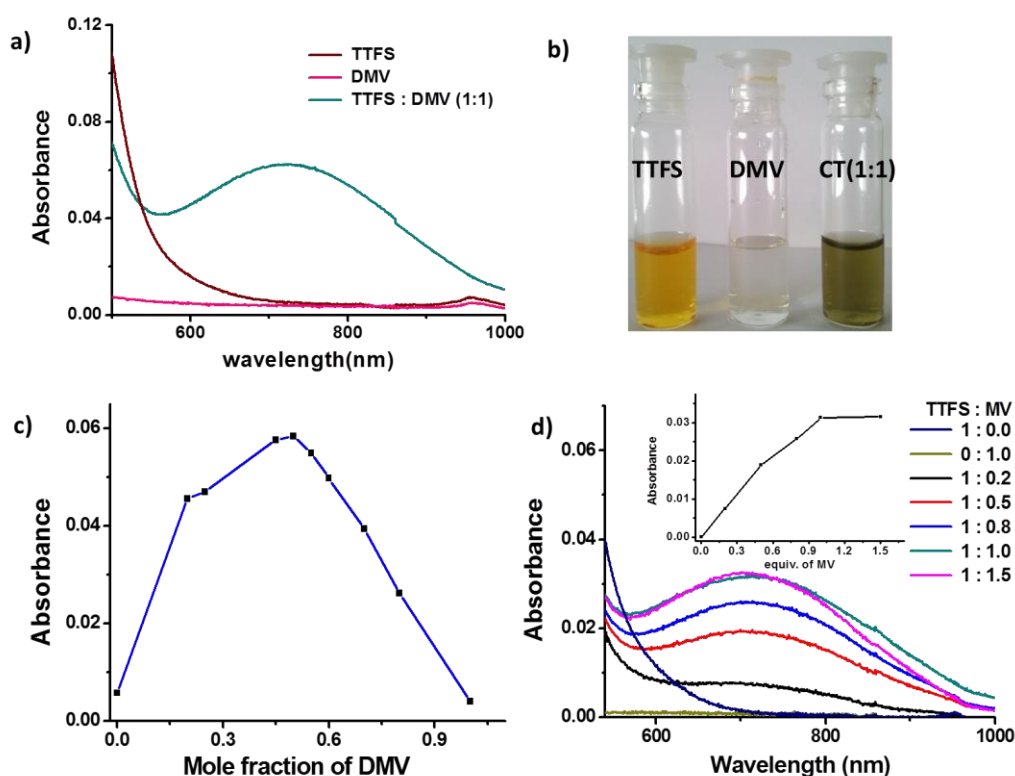
Figure 2.1.4: *a) UV-Vis Absorption spectra of **TTFS** and **DMV** CT complex (1:1) in water at 5 x 10^{-4} M concentration. b) Photographs of **TTFS**, **DMV** and 1:1 CT pair in water. The intense green color of the **TTFS-DMV** solutions clearly suggests the formation of CT complexes. c) Job plot for **TTFS** and **DMV** CT pair at 5 x 10^{-4} M concentration. d) UV-Vis absorption spectra for the titration of **TTFS** with **MV** at 5 x 10^{-4} M concentration in water. Inset shows corresponding titration curve obtained by plotting the absorption changes monitored at 725 nm.*
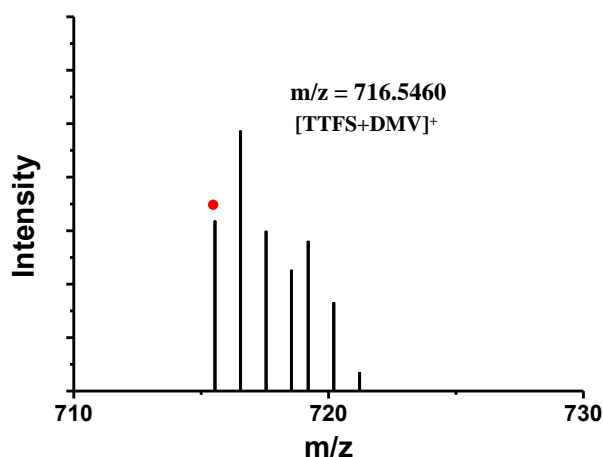
Figure 2.1.5: *High resolution mass spectrum of **TTFS-DMV** (1:1) CT-complex formed in water.*

2.1.5. Face-to-face Organisation of TTF and Viologen Chromophore

^{1}HNMR spectroscopy was used to provide information on the molecular organisation of D and A upon CT formation as attempts to crystallize CT-crystals of **TTFS** with viologen acceptors was unsuccessful. To get deeper insight into the D-A organisation in the 1:1 CT complexes, we have performed NMR measurements for both **TTFS-DMV** and **TTFS-MV** CT pair. Figure 6, shows the ^{1}HNMR spectra of **TTFS** and **DMV** in D_2O, recorded at high concentration (10^{-2} M) to achieve a significant spectral shift upon CT formation. **DMV** alone in D_2O gives three signals, two doublets and a triplet between $\delta = 8$–9 ppm, which corresponds to two types of terminal protons (H_{a1} and H_{a2}) and middle protons (H_{b1} and H_{b2}) respectively. Although H_{b1} and H_{b2} protons should have appeared as separate doublets in the aromatic region, because of similar chemical environments they merged partially and appeared as a triplet.[12] However in the 1:1 CT complex solution (10^{-2} M, D_2O) a spectral splitting pattern change was observed where the triplet corresponding to H_{b1} and H_{b2} protons splits into two clear separated doublets along with an up-field shift (0.1 ppm) for H_{a1} and H_{a2} protons adjacent to the cationic

29

nitrogen. This can be attributed to the strong π-electron cloud shielding of H_{a1} and H_{a2} protons of **DMV,** resulted from the co-facial organisation of **TTFS** and **DMV** which causes significant change in the chemical environment for all the protons.
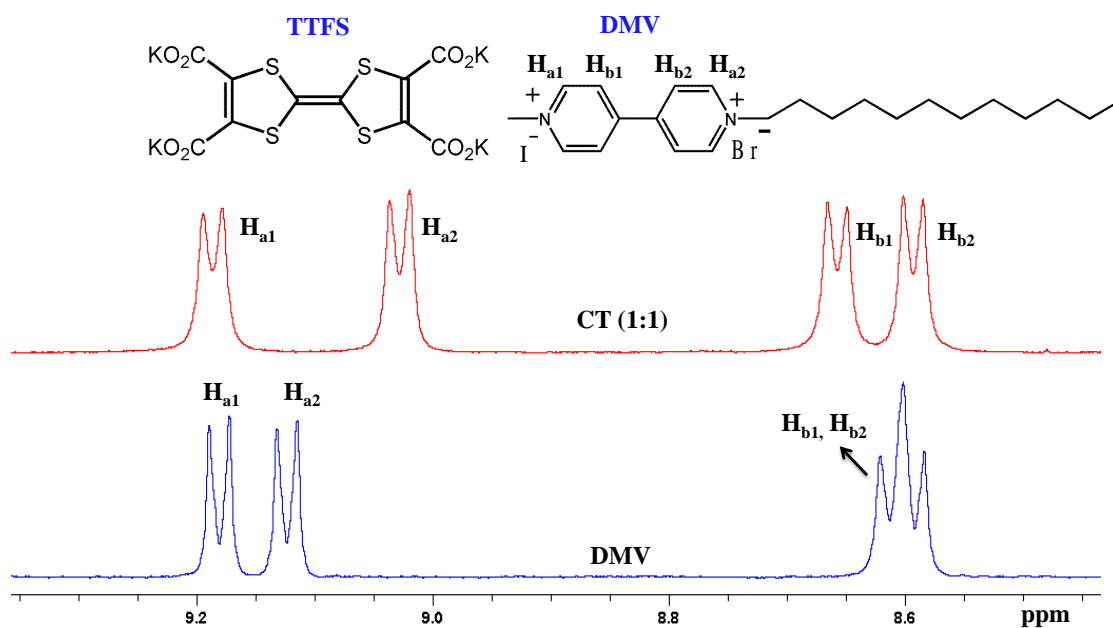
Figure 2.1.6: *Partial ^1H NMR spectra of **TTFS** and **DMV** CT complex (D_2O, 10^{-2} M) along with **DMV** alone showing the variation of proton resonance signal in the aromatic region.*

^1H NMR spectrum for **TTFS** and model compound **MV** in 1:1 composition was also done at 10^{-2} M in D_2O which indicates an up-field shift for bipyridinium aromatic protons (H_a, figure 2.1.7) adjacent to the cationic nitrogen which further indicates the co-facial orientation of D and A in the CT co-assembly.
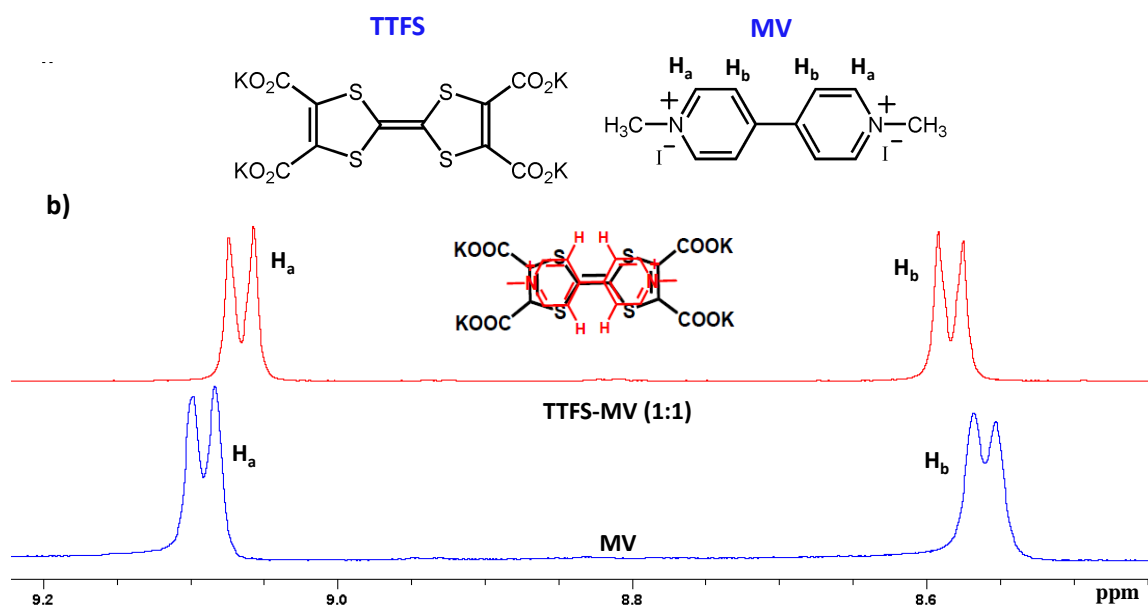
Figure 2.1.7: *Partial ^{1}H-NMR spectra of MV and its 1:1 complex with **TTFS** in D_2O (c = 10^{-2} M). Inset shows the proposed orientation of **TTFS** and **MV** in the CT co-assembly.*

2.1.6. Higher-Order Self-assembly of the CT Amphiphiles

Having established the co-facial orientation of **TTFS** and **DMV** and thereby forming a non-covalent amphiphilic pair in the CT co-assembled state, we have further explored their self-assembly into higher order aggregates. To understand the morphological features of nanostructures formed via self-assembly of non-covalent CT-amphiphile, we have done detailed microscopy experiments and DLS measurements (Figure 2.1.8). FE-SEM image of 1:1 mixture of **TTFS** and **DMV** CT co-assembly in water ($5x10^{-4}$ M) drop casted on glass substrates, reveals the self-assembly of **TTFS-DMV** CT amphiphiles into nanoplates having 0.5–1 mm width and 10–15 mm in length, which was also observed through TEM (Figure 2.1.8 b, c). This suggests a different molecular packing in the CT nanostructures. **DMV** being amphiphilic in nature self-assembles in water and shows a hydrodynamic radius of 100 nm (Figure 2.1.8a) which is further supported from its vesicle formation observed through **FE-SEM** image (Figure

31

2.1.8b).[12] Interestingly, hydrodynamic radius for CT complex in solution is larger than **DMV** aggregates and broad in nature which indicates the formation of higher order aggregates of **TTFS-DMV** co-assembly.[8] This further gives a decisive proof for the formation CT-nanostructures in solution via amphiphilic self-assembly and not due to any surface drying effects.
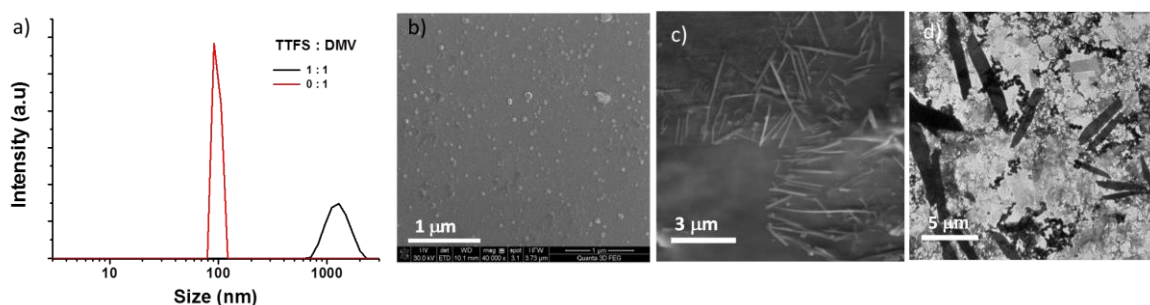
Figure 2.1.8: *a) Dynamic light scattering (DLS) measurements showing the hydrodynamic size distribution of **DMV** and CT co-assembly of **TTFS : DMV** (c = 5 x 10^{-4} M, in water). b) FE-SEM image of the self-assembled spherical objects of **DMV** formed in water (c = 1 x 10^{-4} M, glass substrate). c) and d) are the FE-SEM image and TEM image of the 5 x 10^{-4} M solution of **TTFS-DMV** (1:1) CT complex respectively.*

We have further investigated the structural ordering of these CT-nanostructures using PXRD. The XRD pattern of **TTFS-DMV** nanostructures exhibits a set of ordered reflections in the low angle region which signifies the long-range ordering hierarchical self-assembly of CT-amphiphile (Figure 2.1.9). Careful analysis of these ordered reflection peaks unambiguously demonstrates a lamellar ordering of CT-amphiphile in the self-assembly with d-spacing at 2.72 nm, 1.35 nm, 0.9 nm, 0.67 nm with 1: ½ : $^1/_3$ order. The powder XRD pattern shows a strong peak at $2\theta = 23.26°$ (0.38 nm) which is attributed to the π-π stacking distance between D-A aromatic core. The length of **TTFS-DMV** bilayer with non-interdigitated alkyl chain orientation is ~5.4 nm which is double

of the maximum d-spacing (2.7 nm) obtained in the PXRD pattern. This clearly indicates the lamellar packing of **TTFS-DMV** CT amphiphile in the nanoplates which is also shown in the schematic (Figure 2.1.3).
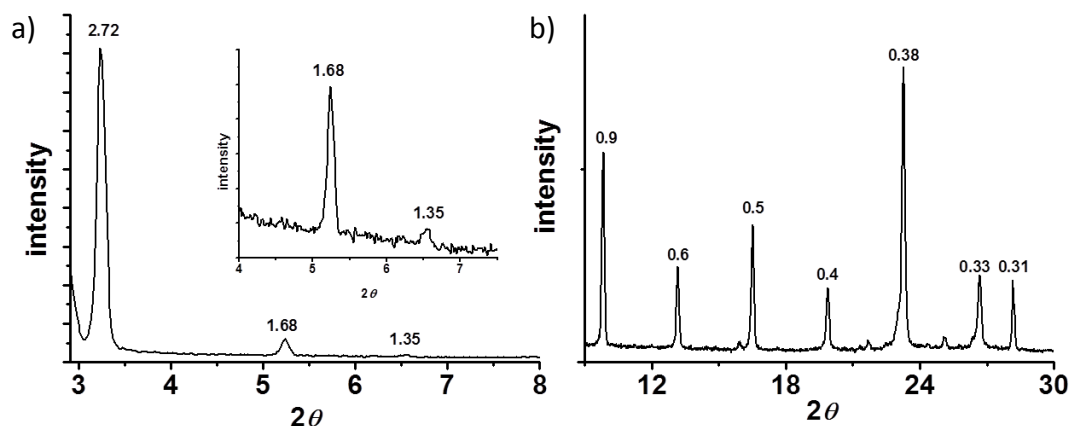
Figure 2.1.9: *a) PXRD profiles of the thin film of **TTFS-DMV** CT co-assembly, obtained by drop-casting the self-assembled solution on glass substrates. The numbers shows the d-spacing in nm. Inset a) shows the zoomed portion of the graph between the angles (2θ) 4 to 8°.*

2.1.7. Conductivity Measurement on the CT Nanostructures

To understand the charge transport properties of the MS-CT nanostructures of **TTFS**-**DMV**, two probe conductivity studies were carried out using these nanostructures as channel elements. The device was fabricated using gold electrodes with a gap of ca. 10 μm on glass substrate. The measurements were done by drop-casting aggregated solutions of the CT complex across the gold electrode which sows a non-linear *I-V* response suggesting the semiconducting behaviour of CT nanostructures (Figure 2.1.10). The estimated conductivity value is 2.32 x 10^{-6} S cm^{-1} and the calculated resistance by fitting to the linear region of the *I-V* curve passing through origin was found to be 1.248 x 10^{6} ohm.
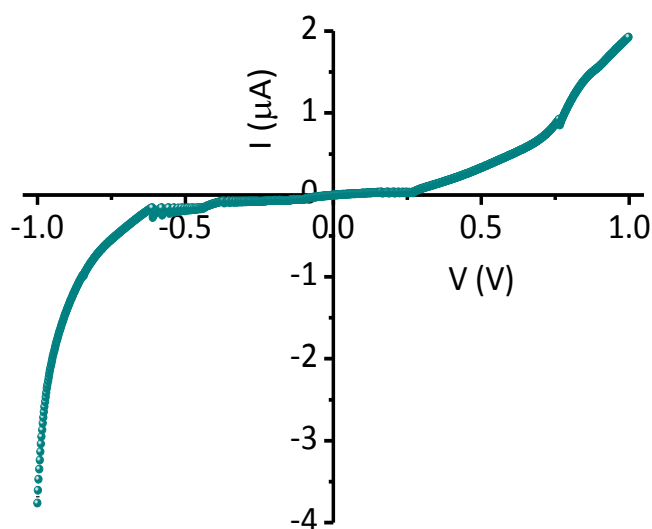
Figure 2.1.10: *I-V curve for **TTFS** and **DMV** CT nanostructures. The sample was prepared by drop-casting the CT solution on a gold-coated glass substrate followed by vacuum drying.*

2.1.8. Conclusion and Outlook

In conclusion we have shown the construction of novel mixed stack CT nanostructures from TTF and viologen derivatives through a non-covalent amphiphilic design strategy. Detailed NMR, optical and mass spectroscopic measurement suggested the formation face-to-face CT co-assembly in solution and provided insight into their self-assembly nature. This is a simple approach to make water soluble mixed-stack CT nanostructures with impressive semiconducting property. We are currently exploring the ionicity of this co-facial D-A arrays in order to evaluate their potential in organic ferroelectrics.

2.1.9. Experimental Section

General Methods

Optical Measurements:

Electronic absorption spectra were recorded on a Perkin Elmer Lambda 900 UV-Vis-NIR Spectrometer and emission spectra were recorded on Perkin Elmer Ls 55 Luminescence Spectrometer. UV-Vis and emission spectra were recorded in 5mm path length cuvette. Fluorescence spectra of solutions were recorded with 340 nm excitation wavelength.

NMR Measurements:

NMR spectra were obtained with a Bruker AVANCE 400 (400 MHz) Fourier transform NMR spectrometer with chemical shifts reported in parts per million (ppm) with respect to residual solvent peak. Titration measurements were done in D_2O.

High-Resolution Mass-Spectrometry (HR-MS):

HRMS measurements were performed with Agilent Technologies Q-TOF-LCMS system, 6538 instrument. Measurements were done in ESI mode.

Transmission Electron Microscopy (TEM):

TEM measurements were performed on a JEOL, JEM 3010 operated at 300 kV. Samples were prepared by placing a drop of the solution on carbon coated copper grids followed by drying at room temperature. The images were recorded with an operating voltage 300 kV. In order to get a better contrast samples were stained with uranyl acetate (1 wt % in water) before the measurements.

Dynamic light scattering Experiments (DLS):

The measurements were carried out using a Nano ZS (Malvern UK) employing a 532 nm laser at a back scattering angle of 173°. 10^{-3} M stock solutions of **TTFS** and **DMV** were prepared in water, which were mixed in equal amount to obtain the required solution mixture.

Conductivity measurement:

Electrical measurements were carried out using micron-sized-gap gold electrodes on glass substrate, and I–V curves were acquired by using a Keithley 236 electrometer at room temperature and in air. Electrical conductivity values were calculated by considering average thickness and area of the drop-coated film.

2.1.9a. Synthetic Procedures

Synthesis of Tetrathiafulvalene tetra-methyl carboxylate ester (2): 2 g (7.98 mmol) of dimethyl 1, 3 dithiole-2-thione-4, 5-dicarboxylate was mixed with 2 g. (12 mmol) of triethyl phosphite and 16 ml of benzene and refluxed at 85 ^{o}C for 15 h. After that benzene was removed under low pressure and added to 16 ml of ethanol to precipitate out the compound and remove the impurity. The compound was further dissolved in 10 ml of MeOH by heating and then cooled to room temperature to recrystallize the product. Yield: 38%. ^{1}H NMR (400 MHz, CDCl$_3$ TMS): δ (ppm) 3.85 (s, 12H); ^{13}C NMR (100 MHz, CDCl$_3$): δ (ppm) 159.85, 132.17, 109.92, 53.62; HRMS (ESI): m/z calcd: C$_{14}$H$_{12}$O$_8$S$_4$: 458.9415, found: 458.9131 [M+Na]$^{+}$.

Synthesis of TTF tetra carboxylate potassium salt (TTFS): 3.5 % (w/v) (100 ml) of aqueous KOH solution was added drop by drop through a pressure equaliser funnel to 0.5

g. (1.146 mmol) of tetrathiafulvalene tetra methyl carboxylate ester (**2**), taken in 100 ml ethanol. The reaction mixture was stirred for 12 hr. at 95 ^{o}C. After completion of the reaction ethanol was removed under vacuum and excess ethanol was added to remove the water completely in vacuum. The product was finally precipitated out in ethanol and dried after filtering. Yield: 84%. ^{13}C NMR (100 MHz, CDCl$_3$): δ (ppm) 167.03, 133.48, 108.23. HRMS (ESI), calculated for corresponding acid, m/z calcd: C$_{10}$H$_4$O$_8$S$_4$: 379.8789, found: 380.8842 [M+H] $^+$.

Synthesis of dodecyl methylviologen (DMV): see the reference. [12]

2.1.10. References

[1] A. S. Tayi, A. K. Shveyd, A. C.-H. Sue, J. M. Szarko, B. S. Rolczynski, D. Cao, T. J. Kennedy, A. Sarjeant, C. L. Stern, W. F. Paxton, W. Wu, S. K. Dey, A. C. Fahrenbach, J. R. Guest, H. Mohseni, L. X. Chen, K. L. Wang, J. F. Stoddart and S. I. Stupp, *Nature*, 2012, **488**, 485; S. Horiuchi and Y. Tokura, *Nature Mater.*, 2008, **7**, 357; A. Girlando, A. Painelli, C. Pecile, G. Calestani, C. Rizzoli and R. M. Metzger, *J. Chem. Phys.*, 1993, **98**, 7692; A. Jain, K.V. Rao, U. Mogera, A.A. Sagade and S.J. George, *Chem. −Eur. J.*, 2011, **17**, 12355; H. Alves, A. S. Molinari, H. Xie, A. F. Morpurgo, *Nat. Mater.,* 2008, **7**, 574; J.-Y. Wang, J. Yan, L. Ding, Y. Ma, J. Pei, *Adv. Funct. Mater.*, 2009, **19**, 1746.

[2] L. Zhu, Y. Yi, Y. Li, E. -G. Kim, V. Coropceanu and J. -L. Brédas, *J. Am. Chem. Soc.*, 2012, **134**, 2340.

[3] S. Horiuchi and Y. Tokura, *Nature Mater.*, 2008, **7**, 357; A. Girlando, A. Painelli, C. Pecile, G. Calestani, C. Rizzoli and R. M. Metzger, *J. Chem. Phys.*, 1993, **98**, 7692.

[4] F. Wudl, D. Wobschall and E. J. Hufnagel, *J. Am. Chem. Soc.,* 1972, **94**, 670; J. L. Segura and N. Marti′n, *Angew. Chem.* 2001, **113**, 1416; M. R. Bryce, *Adv. Mater.,* 1999, **11**, 11.

[5] J. M. Spruell, W. F. Paxton, J.-C. Olsen, D. Benı´tez, E. Tkatchouk, C. L. Stern, A. Trabolsi, D. C. Friedman, W. A. Goddard III and J. F. Stoddart. *J. Am. Chem. Soc.*, 2009, **131**, 11571.

[6] W. R. Dichtel, O. S. Miljani, W. Zhang, J. M. Spruell, K. Patel, I. Aprahamian, J. R. Heath and J. F. Stoddart. *Acc. Chem. Res.***,** 2008, **41**, 1750; A. R. Pease, J. O. Jeppesen, Y. Luo, C. P. Collier, J. R. Heath and J. F. Stoddert, *Acc. Chem. Res.***,** 2001, **34**, 433; K. B. Simonsen, K. Zong, R. D. Rogers and M. P. Cava*, J. Org. Chem.*, 1997, **62**, 679; D. B. Amabilino and J. F. Stoddart*, Chem. Rev.*, 1995**, 95**, 2725; C. O. D-Buchecker and J. P. Sauvage, *Chem. Rev.,* 1987, **87,** 795; L. Raehm, D. G. Hamilton and J. K. M. Sanders, *Synlett,* 2002, 1743; S. A. Vignon, T. Jarrosson, T. Iijima, H.-R. Tseng, J. K. M. Sanders and J. F. Stoddart, *J. Am. Chem. Soc.*, 2004, **126**, 9884; M. A. Olson, A. Coskun, L. Fang, A. N. Basuray and J. F. Stoddart, *Angew. Chem. Int. Ed.,* 2010**, 49**, 3151; G. Koshkakaryan, L. M. Klivansky, D. Cao, M. Snauko, S. J. Teat, J. O. Struppe and Y. Liu, *J. Am. Chem. Soc.,* 2009, **131**, 2078; H. M. Colquhoun and Z. Zhu, *Angew. Chem. Int. Ed.*, 2004, **43***,* 5040; E. A. Appel, F. Biedermann, U. Rauwald, S. T. Jones, J. M. Zayed and O. A. Scherman, *J. Am. Chem. Soc.*, 2010, **132**, 14251; D. Jiao, J. Geng, X. J. Loh, D. Das, T.-C. Lee and O. A. Scherman, *Angew. Chem. Int. Ed.,* 2012, **51**, 9633.

[7] K. B. Simonsen, K. Zong, R. D. Rogers and M. P. Cava, *J. Org. Chem.*, 1997, **62**, 679.

[8] K. V. Rao, K. Jayaramulu, T. K. Maji and S. J. George, *Angew. Chem. Int. Ed.,* 2010, **49**, 4218 .

[9] A. A. Sagade, K. V. Rao, U. Mogera, S. J. George, A. Datta and G. U. Kulkarni, *Adv. Mater.,* 2013, 25, 559.

[10] J. B. Torrance, J. E. Vazquez, J. J. Mayerle, and V. Y. Lee, *Phys. Rev. Lett.,* 1981, **46**, 253.

[11] M. F. Pepitone, G. G. Jernigan, J. S. Melinge and O.-K. Kim, *Org. Lett.,* 2007, **9**, 801

[12] M. R. Bryce, *Adv. Mater.,* 1999, **11**, 11

CHAPTER-2, Part-2

Alternate Tetrathiafulvalene-Naphthalene Diimide D-A Arrays by an Amphiphilic Co-Assembly

Abstract

*One-dimensional (1-D) mixed stack charge transfer (CT) nanostructures, composed of alkyl tetrathiafulvalene dicarboxylate dipotassium salt derivatives (**dbTTFS/Ch-dbTTFS**) and unsymmetrical, dodecyl substituted naphthalene diimide (**NDI-Cat**) amphiphiles were constructed via non-covalent co-assembly process. Detailed spectroscopic measurements revealed efficient co-facial assembly between donor (D, **dbTTFS/ Ch-dbTTFS**) and acceptor (A, **NDI-Cat**) amphiphiles to form 1:1 superamphiphiles. NMR spectroscopy measurements provided insights into the face to face orientation of the D and A molecules in their co-assembly. This efficient D-A CT co-assembly resulted in strong red shifted CT absorption in the near infra-red (NIR, 825 nm) region. Furthermore, two probe electrical measurements on these CT-nanostructures showed that they are semiconducting in nature and can further be useful for supramolecular electronics.*
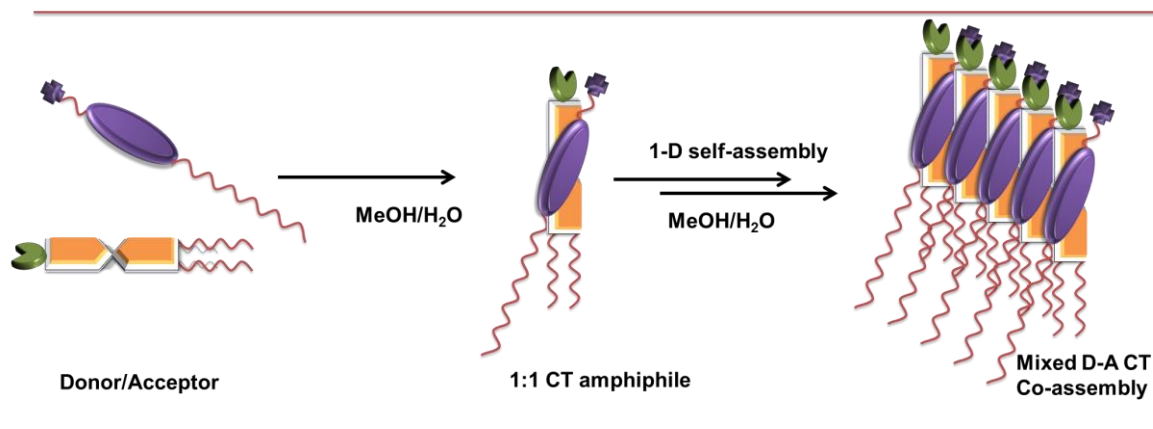
2.2.1. Introduction

Mixed-stack assemblies of electron D and A aromatic molecules formed via charge transfer interactions have attracted much attention in recent years owing to their interesting optoelectronic and ferroelectric properties.[1] In this context 1D stacks of mixed CT complex from the co-assembly of D and A molecules are important because of their highly conducting nature through inherent doping and therefore finds potential application in nanoelectronics.[2] Mixed CT crystals have been well-studied and proposed as potential candidates for ferroelectric applications because of their highly ordered long range orientation of CT dipole and characteristic neutral to ionic phase transition in the CT complex.[3] Tokura and co-workers have shown remarkable ferroelectric property in mixed CT system based on TTF (D) and *p*-chloranil and *p*-bromanil (A), but with ferroelectric curie temperature (T$_c$) well below the ambient temperature.[4]
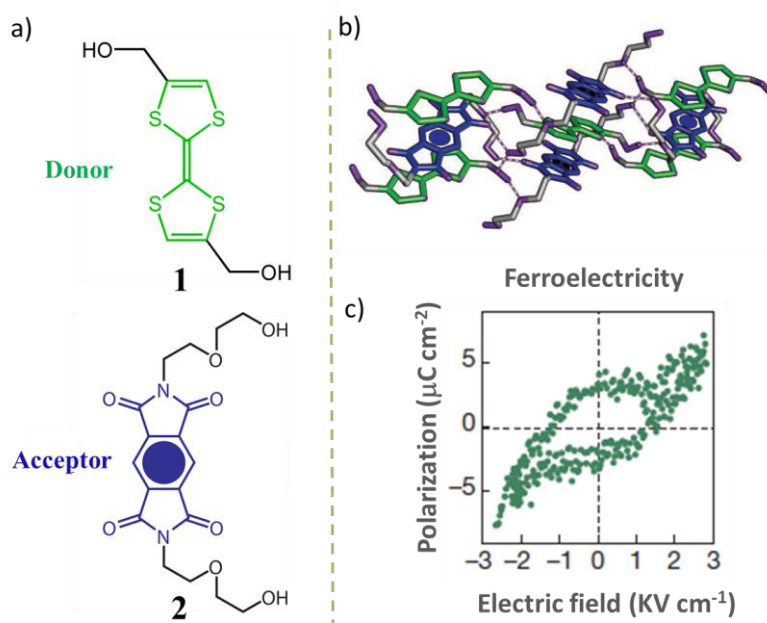

Figure 2.2.1: *a) Molecular structures of TTF donor (**1**) and* pyromellitic diimide *acceptor (**2**). b) Shows the molecular organization in the CT co-crystal. c) Room temperature ferroelectricity exhibited by **1-2** CT co-crystal.*

Recently Stupp *et al*. have come up with an elegant design of mixed stack CT crystals having ferroelectric polarisation switching at room temperature.[5] The mixed CT crystals were formed using TTF (**1**), naphthalene and pyrene as donors and pyromellitic diimide (**2**) as acceptor. Figure 2.2.1 depicts the CT co-crystal formation between TTF-pyromellitic diimide based D-A pair. In this chapter we plan to make the supramolecular analogues of CT co-crystals with higher ionicity. We have selected tetrathiafulvalene molecule as the donor and naphthalene diimide as the acceptor to achieve the same. In literature, individually tetrathiafulvalenes and naphthalene diimides are well known to form various rotaxanes and catenanes but their CT complex and corresponding macromolecular assemblies in solution are not known.[6] Although, D. Zhang and co-workers have also done research on metal induced electron transfer process in covalently linked TTF-NDI D-A systems, their CT nanostructures in solution are not yet reported.[7]

In order to construct TTF-NDI based CT nanostructures, we have adopted an amphiphilic design strategy. We have designed TTF and NDI amphiphilic derivatives and attempted their co-assembly in polar solvents (Figure 2.2.2).

2.2.2. Design and Molecular Structure
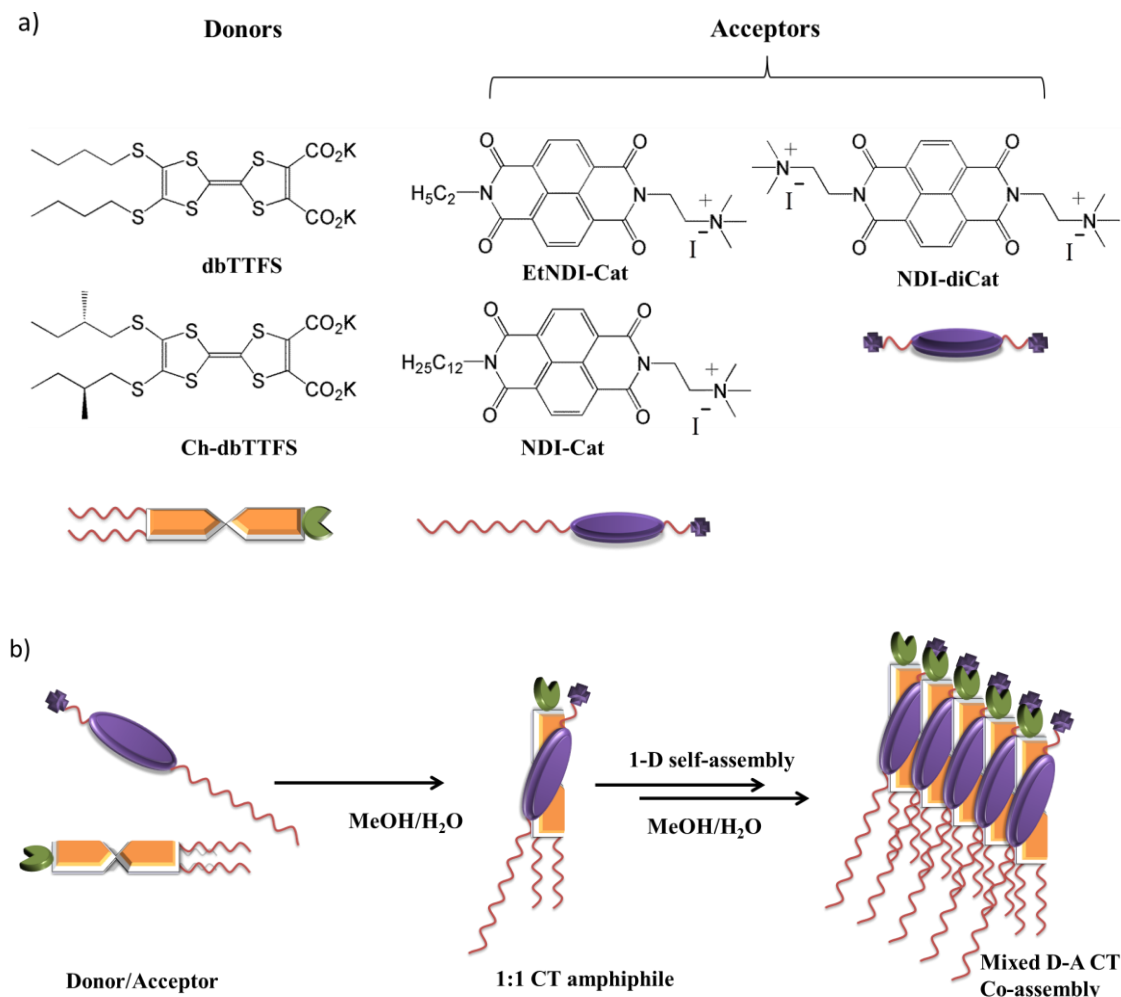
Figure 2.2.2: *a) Molecular structures of TTF (D) and NDI (A) derivatives used in this chapter. b) Amphiphilic design strategy for mixed donor-acceptor (D-A) supramolecular assemblies.*

In this study we have designed and synthesised water soluble amphiphilic tetrathiafulvalene donor, **dbTTFS** and its chiral analogue, **Ch-dbTTFS** decorated with butyl or (S)-2-methyl butyl chains on one side and polar carboxylate anionic group on the other side which imparts the amphiphilic nature to the donor. As an acceptor counterpart we have synthesised **NDI-Cat**, with an unsymmetrical amphiphilic structure containing a

trimethyl ammonium group at one end, and a long hydrophobic alkyl chain on the other end which can form a non-covalent amphiphilic pair with donor molecules, possibly through synergistic CT, π-π and electrostatic interactions (Figure 2.2.2). **EtNDI-cat** and **NDI-diCat** were used as model compounds for NMR measurement as those are well-soluble in water. **Ch-dbTTFS** was synthesised to see the effect of chiral nature of the donor onto the aggregation behaviour of the CT amphiphiles. However, they failed to induce any chiroptical property upon CT co-assembly.

2.2.3. Synthetic Schemes for TTF and NDI Amphiphiles

The synthesis of donors **dbTTFS**, **Ch-dbTTFS** and the acceptor **EtNDI-Cat** are shown in Scheme 2.2.1 and Scheme 2.2.2 respectively.
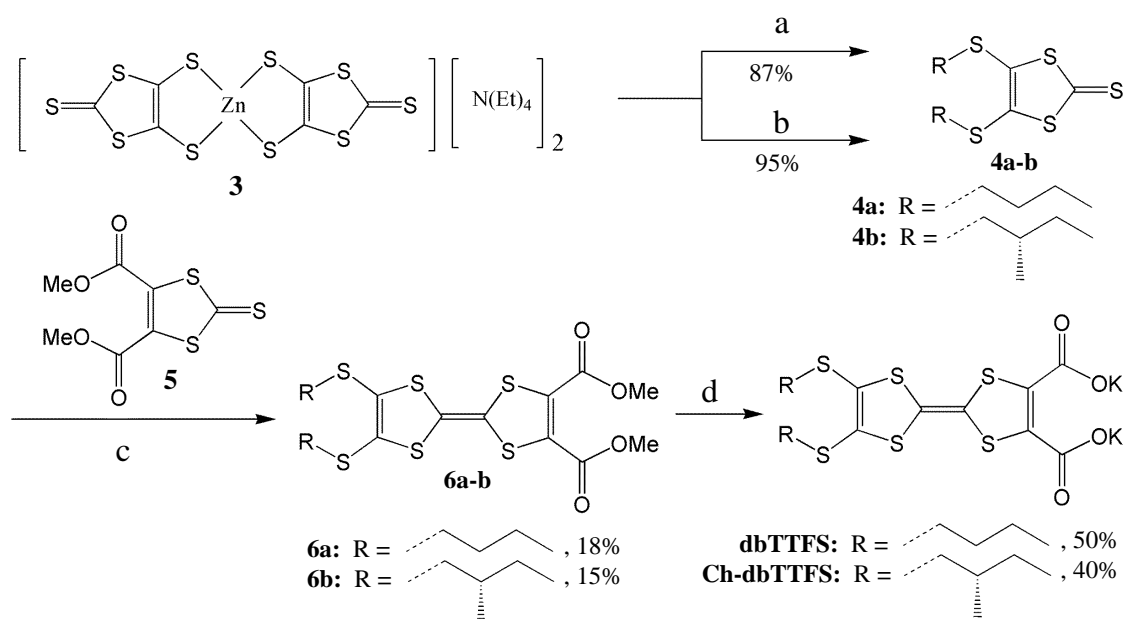
Scheme 2.2.1: *Synthesis of dbTTFS: a) Butyl bromide, CH₃CN, reflux, Ar, 90 °C, 4 h. b) (S)-2-methyl butyl bromide, CH₃CN, reflux, Ar, 55 °C, 24 h. c) P(OEt)₃, p-xylene, reflux, 120 °C, 5 h. d) 3.5% aq KOH, EtOH, reflux, 95 °C, 12 h.*
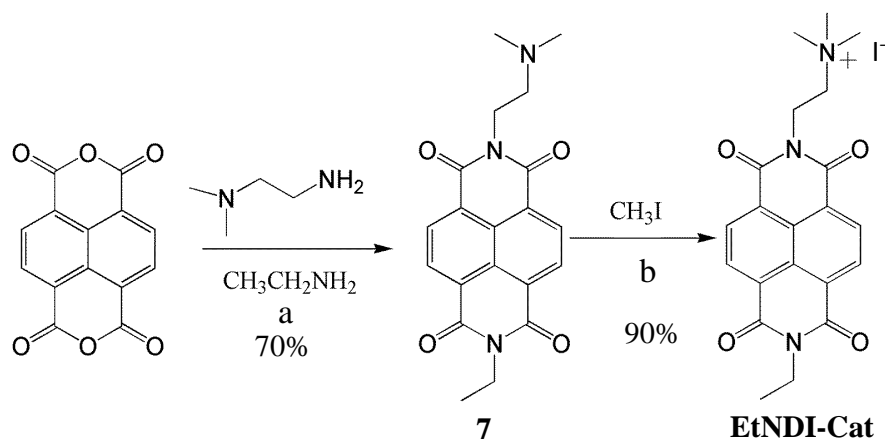
Scheme 2.2.2: *Synthesis of **EtNDI-Cat**: a) Isopropanol, 80 °C, reflux, Ar, 12 h; b) Toluene, 80 °C, 4 h.*

NDI-Cat and **NDI-diCat** acceptors were synthesised according to literature procedure.[8,9]

2.2.4. CT Co-Assembly in Solution

The aggregation behaviour of the individual molecules were studied in detail by optical spectroscopic measurements. The donor **dbTTFS** and **Ch-dbTTFS** self-assemble in water-methanol (30:70 v/v) mixture at 5 x 10^{-4} M concentration (as evident from the dynamic light scattering studies, Figure 2.2.24) (*vide infra*). The acceptor **NDI-cat** is molecularly dissolved in methanol whereas the addition of increasing amount of water (bad solvent) renders a surfactant like self-assembly because of its amphiphilic nature. Accordingly the self-assembly behaviour of **NDI-Cat** was first probed by UV-Vis spectroscopic study in water-methanol solvent mixture where the absorption spectra of **NDI-cat** showed significant changes consistent with the aggregates formation in higher water percentage (Figure 2.2.3). The addition of increasing amount of water (20-100%) to a molecularly dissolved solution of **NDI-Cat** at 10^{-4} M concentration leads to the broadening of the absorption band with a red shift of 6 nm in 100% water, suggesting the formation of J-aggregates in solution.
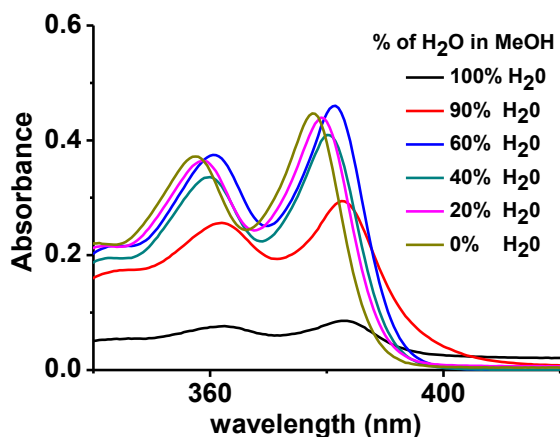
Figure 2.2.3: *Solvent dependent UV-Vis spectra of* **NDI-Cat** *(c = 10^{-4}M) in varying percentage of MeOH in water.*
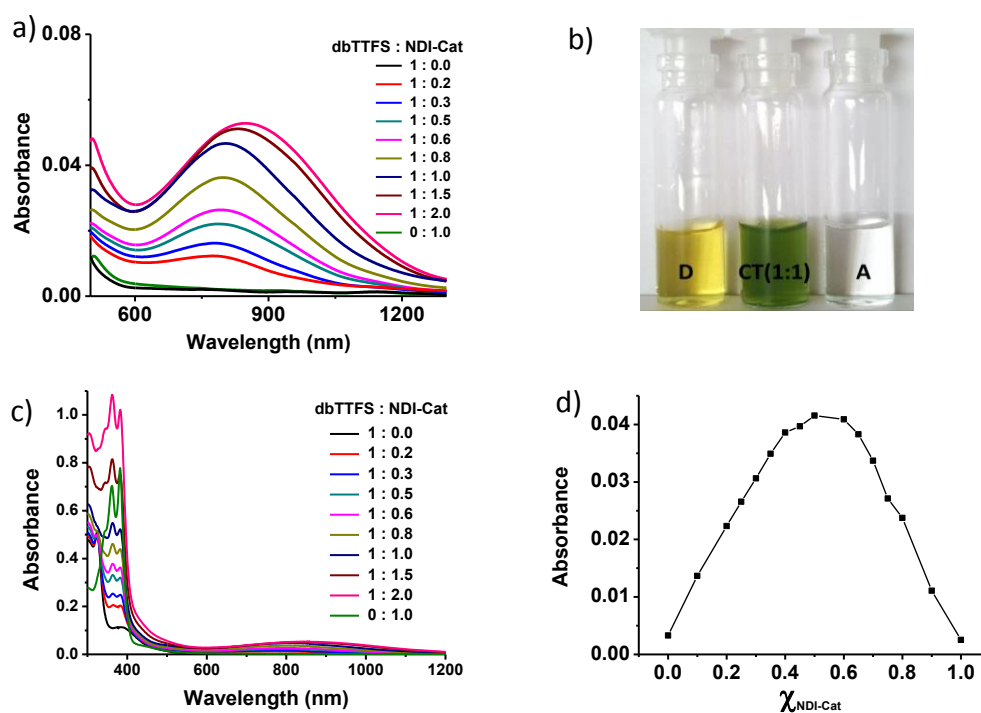
Figure 2.2.4: *a) UV-Vis-NIR titration of* **dbTTFS** *and* **NDI-Cat** *CT complex at 5 x 10^{-4} M concentration in 30% methanol containing water (v/v). b) Shows the colour change upon 1:1 CT formation. D =* **dbTTFS**, *A =* **NDI-Cat** *and their 1:1 CT co-assembly (green solution in the middle). c) Full spectra of UV-Vis-NIR spectroscopic titration of* **dbTTFS** *and* **NDI-Cat** *CT at 5 x 10^{-4} M concentration in 30% MeOH in H_2O, showing the reversal of relative intensity of vibronic bands of* **NDI-Cat.** *d) Job plot for* **dbTTFS** *and* **NDI-Cat** *CT pair at 5 x 10^{-4} M concentration.*

Figure 2.2.5: *UV-Vis-NIR spectra corresponding to **dbTTFS**, oxidised with Cu(ClO$_4$)$_2$ and 1:1 CT band of **dbTTFS** + **NDI-Cat** pair (c = 5 x 10^{-4} M, 30% MeOH in H$_2$O).*

The D-A mixture for optical study was prepared by injecting the molecularly dissolved solution of **NDI-Cat** (in methanol) to a solution of **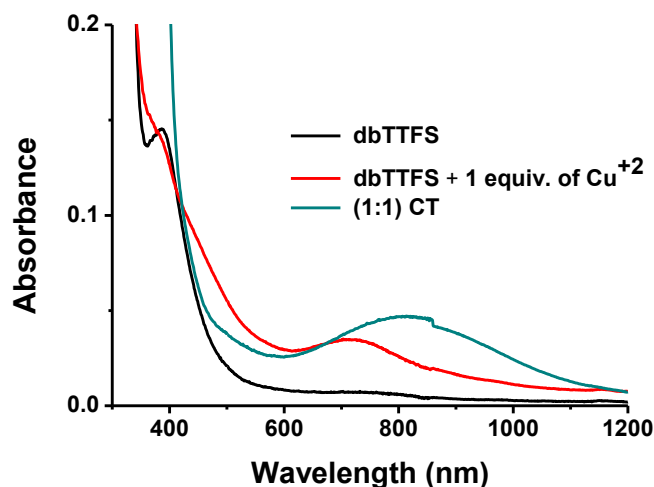dbTTFS** in methanol-water mixture in appropriate ratio. The UV-Vis-NIR spectrum of the 1:1 mixture (5 x 10^{-4} M) of **dbTTFS** and **NDI-Cat** in 30% methanol in water (v/v) showed the appearance of a new broad absorption band in the NIR region centred at 825 nm corresponding to the CT interaction between D-A pair (*vide infra*).[7] UV spectroscopic titration of **dbTTFS** and **NDI-Cat** CT pair at 5 x 10^{-4} M concentration suggest the 1:1 stoichiometry (Figure 2.2.4a) which is also evident from Job plot of **dbTTFS** and **NDI-Ca**t CT pair (Figure 2.2.4d). Formation of CT co-assembly can also be visualised by the dramatic colour change upon mixing the corresponding D and A pair in 1:1 ratio in the same solvent system (Figure 2.2.4b). The reversal of relative intensity of the vibronic bands of **NDI-Cat** with its increasing equivalents with respect to **dbTTFS** in the UV titration experiment suggests a ground state inter-chromophoric interaction (Figure 2.2.4c). Further to prove that the band at λ_{max} = 850 nm is the CT band and not related to any TTF radical ion band, we have performed oxidation of **dbTTFS** with copper perchlorate which

indicates that the resulting TTF-radical cation band does not match with the CT band (Figure 2.2.5).[10]

The chiral donor molecule **Ch-dbTTFS** also forms strong CT complex with **NDI-Cat** and shows similar spectroscopic features (Figure 2.2.6). The plot of absorbance vs. equivalent of **NDI-Cat** for the UV-Vis-NIR spectroscopic titration of **Ch-dbTTFS** with **NDI-Cat** clearly shows saturation at one equivalent of **NDI-Cat** which is also evident in the Job plot (Figure 2.2.6d). Interestingly the high resolution ESI-MS (HRMS) spectra of **dbTTFS + NDI-Cat** 1:1 CT pair show the m/z: 1038.1548 mass, corresponding to 1:1 CT pair which suggest the strong 1:1 D-A binding behaviour (Figure 2.2.7).
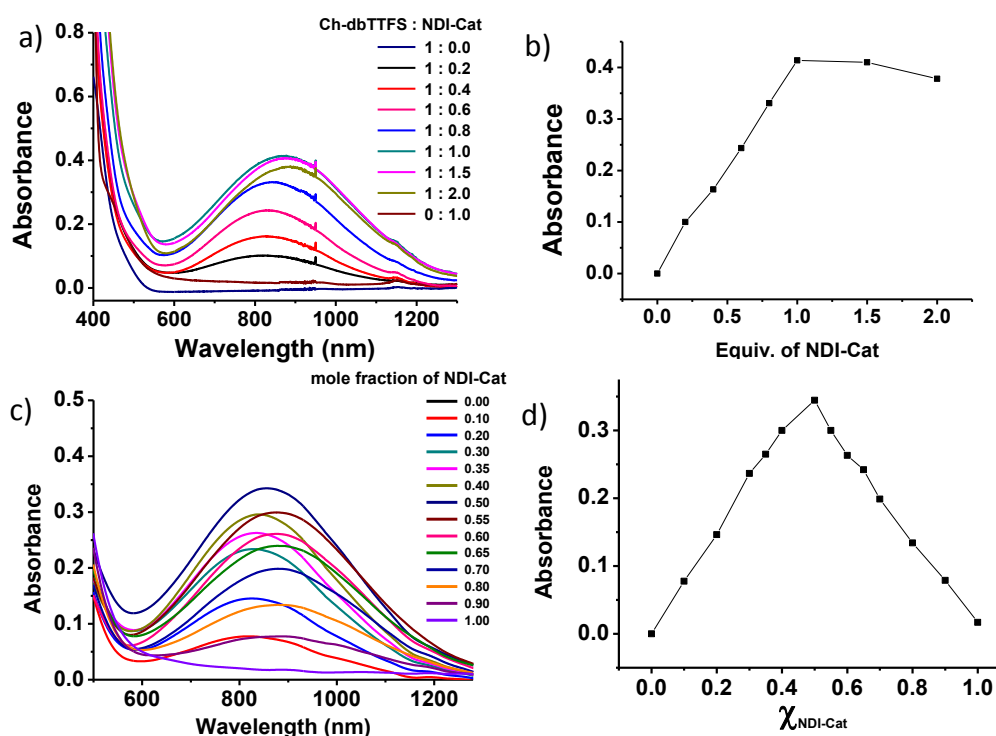
Figure 2.2.6: *a) UV-Vis-NIR titration of **Ch-dbTTFS** and **NDI-Cat** CT complex at 5 x 10^{-4} M concentration in 30% methanol containing water (v/v) b) shows the plot of absorbance vs. equivalent of **NDI-Cat** for UV-Vis-NIR titration of **Ch-dbTTFS** and **NDI-Cat**. c) Job method of titration for **Ch-dbTTFS** and **NDI-Cat** CT complex at 5 x 10^{-4} M concentration in 30% MeOH in H_2O and d) corresponding Job plot.*
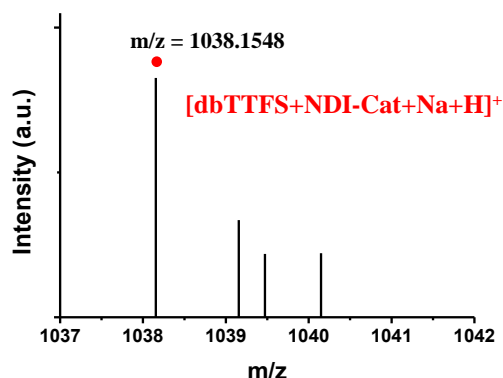
Figure 2.2.7: *The high resolution ESI-MS spectra of **dbTTFS** + **NDI-Cat** 1:1 CT pair.*

NDI-Cat, being hydrophobically modified with long alkyl substituent, tends to self-assemble in solution, which would hamper detailed NMR measurements. Therefore to get a better insight into the CT co-assembly process, we have synthesised **EtNDI-Cat** and **NDI-diCat** as model compounds which are soluble in water as expected because of their short alkyl chains. However both the molecules have strong CT co-assembly with **dbTTFS** molecule. This is evident from the strong CT band at $\lambda_{max} = 800$ nm when co-assembled with 1 equivalent of **dbTTFS** similar to **NDI-Cat** (Figure 2.2.8a-b), suggesting that they can be used as suitable model compounds for **NDI-Cat**.
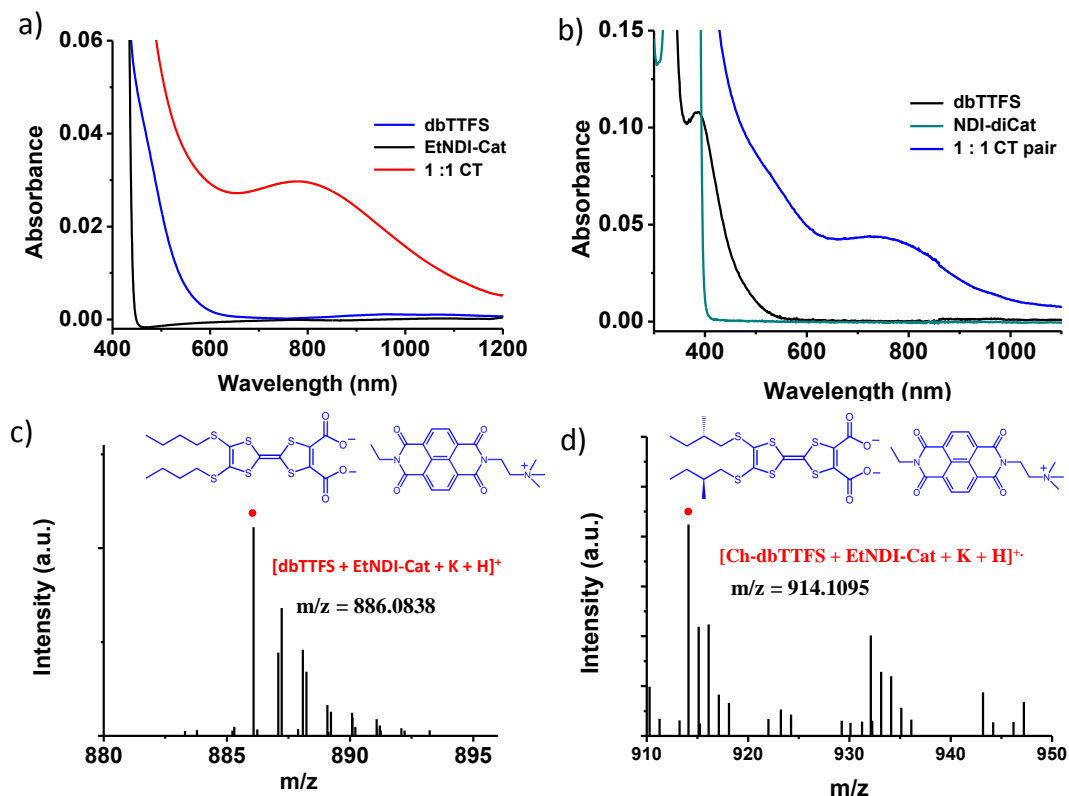
Figure 2.2.8: *a) and b) corresponds to the absorption spectra of **dbTTFS + EtNDI-Cat** and **dbTTFS + NDI-diCat** 1:1 CT pair respectively along with the individual D and A in H_2O at 5 x 10^{-4} M concentration. c) and d) are the high resolution ESI-MS spectra of 1:1 CT complex for **dbTTFS + EtNDI-Cat** and **Ch-dbTTFS + EtNDI-Cat** along with their molecular structures.*

The high resolution ESI-MS spectra of both **dbTTFS** and **Ch-dbTTFS** with **EtNDI-Cat** in their CT co-assembly state in water also showed the mass corresponding to their 1:1 CT pair, which clearly proved their stoichiometry and their co-assembly in solution (Figure 2.2.8c-d).

To further investigate the binding behaviour of D and A chromophore in their co-assembly, we made 1:1 CT co-crystals for **dbTTFS + NDI-Cat** as well as **Ch-dbTTFS + NDI-Cat** co-assembly. However they showed poor X-ray diffraction pattern and hence

resolving the crystal structure was unsuccessful. Hence we have studied detailed ^{1}H NMR spectroscopy to determine the D-A organisation in their co-assembly (*vide infra*).

UV titration and Job plot experiment showed that at higher equivalents of NDI (beyond 1 equiv.) a red shift in the CT band maxima was observed suggesting the formation of higher stoichiometry which will be discussed later in the chapter. This is evident from the plot of λ_{max} versus the equivalent of **NDI-Cat** and mole fraction of **NDI-Cat** from UV-titration and Job method of titration, respectively.
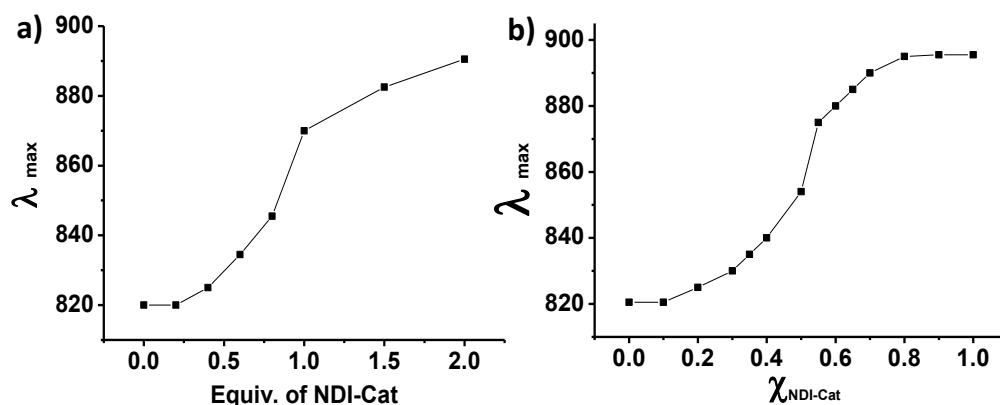
Figure 2.2.9: *a) λ_{max} vs. equivalent of NDI-Cat plot for UV-titration of Ch-dbTTFS/NDI-Cat CT pair. b) λ_{max} vs. mole fraction of NDI-cat plot for Job method titration of the same CT pair.*

These graphs shows an abrupt change in the λ_{max} at one equivalent of **NDI-cat** (Figure 2.2.9a) indicating different types of packing behaviour. Similar abrupt change in λ_{max} is visible in Figure 2.2.9b, above 0.5 mole fraction of NDI.

2.2.5. NMR probing of Co-facial Organisation in the CT states

^{1}H NMR spectroscopy was used to get a deeper insight into the molecular organisation of TTF and NDI in their CT-complex state. Since ^{1}H NMR spectra of 1:1 co-assembly of **dbTTFS** and **NDI-Cat** failed to show any signal probably because of aggregation in 30% MeOH containing water, we have used **EtNDI-Cat** and **NDI-diCat** as

model donor compounds which are soluble in water. As there is no aromatic proton in the TTF core, we have probed the NDI aromatic protons for the NMR measurements.

The ^{1}H NMR spectra of **dbTTFS** and **EtNDI-Cat** CT co-assembly in D$_2$O (5 x 10^{-3} M) with 1:1 composition showed strong up-field shift of NDI aromatic protons which indicates the strong π-electron cloud shielding by TTF aromatic core suggesting the face to face organization of **dbTTFS** and **EtNDI-Cat** in their co-assembly (Figure 2.2.10). Additionally, the broad doublet, corresponding to the four NDI aromatic hydrogens, further splitted into two sets of doublet of doublet in their CT co-assembly. This further indicates the unsymmetrical face-to-face organization resulting from the unsymmetrically structured TTF and NDI chromophores in which all four protons are experiencing different chemical environments. Inset of Figure 2.2.10, shows the proposed co-facial organisation of CT pair. According to the proposed structure in Figure 2.2.10, H$_a$ and H$_c$ protons are closer to carbonyl and sulphur groups of **dbTTFS,** respectively which causes a deshielding effect and thereby the two doublets which are merged partially to give a triplet, stays in the downfield region (δ = 8.55) of the NMR spectra (Figure 2.2.10). On the other hand the H$_b$ and H$_d$ protons are far away from the TTF carbonyl groups and thus experiences the strong shielding effect from TTF π-conjugated core compared to that of H$_a$ and H$_b$ protons and hence shifted up field (δ = 8.6 ppm to δ = 7.95 ppm) in the NMR spectra.
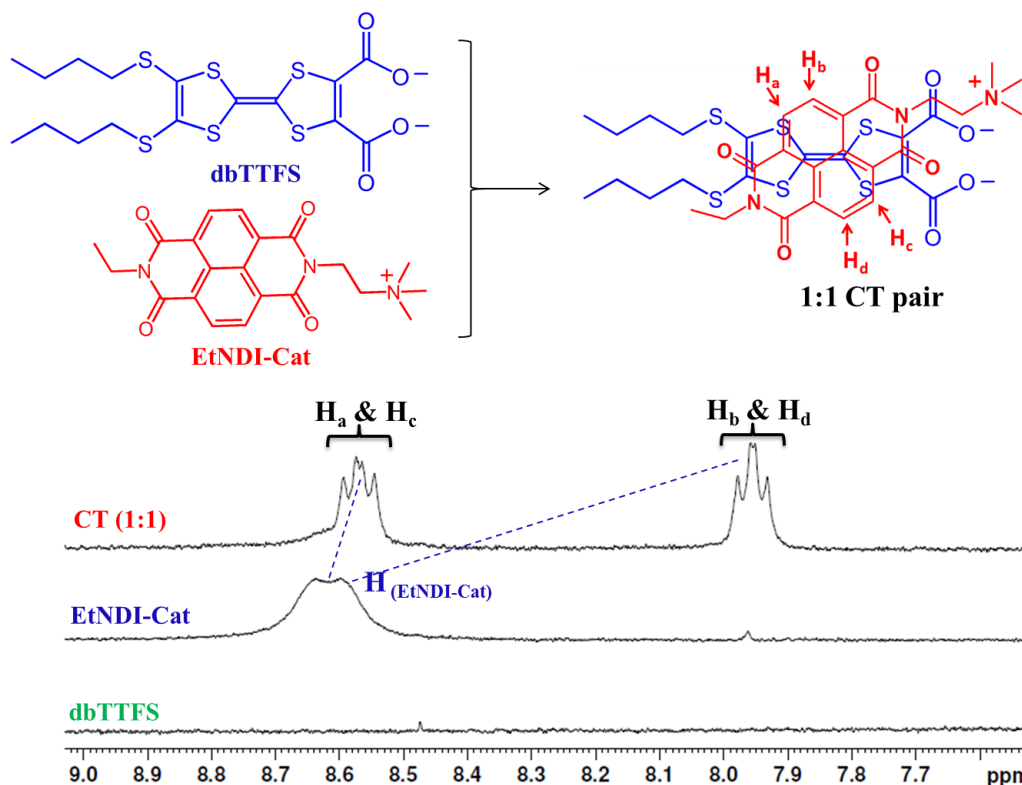
Figure 2.2.10: *^{1}H NMR spectra of **dbTTFS** and **EtNDI-Cat** CT pair (showing the aromatic region) at 5 x 10^{-3} M concentration (400 MHZ, D_2O). Inset shows proposed molecular structure of face-to-face stacking orientation of **dbTTFS** and **EtNDI-Cat** in their 1:1 MS-CT pair.*

Apart from the aromatic region, a significant amount of upfield shift was observed for remaining protons of the **EtNDI-Cat** which are shown in Figure 2.2.11. The free **EtNDI-Cat** should have three triplets in the alkyl region corresponding to two N-CH$_2$ groups on the cationic side and one CH$_3$ group in the ethyl side chain. Apart from this there should be a quartet corresponding to N-CH$_2$ group of ethyl side chain and one singlet corresponding to the $^+N(CH_3)_3$ protons. In free **EtNDI-Cat,** the triplet of the $^+NCH_2$ proton (marked as triangle) adjacent to trimethyl ammonium group, merged with the water peak at $\delta = 4.79$ ppm in the ^{1}H NMR spectra, hence not visible in the spectra, but it shifts to the upfield region ($\delta = 4.79$ ppm to $\delta = 3.95$ ppm) after binding with

dbTTFS which is attributed to a change in the chemical environment in the CT co-assembly. The remaining two triplets (marked as circle and star) and one singlet (marked as square) also shifts upfield because of the strong co-facial organisation of the D and A in the CT complex (Figure 2.2.11).
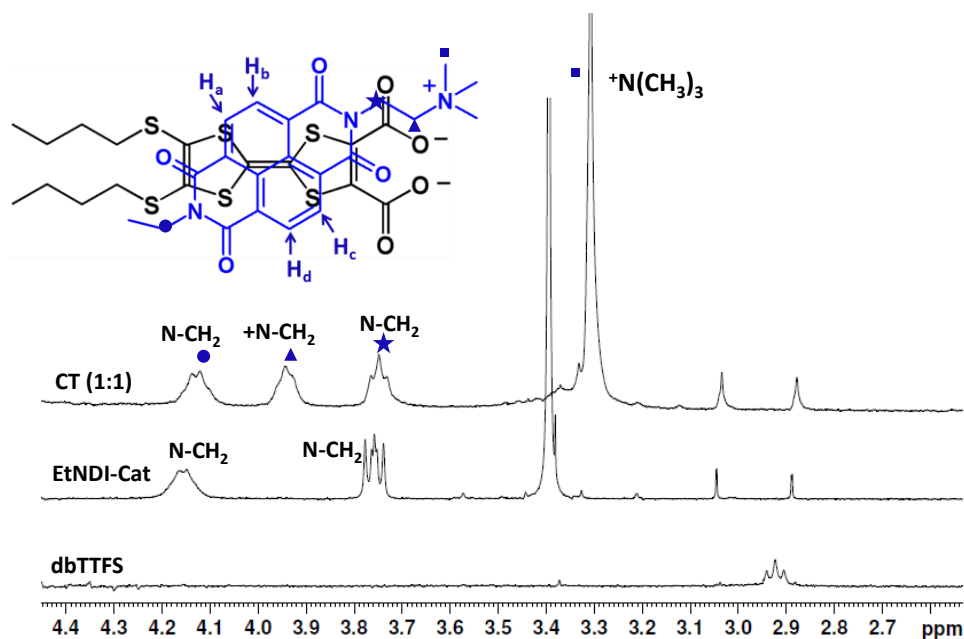
Figure 2.2.11: *Partial ^1H NMR spectra of **dbTTFS** and **EtNDI-Cat** 1:1 CT pair (showing the alkyl region) at 5 x 10^{-3} M concentration (400 MHZ, D$_2$O).*

A decisive proof of face-to-face binding of **dbTTFS** and **EtNDI-Cat** D-A pair in their co-assembly comes from the ^{13}C NMR data which is further supported by Heteronuclear single quantum coherence spectroscopy (HMQC) and Heteronuclear Multiple Bond Correlation spectroscopy (HMBC) NMR measurements. Here we have observed four types of NDI aromatic carbons attached with H$_a$, H$_b$, H$_c$ and H$_d$ protons which are denoted as c$_a$, c$_b$, c$_c$ and c$_d$ respectively (Figure 2.2.12 and 2.2.13). The carbons c$_a$, c$_c$ (δ = 132.56 ppm and 131.40 ppm, respectively) corresponds to the protons H$_a$ and H$_c$ (δ = 8.75 ppm to 8.70 ppm respectively) which was assigned from the ^1H vs. ^{13}C signal

correlation in the HMQC spectra (Figure 2.2.15). It further shows that the carbons c_b, c_d corresponds to the protons H_b and H_d (δ = 8.15 to 8.05 ppm). In the ^{13}C spectra c_a and c_c comes as two separate signals as they face different chemical environment in the co-assembly (Figure 2.2.12), on the other hand c_b and c_d are merged together being in the similar environment and also far from the TTF carbonyls (the observed upfield shift is because of π-electron cloud shielding from TTF core).

The offset binding of the **EtNDI-Cat** onto **dbTTFS** was further proved by the splitting pattern, observed in case of carbonyl carbons of **EtNDI-Cat** which is also supported by the HMBC NMR data of the the 1:1 CT co-assembly. The four carbonyl groups of the **EtNDI-Cat** are numbered in the ^{13}C spectra as well as in the proposed structure (Figure 2.2.12, 2.2.13). Here we observed two sets of carbon signal, one at δ = 175.41 ppm and 171.80 ppm and another one at δ = 144.88 ppm and 140.02 ppm. It was observed that the C=O (2, 4) drastically shifted upfield from its normal position δ = 161.5 ppm (in the free state) as it directly face the double bond of the **dbTTFS** (shown in the proposed structure) thereby experience a huge π-electron cloud shielding compared to C=O (1, 3) carbons. Further, the correlation of carbon signals corresponding to C=O (2, 4) with H_a and H_c protons signal in the HMBC spectra suggests that c_a is adjacent to C=O (4) and c_c is adjacent to C=O (2), which justifies well the proposed orientation of D-A binding (Figure 2.2.16).
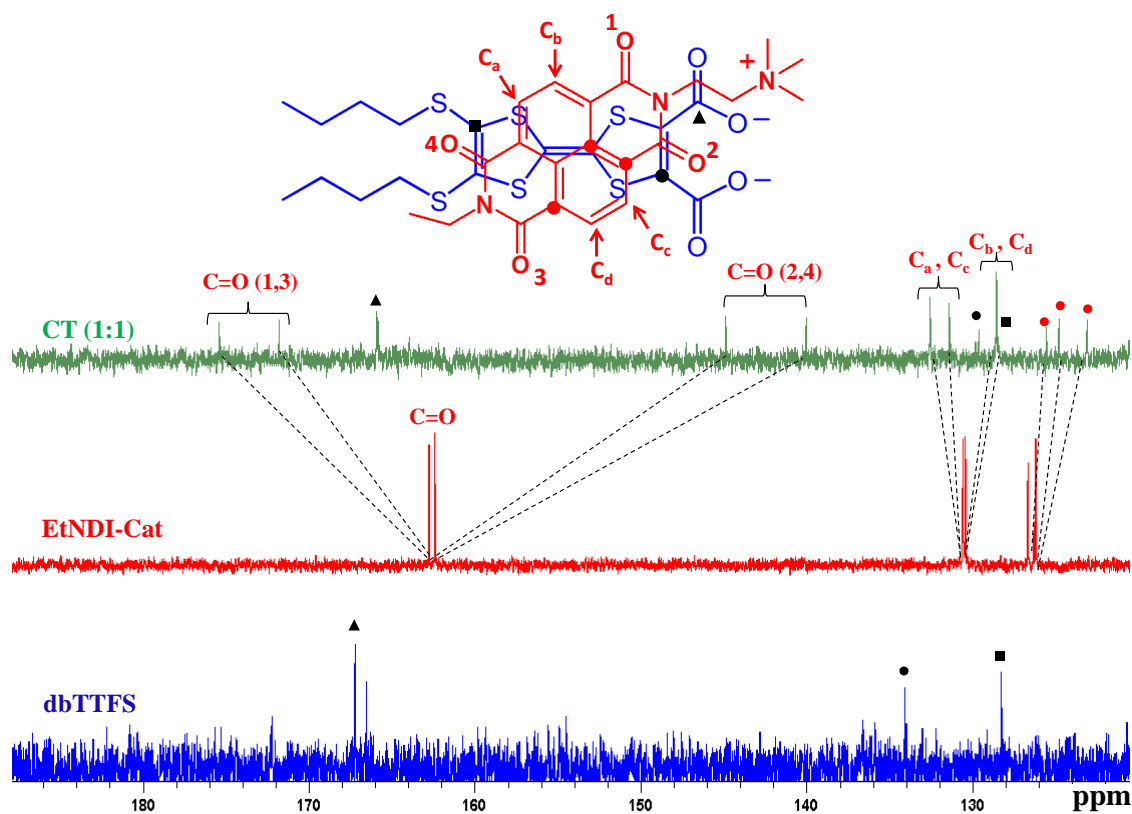
Figure 2.2.12: *Partial ^{13}C NMR spectra of **dbTTFS**, **EtNDI-Cat** and their 1:1 mixture in 20% CD_3CN in D_2O (100 MHZ, c = 1.2 x 10^{-2} M). Inset shows the proposed structure of binding.*
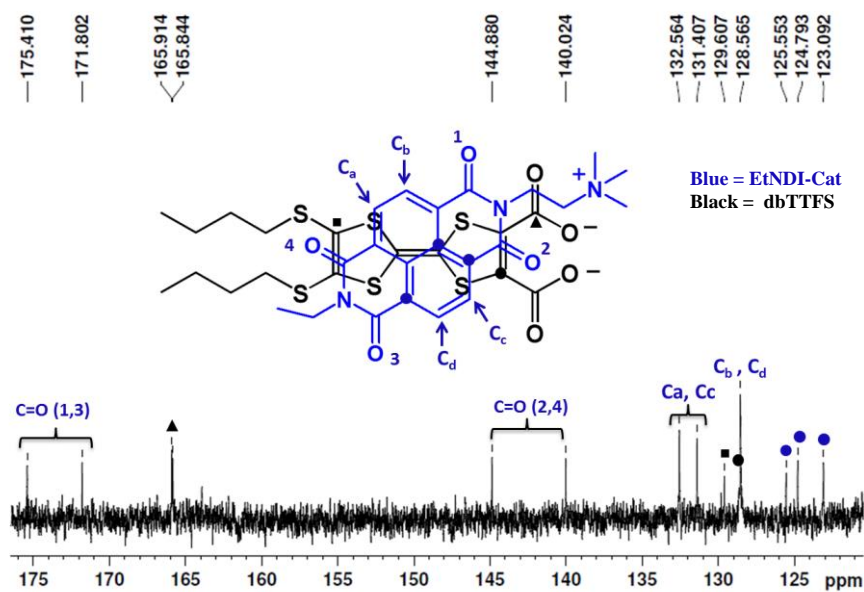
Figure 2.2.13: *Partial ^{13}C NMR spectra of **dbTTFS** and **EtNDI-Cat** CT pair (showing the aromatic region) at 1.2 x 10^{-2} M concentration (100 MHZ, 20% CD_3CN in D_2O).*
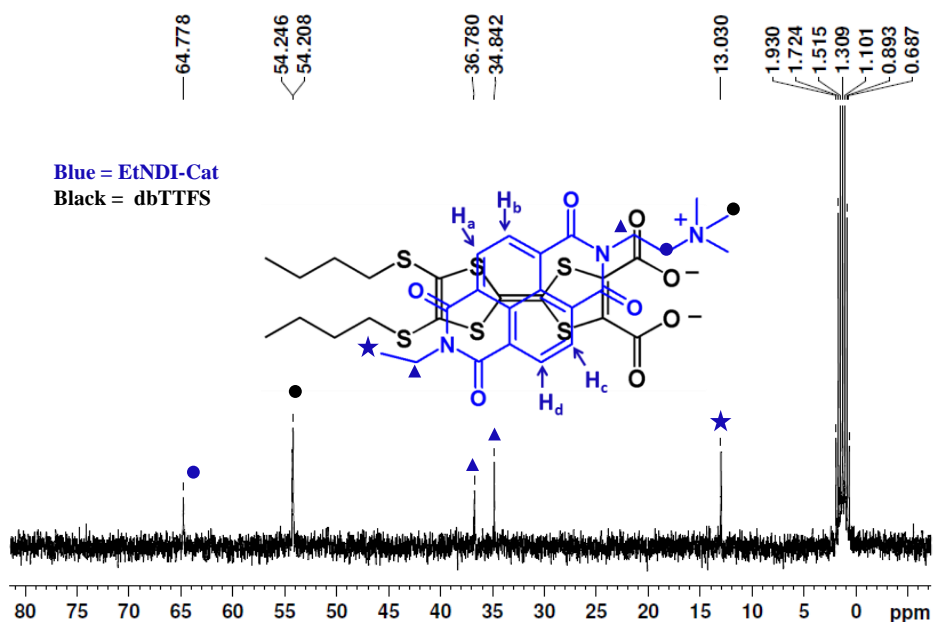
Figure 2.2.14: *Partial ^{13}C NMR spectra of **dbTTFS** and **EtNDI-Cat** CT pair (showing the alkyl region) at 1.2 x 10^{-2} M concentration (100 MHZ, 20% CD$_3$CN in D$_2$O).*
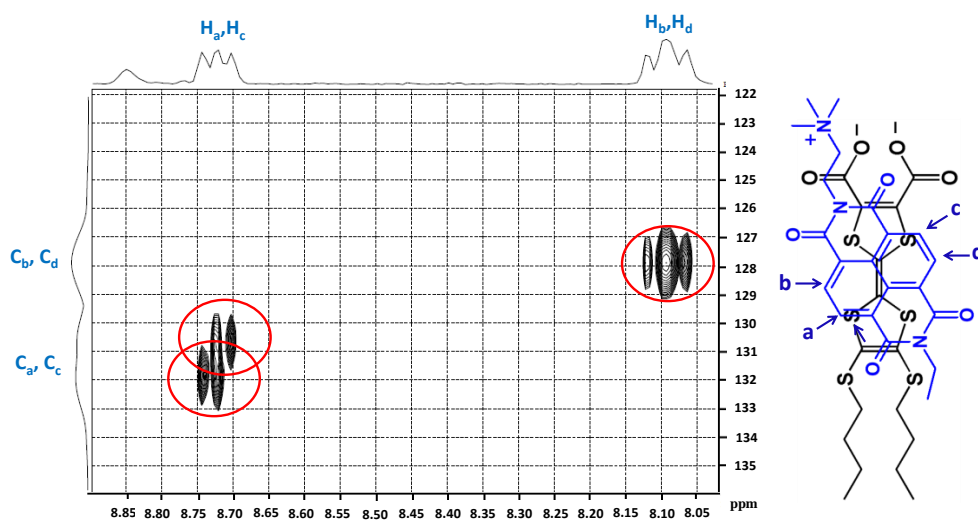
Figure 2.2.15: *HMQC spectra of **dbTTFS/NDI-Cat** CT complex at 1.2 x 10^{-2} M concentration (400 MHZ, 20% CD$_3$CN in D$_2$O).*
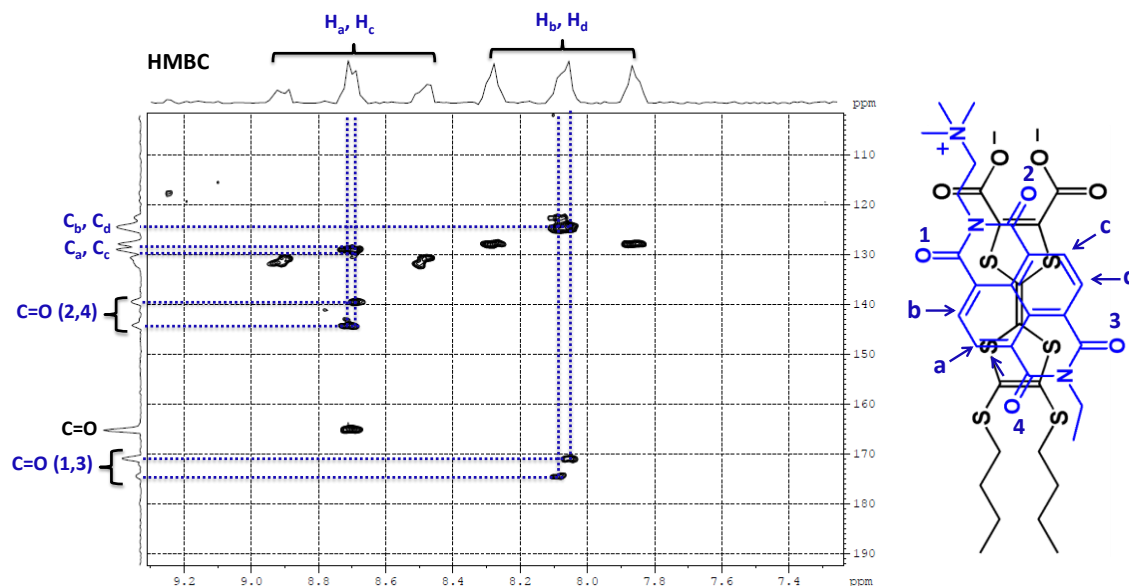
Figure 2.2.16: *HMBC spectra of **dbTTFS/NDI-Cat** CT complex at 1.2 x 10^{-2} M concentration (400 MHZ with respect to ^1H nuclei, 20% CD_3CN in D_2O).*

We have further performed the NMR measurements on **dbTTFS** and **NDI-diCat** CT co-assembly. Interestingly this D-A pair forms even stronger CT complex than **dbTTFS** and **EtNDI-Cat** CT pair which immediately precipitates in water after mixing corresponding D and A molecules. The precipitate does not go back to solution even after heating at high temperature. However d**bTTFS** and **NDI-diCat** form a stable 1:1 CT complex in 22% acetonitrile in water. The ^1H NMR spectroscopy shows a clear splitting of the singlet corresponding to four NDI aromatic hydrogens into four doublets in the same manner as described earlier which proves that it indeed forms 1:1 face to face D-A complex (Figure 2.2.17a). The high resolution mass spectrometry (HRMS) of this CT co-assembly solution shows a strong peak at m/z 905.1823 corresponding to [**dbTTFS +NDI-diCat + H**]^+ ion confirming strong 1:1 CT co-assembly (Figure 2.2.17b).
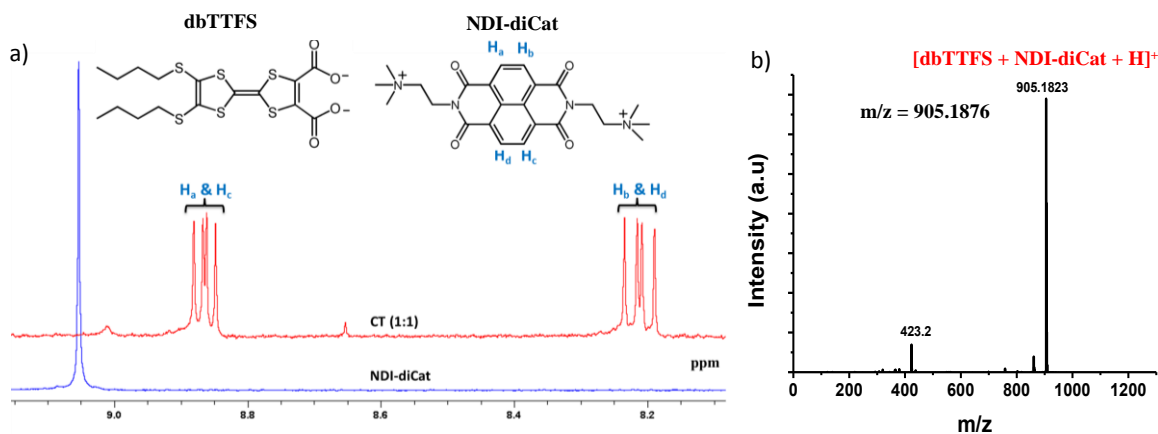
Figure 2.2.17: a) *Partial ^1H NMR spectra of **dbTTFS** and **NDI-diCat** CT pair at 2 x 10^{-3} M concentration in 22% acetonitrile in water (400 MHz, D_2O). b) High resolution mass spectrometry (HRMS) of **dbTTFS/NDI-diCat** 1:1 CT complex showing m/z = 905.1823.*

Figure 2.2.18: *ESI tandem MS/MS pattern of 1:1 CT complex between **dbTTFS** and **NDI-diCat** (m/z = 905.1876) with varying accelerating voltages.*

Tandem mass spectroscopy (MS/MS) experiments on the complex ion peak further showed its dissociation into individual components with increase in accelerating voltage (Figure 2.2.18). At low vol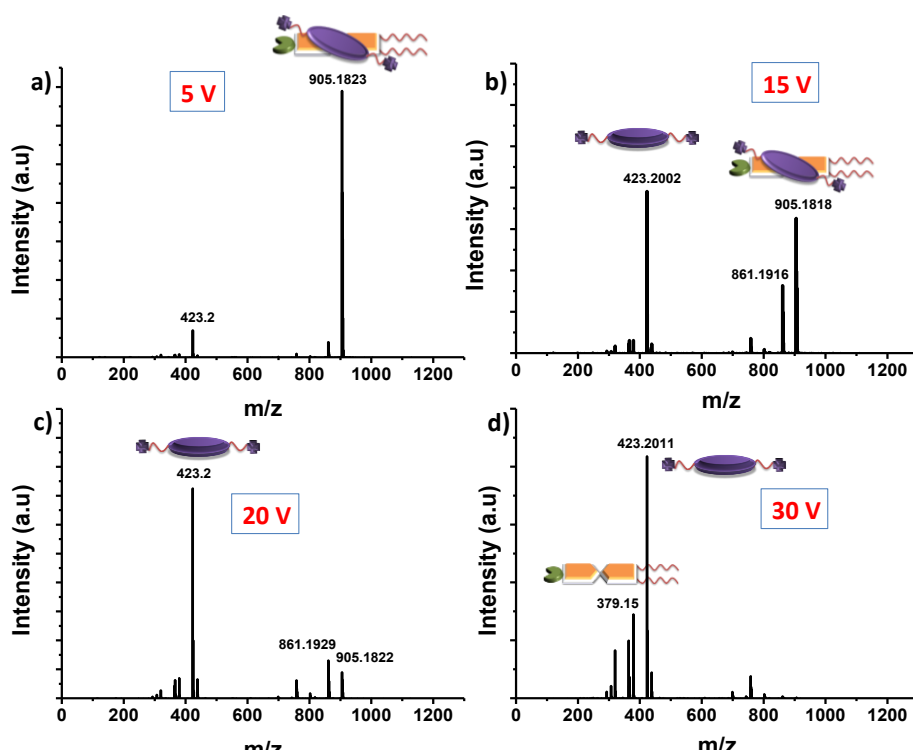tage (5 V), a major peak corresponding to 1:1 CT mass was observed, whereas on increasing voltage we see a gradual increase of the peak m/z 423.2 which corresponds to **NDI-diCat** with the loss of one CH_3 group along with the appearance of mass 379.15 corresponding to **dbTTFS** with the loss of two CO_2 groups. At high voltage (30 V) only fragmented mass of CT complex was seen.

2.2.6. Investigations of 1:2 CT Formation

In the previous section (Sec. 2.2.4), we have seen that after adding two equivalent of **NDI-cat** to **dbTTFS** in 30% MeOH in water, the λ_{max} value shifts 50 nm compared to the λ_{max} of 1:1 CT band (figure 2.2.9a). In order to get a deeper insight into these spectral changes at higher equivalent of NDI, we have done detailed ^{1}H NMR spectroscopy and mass spectroscopy measurements using **EtNDI-Cat** as a model compound. **EtNDI-Cat** shows a broad aromatic signal in ^{1}H NMR experiment because of its highly aggregated state (Figure 2.2.10). ^{1}H NMR measurements on **Ch-dbTTFS** + **EtNDI-Cat** 1:2 CT co-assembly in solution showed further upfield shift of the aromatic protons of NDI compared to its 1:1 CT co-assembly (Figure 2.2.19). The proton signals in the alkyl region also shifted upfield which suggests the co-facial binding of **EtNDI-Cat** with TTF. Further we have added three equivalents of **EtNDI-Cat** to **Ch-dbTTFS** which shows peaks corresponding to excess **EtNDI-Cat** in the aromatic region (figure 2.2.21). The appearance of extra $^+N(CH_3)_3$ peak and CH_3 peak with 1:3 CT solution further suggests the presence of uncomplexed NDI (Figure 2.2.20), therefore proving the formation of 1:2 complex. However, further upfield shifts of **EtNDI-Cat** aromatic protons (involved in the

1:2 CT with 1:3 CT solution, suggests that more than two equivants of NDI molecules is necessary for the efficient formation of 1:2 complex, hinting towards a weak association constant (Figure 2.2.19).
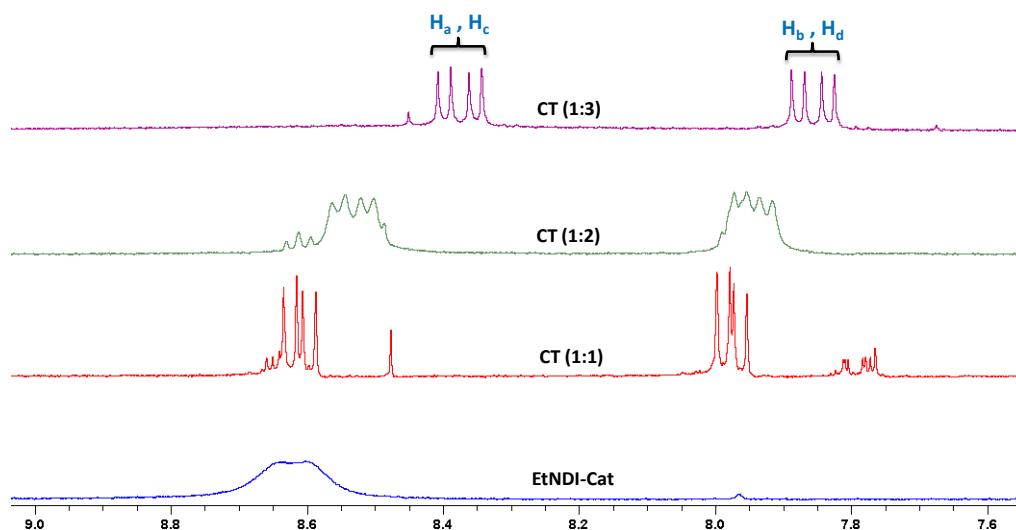
Figure 2.2.19: *Aromatic region of the ^1H NMR spectra for **Ch-dbTTFS** and **EtNDI-Cat** CT pair with various composition of D:A ratio at 5 x 10^{-3} M concentration (400 MHZ, D_2O).*
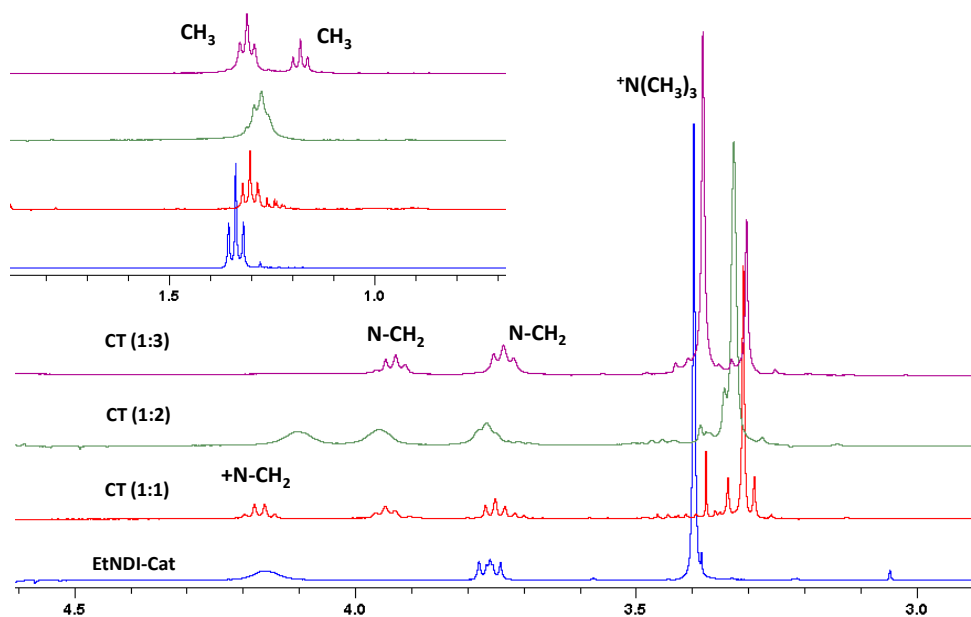
Figure 2.2.20: *Alkyl region of the ^1H NMR spectra for **EtNDI-Cat** and the **ch-dbTTFS** + **EtNDI-ca**t CT complex solution at different D:A ratio (c = 5 x 10^{-3} M, D_2O).*
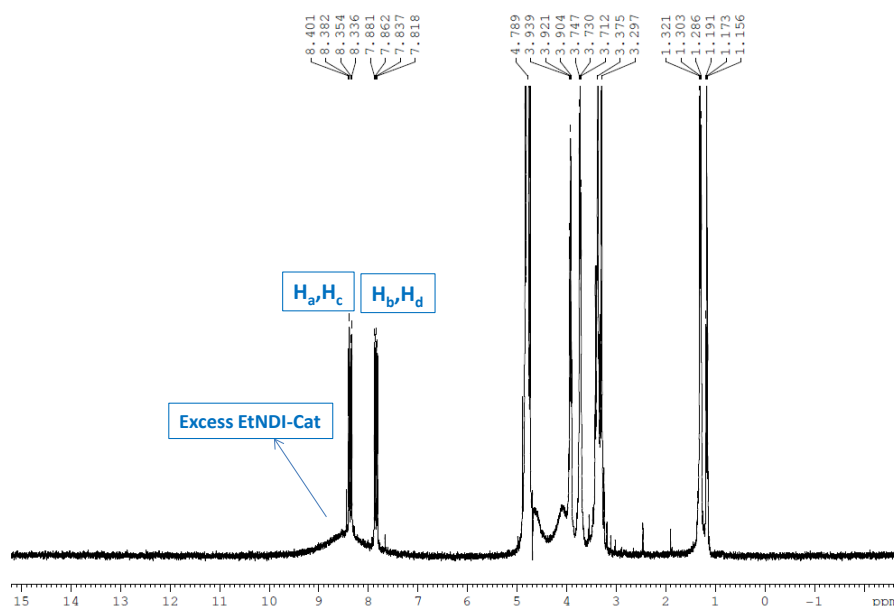
Figure 2.2.21: *^1H NMR spectra of **Ch-dbTTFS + EtNDI-Cat** 1:3 CT complex at 5 x 10^{-3} M concentration in D_2O which shows excess **EtNDI-Cat** in the aromatic region.*

ESI HRMS spectra shows intense peak corresponding to the mass of 1:2 CT pairs for **dbTTFS + NDI-Cat, dbTTFS + EtNDI-Cat** as well as **Ch-dbTTFS + EtNDI-Cat,** which suggest the formation of strong 1:2 CT co-assembly in solution. The proposed molecular structure for 1:2 CT co-assembly is shown in Scheme 2.2.4 (below). Unfortunately attempt to make 1:2 CT co-crystal was unsuccessful.
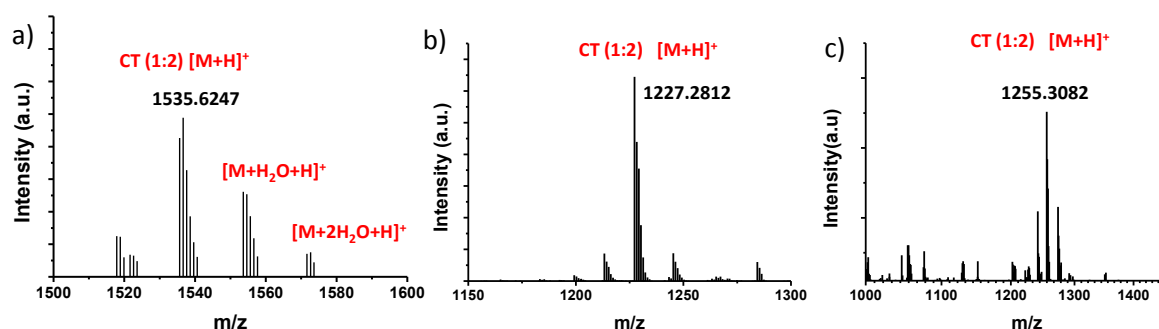
Figure 2.2.22: *High resolution ESI-MS spectra for 1:2 CT co-assembly of [**dbTTFS +NDI-Cat**], **dbTTFS + EtNDI-Cat** and **Ch-dbTTFS + EtNDI-Cat** respectively where M is the mass of the corresponding 1:2 CT pair.*
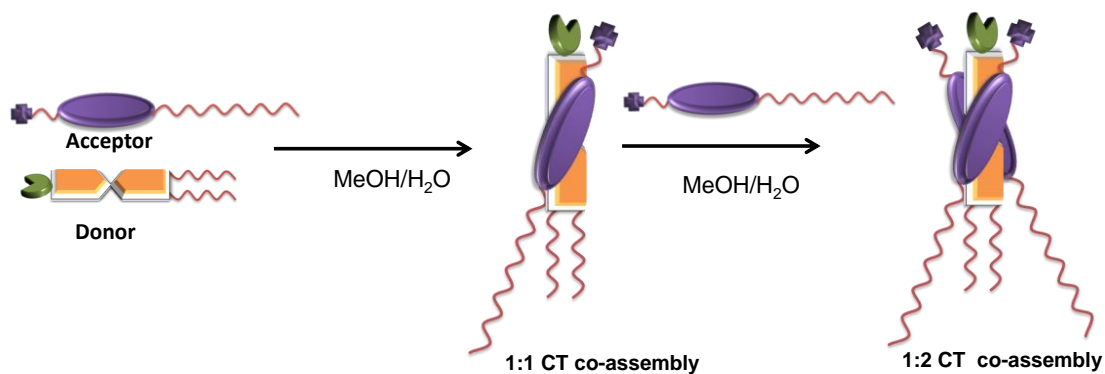
Scheme 2.2.4: *Schematic shows the formation of 1:2 CT co-assembly along with the proposed molecular orientation.*

2.2.7 Morphology
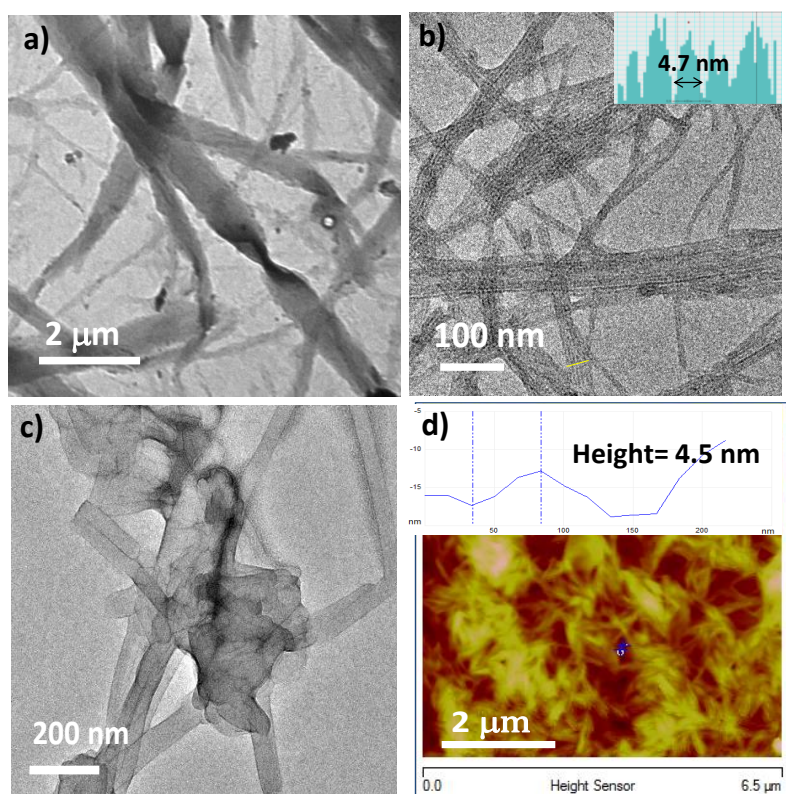
Figure 2.2.23: *a) TEM image of **dbTTFS** at 5 x 10⁻⁴ M concentration (30% methanol in water). b) and c) TEM image of **NDI-Cat** alone and its 1:1 CT complex with **dbTTFS** respectively at 3 x 10^{−4} M concentration (20% MeOH in water). d) AFM image of the **dbTTFS** and **NDI-Cat** CT pair.*

The self-assembly features and morphology of the non-covalent CT-amphiphiles were investigated by various microscopic techniques. As **dbTTFS** self-assemble in water we have done TEM measurements, which show tape like morphology in the micrometre regime (Figure 2.2.23a). The TEM image of **NDI-Cat** alone in 20% MeOH in H_2O (3 x 10^{-4} M) dried on a carbon-coated copper grid, showed the formation of long nanofibers each of which are 4.7 nm in diameter (Figure 2.2.23b). On the other hand 1:1 CT co-assembly of **NDI-Cat** with **dbTTFS** reveals the formation of nanotape morphology (Figure 2.2.23c). AFM image of 1:1 mixture of **dbTTFS** and **NDI**-**Cat** CT complex in 20% methanol in water (v/v) (3 x 10^{-4} M) drop casted on glass substrates showed the formation of nanostructures supporting the TEM observation.

The formation of CT co-assembly in solution was further supported by DLS measurements performed in methanol-water mixture (30:70, v/v). The DLS measurements for **dbTTFS**, **NDI-Cat** and CT co-assembly were carried out in 30% MeOH in H_2O at 5 x 10^{-4} M concentration (Figure 2.2.24). The **dbTTFS** shows a hydrodynamic radius of 100 nm due to its self-assembly in agreement with the TEM studies. A large hydrodynamic radius (450 nm) for **NDI-Cat** alone was observed, which is in consistent with the formation of dense fibre network in solution. The CT co-assembly of 1:1 **dbTTFS** + **NDI-Cat** shows a hydrodynamic radius of 150 nm because of self-assembly in solution phase whereas the 1:2 CT co-assembly shows a broad size distribution (20 nm 450 nm) in solution because of the more aggregated state. This fact is more prominent in case of **Ch-dbTTFS** + **NDI-Cat** CT pair where the 1:2 CT solution shows a large hydrodynamic radius (500 to 2000 nm), which is further supported by the sheets type morphology observed in the TEM image (Figure 2.2.24c). The extended molecular length of **NDI-Cat** obtained from CPK model is 2.5 nm. Hence the height 4.5

nm obtained from the AFM images suggests a lamellar organisation of the charge-tansfer amphiphiles in their 1:1 CT complex solution. This is further supported by the PXRD pattern for CT nanostructures where the maximum d-spacing obtained is 2.42 nm and also shows three low-angle peaks with *d* spacing of 24.2, 12, and 8 Å. (Figure 2.2.25) with 1: 1/2: 1/3 orders

.
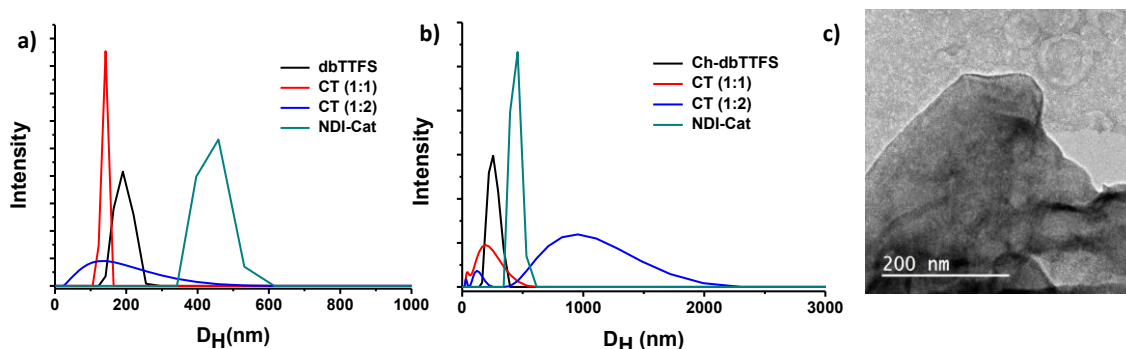
Figure 2.2.24: *a) and b) corresponds to dynamic light scattering (DLS) measurements showing the hydrodynamic size distribution of individual D, A and the CT co-assembly of **dbTTFS + NDI-Cat** and **Ch-dbTTFS + NDI-Cat** CT pair for (1:1) and (1:2) composition. (c = 5 x 10^{-4} M, 30 % Methanol in water). c) TEM image of the 1:2 CT complex solution, measured at c = 5 x 10^{-4} M, 30 % Methanol in water.*
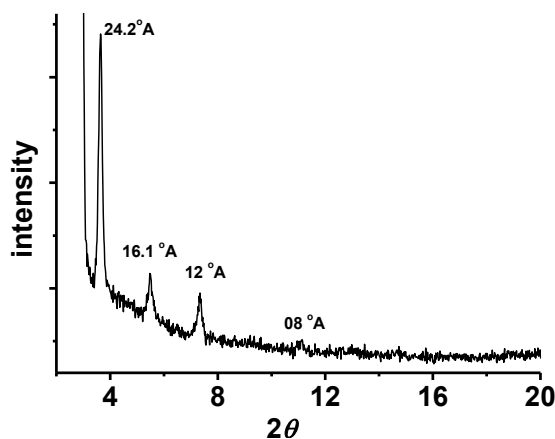
Figure 2.2.25: *PXRD profiles of the **dbTTFS-NDI-Cat** CT complex in the film state obtained by drop-casting the self-assembled solution on glass substrate. The numbers shows the d-spacing in Å.*

2.2.8. Conductivity Measurement

Two probe conductivity studies were carried out on **dbTTFS** and **NDI**-**Cat** self-assembled CT fibres by drop-casting CT solution across a gap of gold electrodes on glass substrate where the gap between two electrodes is 2μm. The *I-V* response of the CT nanostructures was found to be non-linear (Figure 2.2.26) suggesting the semiconducting behaviour of CT nanostructures and the estimated conductivity was 6.24×10^{-5} S cm^{-1}. The calculated resistance by fitting to the linear region of the *I-V* curve passing through origin was found to be 1.248×10^{-6} ohm.
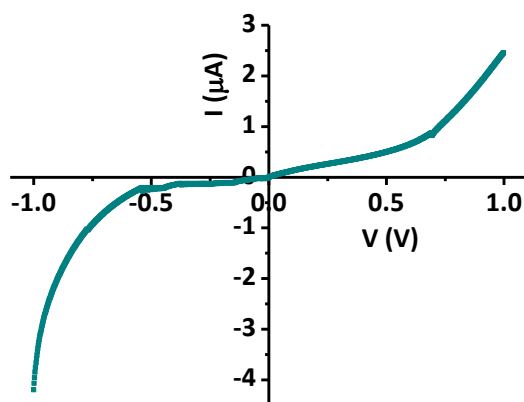
Figure 2.2.26: *I-V curve for **dbTTFS** and **NDI**-**Cat** CT nanostructures. The sample was prepared by drop-casting the CT solution on a gold-coated glass substrate followed by vacuum drying.*

2.2.9. Conclusion

In summary for the first time we have shown a novel supramolecular design for the construction of mixed-stack CT-nanostructures of TTF-NDI chromophores. This was achieved through amphiphilic design in which amphiphilic D (**dbTTFS**) and A (**NDI**-**Cat)** co-assemble to form supramolecular amphiphile. This further enables the formation of well-defined CT-nanostructures with lamellar packing via amphiphilic self-assembly in

solution. Here the strength of the π-π stacking between D-A pair, hydrophobic, electrostatic and solvophobic interactions also play a crucial role in guiding the self-assembly of the present non-covalent CT-amphiphile. Moreover this is a simple and unprecedented example of constructing mixed-stalk stack D-A CT complex obtained from TTF and NDI derivative affording a strong CT band in the NIR region. The amphiphilic nature of CT co-assembly plays a crucial role in the formation of well-defined nanostructures with interesting conducting properties. We hope this supramolecular approach of making CT nanostructure will further help in organic optoelectronics and can show ferroelectric property which will be investigated in future.

2.2.10. Experimental Section

General Methods

Optical Measurements:

Electronic absorption spectra were recorded on a Perkin Elmer Lambda 900 UV-Vis-NIR Spectrometer and emission spectra were recorded on Perkin Elmer Ls 55 Luminescence Spectrometer. UV-Vis and emission spectra were recorded in 1 cm path length cuvette. Fluorescence spectra of solutions were recorded with 340 nm excitation wavelength.

1-D NMR Measurements:

NMR spectra were obtained with a Bruker AVANCE 400 (400 MHz) Fourier transform NMR spectrometer with chemical shifts reported in parts per million (ppm) with respect to residual solvent peak.

Two-Dimensional NMR measurements:

All 2D NMR spectra were recorded on a Bruker AVANCE(III) 400 MHZ NMR, SIF,NRC by means of a 5mm 1H/X Inverse BBFO Detection probe equipped with gradient capabilities at 298K.

HMQC: Gradient selective HMQCPHPR experiments were performed using a relaxation delay time of 1.5 s, a sweep width of 4807.692 Hz for proton dimension and 22142.533 Hz for the carbon dimension and aquestion mode States-TPPI. All 2D-data were collected in the phase-sensitive mode using the States-Haberkorn method. A total of 400 FIDs of 2K complex data points, collected in t2 with 32 scans per increment. $^1J_{C-H}$ coupling constant was set to 160 Hz. The suppression was applied to filter residual ^1H coupled to ^{12}C. Processing was done after Gaussian apodization in both dimensions. Calibration of the decoupler pulse widths and decoupler strength was achieved by using the States-Haberkorn method.

HMBC: Gradient selective HMBCGPNDQF experiments were performed using a relaxation delay time of 1.5 s, a sweep width of 4807.692 Hz for proton dimension and 22142.533 Hz for the carbon dimension and aquestion mode QF. All 2D-data were collected in the phase-sensitive mode, collected in t2 with 32 scans per increment. The suppression was applied to filter residual ^1H coupled to 12C. Processing was done after Gaussian apodization in both dimensions. Calibration of the decoupler pulse widths and decoupler strength was achieved by using the States-Haberkorn method. A total of 400 FIDs of 2K complex data points were $^1J_{C-H}$ coupling constant was set to 145 Hz.

High-Resolution Mass-Spectrometry (HR-MS):

HRMS measurements were performed with Agilent Technologies Q-TOF-LCMS system, 6538 instrument. Measurements were done in ESI mode.

Transmission Electron Microscopy (TEM):

TEM measurements were performed on a JEOL, JEM 3010 operated at 300 kV. Samples were prepared by placing a drop of the solution on carbon coated copper grids followed by drying at room temperature. The images were recorded with an operating voltage 300 kV. In order to get a better contrast samples were stained with uranyl acetate (1 wt % in water) before the measurements.

Dynamic Light scattering Experiments (DLS):

The measurements were carried out using a Nano ZS (Malvern UK) employing a 532 nm laser at a back scattering angle of 173°.

Conductivity measurement:

Electrical measurements were carried out using micron-sized-gap gold electrodes on glass substrate, and I–V curves were acquired by using a Keithley 236 electrometer at room temperature and in air. Electrical conductivity values were calculated by considering average thickness and area of the drop-coated film.

2.2.10a. Synthetic Procedures

4, 5-Bis(butylthio)-1, 3-dithiole-2-thione (**4a**): Butyl bromide (3.9 g, 28.46 mmol) and [Zn(dmit)$_2$](NEt$_4$)$_2$ (5 g, 6.96 mmol) were mixed in 75 ml of acetonitrile. The solution was refluxed for 4 hrs at 90 ^{o}C under inert atmosphere, changing in colour from red to brown. The mixture was then extracted with hexane followed by the evaporation of the

organic layer. The product was purified by chromatography on a silica column with CHCl$_3$/Hexane (1:1) solvent mixture. Yield 87%. ^{1}H NMR (400 MHz, CDCl$_3$ TMS): δ (ppm) 2.87 (t, J = 7.2 Hz, 4H), 1.69-1.61 (m, 4H), 1.49-1.40 (m, 4H), 0.93 (t, *J* = 7.2 Hz, 6H). ^{13}C NMR (100 MHz, CDCl$_3$): δ (ppm) 211.5, 136.4, 35, 28.4, 18.6, 11.2.

4,5-Bis(2-methylbutylthio)-1,3-dithiole-2-thione ((*S,S*) **4b**): 2-methyl butyl bromide (5 g, 33.1 mmol) and [Zn(dmit)$_2$](NEt$_4$)$_2$ (4 g, 5.57 mmol) were mixed in 50 ml of acetonitrile. The solution was refluxed for 48 hrs at 55 ^{o}C under inert atmosphere, changing in colour from red to brown and forming a yellow precipitate. The mixture was then extracted with hexane followed by the evaporation of the organic layer. The product was purified by chromatography on a silica column with CHCl$_3$/Hexane (1:4) solvent mixture. Yield 99%. ^{1}H NMR (400 MHz, CDCl$_3$ TMS): δ (ppm) 2.88 (dd, J = 6 Hz, J = 5.2 Hz, 2H), 2.70 (dd, J = 7.2 Hz, J = 7.2 Hz, 2H), 1.69-1.47 (m, 4H), 1.29-1.22 (m, 2H), 1.00 (d, J = 6.8 Hz, 6H), 0.91 (t, J = 6.8 Hz, 6 H). ^{13}C NMR (100 MHz, CDCl$_3$): δ (ppm) 211.5, 136.4, 43.7, 35, 28.4, 18.6, 11.2.

Synthesis of Bis(butylthio)-bis(methoxycarbonyl)-tetrathiafulvalene (6a):

1.068 g (4.56 mmol) of dimethyl-1,3-dithiole-2-thione-4,5-dicarboxylate (**5**) and 1.84 g (5.93 mmol) of **4a** was added in 6 ml of freshly prepared triethyl phosphite and refluxed overnight under Ar at 120 ^{o}C. After completion of the reaction triethyl phosphite was removed under high vacuum followed by purification through silica-gel column chromatography using 50% (v/v) chloroform-Hexane mixture as eluent affording 18% yield of the desired product. ^{1}H NMR (400 MHz, CDCl$_3$ TMS): δ (ppm) 3.84 (s, 6H), 2.83 (t, J = 8 Hz, 4H), 1.59 (m, 4H), 1.4 (m, 4H), 0.92 (t, J = 8 Hz, 6H); ^{13}C NMR (100 MHz, CDCl$_3$): δ (ppm) 160.12, 132.16, 128.15, 53.48, 36.26, 31.90, 21.77, 13.70.

Synthesis of Bis(2-methylbutylthio)-bis(methoxycarbonyl)-tetrathiafulvalene (S,S)-(6b):

3.96 g (11.73 mmol) of 4,5-Bis(2-methylbutylthio)-1,3-dithiole-2-thione ((S,S), **4b**) and 2.43 g (10.38 mmol) of **5** was added in 20 ml of freshly prepared triethyl phosphite and refluxed overnight under Ar at 120 ^{o}C. After completion of the reaction, triethyl phosphite was removed under high vacuum followed by purification through silica-gel column chromatography using chloroform-Hexane solvent mixture as eluent affording 15% yield of the desired product. ^{1}H NMR (400 MHz, CDCl$_3$ TMS): δ (ppm) 3.84 (s, 6H), 2.83 (dd, J = 6 Hz, J = 5.2 Hz, 2H), 2.64 (dd, J = 7.2 Hz, J = 7.2 Hz, 2H), 1.66-1.48 (m, 4H), 1.24 (m, 2H), 1.00 (d, J = 6.8 Hz, 6H), 0.9 (t, J = 6.8 7.2 Hz, 6H); ^{13}C NMR (100 MHz, CDCl$_3$): δ (ppm) 158.95, 131.02, 127.02, 112.01, 52.30, 42.42, 34.09, 27.40, 17.57, 10.17. HRMS (ESI): m/z calcd: C$_{20}$H$_{29}$O$_4$S$_6$: 525.0312, found: 525.0397, [M+H]$^+$.

Synthesis of Bis(butylthio)-tetrathiafulvalene dicarboxylate (dbTTFS):

3.5 % (w/v) (30 ml) of aqueous KOH solution was added drop by drop through a pressure equalising funnel to the 0.168 g. (168 mmol) of 1,3 dithiol dibutyl TTF dimethyl carboxylate (**6a**), taken in 100 ml ethanol. The reaction mixture was stirred for 12 hr at 95 ^{o}C. After completion of the reaction ethanol was removed in vacuum and excess ethanol was added to remove the water completely in vacuum. The product was finally precipitated out in ethanol and dried after filtering. Yield: 50%. ^{1}H NMR (400 MHz, CDCl$_3$ TMS): δ (ppm) 2.92 (t, J = 8 Hz, 4H), 1.62 (m, 4H), 1.45 (m, 4H), 0.91 (t, J =11.2 Hz, 6H); ^{13}C NMR (100 MHz, CDCl$_3$): δ (ppm) 166.82, 133.52, 127.75, 35.87, 31.61, 21.38, 16.83, 13.36; HRMS (ESI): m/z calcd: C$_{16}$H$_{24}$S$_6$: 506.9540, found: 506.9289, [M+K+2H]$^+$.

Synthesis of Bis(2-methylbutylthio)-tetrathiafulvalene dicarboxylate (*S,S*) (Ch-dbTTFS):

3.5 % (w/v) (30 ml) of aqueous KOH solution was added drop by drop through a pressure equalising funnel to the 0.6 g. (1.14 mmol) of chiral 1,3 dithiol dibutyl TTF dimethyl carboxylate (**6b**), taken in 100 ml ethanol. The reaction mixture was stirred for 12 hrs at 95 $^\circ$C. After completion of the reaction ethanol was removed in vacuum and excess ethanol was added to remove the water completely in vacuum. The product was finally precipitated out in ethanol and dried after filtering. Yield: 50%. ^{1}H NMR (400 MHz, CDCl$_3$ TMS): δ (ppm) 2.93 (dd, J = 6 Hz, J = 5.2 Hz, 2H), 2.77 (dd, J = 7.2 Hz, J = 7.2 Hz, 2H), 1.67-1.48 (m, 4H), 1.31-1.24 (m, 2H) 1.00 (d, J = 6.4 Hz, 6H), 0.90 (t, 6H, J = 7.6 Hz), δ (ppm) 166.62, 133.86, 127.63, 43.07, 35.01, 28.37, 18.64, 11.33; HRMS (ESI): m/z calcd: C$_{16}$H$_{24}$S$_6$: 493.9853, found: 496.9949, [M+3H]$^+$.

Synthesis of compound (7):

1,4,5,8-Naphthalenetetracarboxylic dianhydride (1g, 3.728 mmol) was added to N,N-dimethylethylene diamine (0.33 g, 3.728 mmol) and aqueous ethylamine, 70% (v/v) (0.25 ml, 3.728 mmol) in 50 ml of isopropanol and the reaction mixture was stirred at 80 °C for 12 h under inert atmosphere. Isopropanol solvent was then evaporated under high vacuum. The resulting residue was dissolved in chloroform and filtered. The filtrate was evaporated and purified by column chromatography (silica, 100-200 mesh, 5% methanol/chloroform (v/v) solvent mixtures to give 1g of desired product in 70% yield. ^{1}H NMR (400 MHz, CDCl$_3$ TMS): δ (ppm) 8.76 (s, 4H), 4.35 (t, J = 8 Hz, 2H), 4.2 (m, 2H), 2.67 (t, J = 6.8 Hz, 2H), 2.34 (s, 6H), 1.36 (t, J = 7.2 Hz, 3H). ^{13}C NMR (100 MHz, CDCl$_3$): δ (ppm) 163.18, 162.66, 131.03, 130.85, 126.89, 126.82, 126.70, 126.62, 56.60,

45.23, 36.03, 13.30; HRMS (ESI): m/z calcd: $C_{20}H_{20}N_3O_4$: 366.1375, found: 366.1439, $[M+H]^+$.

Synthesis of EtNDI-Cat:

Methyl iodide (0.8 ml, 12.84 mmol) was added to 125 mg (0.34 mmol) of **7** in 20 ml of toluene and stirred for 4 h at 80 ^{o}C under inert atmosphere. The shiny yellow precipitate formed during the reaction was filtered, washed with diethyl ether and dried under vacuum to give 155 mg of pure **EtNDI-Cat**. in 90% yield. ^{1}H NMR (400 MHz, CDCl$_3$ TMS): δ (ppm) 8.7 (s, 4H), 4.48 (t, J = 8 Hz, 2H), 4.12 (m, 2H), 3.63 (t, J = 8 Hz, 2H), 3.23 (s, 9H), 1.25 (t, J = 7.2 Hz, 3H); ^{13}C NMR (100 MHz, CDCl$_3$): δ (ppm) 162.7, 162.41, 130.58, 130.43, 126.67, 126.31, 126.19, 61.75, 52.57, 35.37, 33.94, 13.03; HRMS (ESI): m/z calcd: $C_{21}H_{22}N_3O_4$: 380.1610, found: 380.1598, $[M]^+$.

Synthesis of dodecyl derivative of naphthalene diimide (NDI-Cat): See the reference [8]

Synthesis of didodecyl derivative of naphthalene diimide (NDI-diCat): See the reference [9]

2.2.11. References

[1]   A. Jain, K.V. Rao, U. Mogera, A. A. Sagade and S.J. George, *Chem. −Eur. J.* 2011, **17**, 12355; H. Alves, A. S. Molinari, H. Xie and A. F. Morpurgo, *Nat. Mater.,* 2008, **7**, 574; J.-Y. Wang, J. Yan, L. Ding, Y. Ma and J. Pei, *Adv. Funct. Mater.*, 2009, **19**, 1746.

[2]   H.-D. Wu, F.-X. Wang, Y. Xiaoa and G.-B. Pan, *J. Mater. Chem. C*, 2013, **1,** 2286; A. A. Sagade, K. V. Rao, S. J. George, A. Datta and G. U. Kulkarni, *Chem.*

Commun. 2013, 5847; M. Kumar, K. V. Rao and Subi J. George, *Phys. Chem. Chem. Phys.,* 2014, **16**, 1300.

S. K. Park, S. Varghese, J. H. Kim, S.-J Yoon, O.-K. Kwon, B. An, J. Gierschner and S. Y. Park, *J. Am. Chem. Soc*. 2013, **135**, 4757.

[3]   S. Horiuchi and Y. Tokura, *Nature Mater*. 2008, **7**, 357; A. Girlando, A. Painelli, C. Pecile, G. Calestani, C. Rizzoli and R. M. Metzger, *J. Chem. Phys*. 1993, **98,** 7692.

[4]   Y. Tokura and S. Koshihara, *Phys. Rev. Lett.,* 1989, **63**, 2405; H. Okamoto and T. Mitani,   *Phys. Rev. B.,* 1991, **43**, 8224.

[5]   A. S. Tayi, A. K. Shveyd, A. C.-H. Sue, J. M. Szarko, B. S. Rolczynski, D. Cao, T. J. Kennedy, A. Sarjeant, C. L. Stern, W. F. Paxton, W. Wu, S. K. Dey, A. C. Fahrenbach, J. R. Guest, H. Mohseni, L. X. Chen, K. L. Wang, J. F. Stoddart and S. I. Stupp, *Nature*, 2012, *488*, 485.

[6]   W. R. Dichtel, O. S. Miljani, W. Zhang, J. M. Spruell, K. Patel, I. Aprahamian, J. R. Heath and J. F. Stoddart. *Acc. Chem. Res*. 2008, **41**, 1750;   A. R. Pease, J. O. Jeppesen, Y. Luo, C. P. Collier, J. R. Heath and J. F. Stoddert, *Acc. Chem. Res*., 2001, **34**, 433; K. B. Simonsen, K. Zong, R. D. Rogers and M. P. Cava*, J. Org. Chem.*, 1997, **62**, 679; D. B. Amabilino and J. F. Stoddart*, Chem. Rev*., 1995**, 95**, 2725; C. O. D.-Buchecker and J. P. Sauvage, *Chem. Rev.,* 1987, **87,** 795; L. Raehm, D. G. Hamilton and J. K. M. Sanders, *Synlett,* 2002, 1743; S. A. Vignon, T. Jarrosson, T. Iijima, H.-R. Tseng, J. K. M. Sanders and J. F. Stoddart, *J. Am. Chem. Soc*., 2004, **126**, 9884; M. A. Olson, A. Coskun, L. Fang, A. N. Basuray and J. F. Stoddart, *Angew. Chem., Int. Ed.,* 2010**, 49**, 3151; G. Koshkakaryan, L. M. Klivansky, D. Cao, M. Snauko, S. J. Teat, J. O. Struppe and Y. Liu, *J. Am. Chem. Soc.,* 2009, **131**, 2078; H. M. Colquhoun and Z. Zhu, *Angew. Chem., Int. Ed*., 2004, **43**, 5040; E. A. Appel, F. Biedermann, U. Rauwald, S. T. Jones, J. M. Zayed and O. A. Scherman, *J. Am. Chem. Soc*., 2010, **132**, 14251; D. Jiao, J. Geng, X. J. Loh, D. Das, T.-C. Lee and O. A. Scherman, *Angew. Chem., Int. Ed.,* 2012, **51**, 9633; B. V. V. S. P. Kumar, K. V. Rao, T. Soumya, S. J. George and M. Eswaramoorthy, *J. Am. Chem. Soc*., 2013, **135**, 10902.

[7]   X. Guo, Z. Gan, H. Luo, Y. Araki, D. Zhang, D. Zhu and O. Ito, *J. Phys. Chem. A*., 2003, **107**, 9747.

[8]   K. Jalani, M. Kumar and S. J. George*, Chem. Commun*., 2013, 5174.

[9]   L. Chen, Y.-M. Zhang, L-H. Wang and Yu Liu, *J. Org. Chem.,* 2013, **78**, 5357.

[10]   Q.-Y. Zhu, Q.-H. Han, M.-Y. Shao, J. Gu, Z. Shi and J. Dai, *J. Phys. Chem. B*., 2012, **116**, 4239.

CHAPTER - 3

Non-covalent Amphiphilic Foldameric Design for Mixed-CT Nanostructures*

Abstract

A non-covalent, amphiphilic foldamer design leads to an efficient charge transfer complex between dipyrene (donor) and naphthalene diimide (acceptor) derivatives, which further self-assembles into one-dimensional nanofibers with an alternate (mixed) donor– acceptor arrangement.
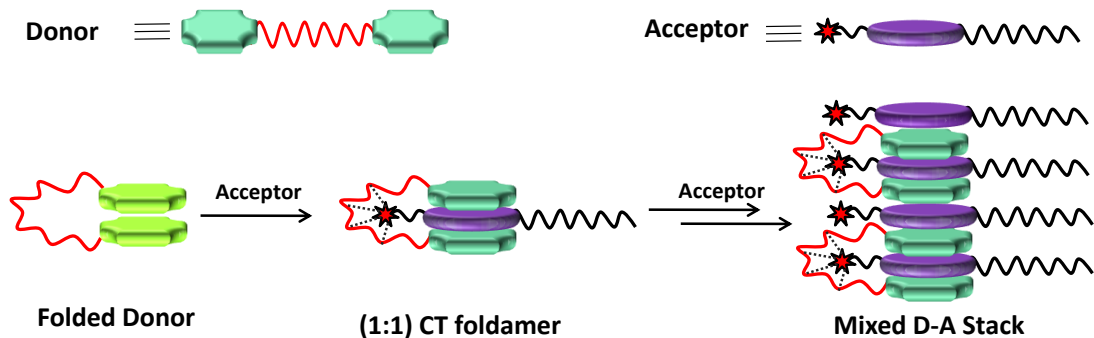
3.1. Introduction

Charge-transfer (CT) assemblies with mixed (alternate or face-to-face) organization of donor (D) and acceptor (A) aromatic molecules are of great importance because of their inherent conducting properties.[1] Mixed CT crystals have been well-studied,[2] however, the construction of corresponding macromolecular assemblies with simple designs remains a challenge.[3] More recently, mixed D–A crystals have been predicted[4] and also shown to exhibit promising ambipolar charge transport properties[5] and room-temperature ferroelectricity.[6] These novel functions have inspired researchers to revisit the design of analogous macromolecular architectures, to render them processable and achieve better structural control of their design. Especially, one-dimensional (1-D) CT nanostructures are interesting, as they can be obtained by molecular self-assembly in solution and would be of great significance in organic nanosized electronics.[7] In the previous chapter, we have shown that CT nanostructures with alternate D–A organization can be efficiently constructed using a non-covalent amphiphilic design of appropriately functionalized molecules.[8] In this construct, the D and A molecules are designed in such a way that the face-to-face CT pair resembles surfactant structure, which ensures its extended self-assembly in polar solvents.[9] However, the efficiency of this approach also depends on the electrostatic interactions between the ionically designed chromophores, thus limiting the variety of molecules. Ramakrishnan *et al*. have introduced a conceptually elegant design of small molecule induced folding of CT-polymers, exploiting ammonium–glycol interactions between them (Figure 3.1).[10] Here they have used a polyimide (**1**) synthesised from pyromellitic dianhydride and appropriate diamine derivative of hexaethylene glycol where pyromellitic units act as acceptor chromophore. As an external folding agent they have synthesised naphthalene donor linked to an

ammonium group through a two or a three-carbon-atom spacer, **2** and **3** respectively, along with 1, 5-dimethoxynaphthalene (**4**) that serves as a model donor which is devoid of the ammonium group. Both the donors **2** and **3** could induce the folding of the polyimide (**1**) by synergistic CT and ammonium-glycol interactions. However **1-2** binding has higher association constant than **1-3** binding thereby suggesting the importance of proper choice of spacer segment in the donor. On the other hand, the molecule **4** has extremely low association constant with **1** and also no folding was observed in this case, which reflects the importance of synergistic CT and electrostatic interaction used in the folding.
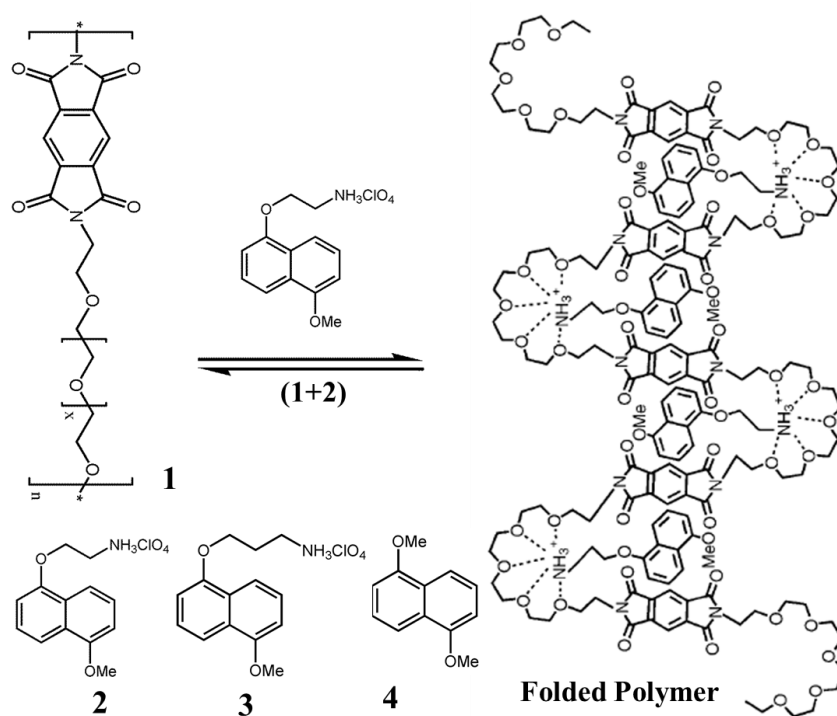
Figure 3.1: *Folding of a synthetic polymer (**1**) aided by two-point interactions with a folding agent. **2, 3** are the molecular structures of various naphthalene donors used as an external folding agent. The molecule **4** corresponds to the model compound without any ammonium group.*

Combining the non-covalent amphiphilic and foldameric designs discussed here, we target the self-assembly of a non-covalent amphiphilic CT foldamer in a bid to broaden

the scope of our CT nanostructure design. In this chapter, we describe the non-covalent synthesis of a CT foldamer, an amphiphilic super molecule, and its self-assembly into 1-D mixed D–A nanostructures. We further show that this co-assembly occurs through a hierarchical (two step) process as confirmed by various spectroscopic techniques.

3.2. Non-Covalent Amphiphilic Foldamer Design
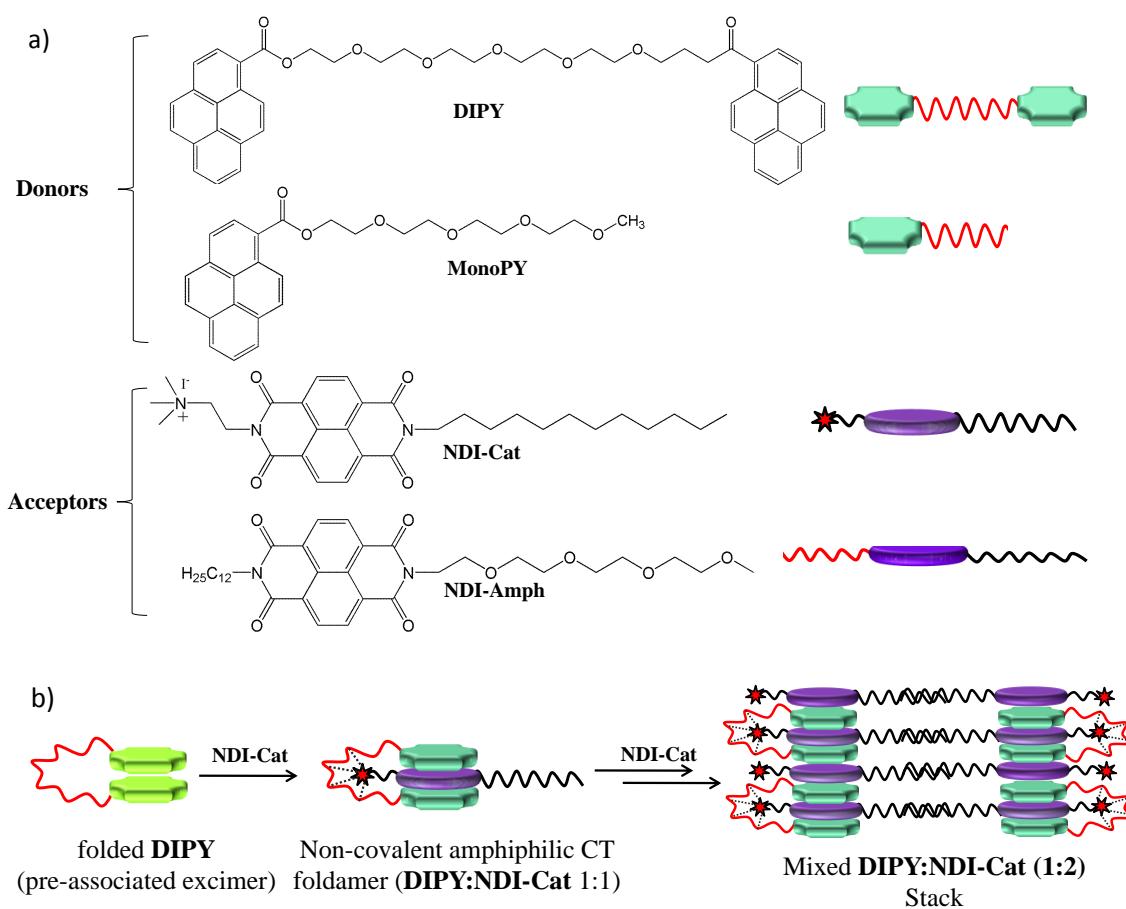
Figure 3.2: *a) Molecular structures of various D and A molecules used in this chapter. b) Foldameric design strategy for the mixed donor–acceptor (D–A) supramolecular assemblies.*

In this design, we have selected dipyrene (**DIPY**) as a donor molecule consisting of two pyrene chromophoric units connected by a flexible hexaethylene glycol (HEG) linker.[11] This molecule can fold under suitable solvent condition or upon the binding of metal ions or small cationic molecules.[12] As a control molecule of **DIPY** we have

synthesised **MonoPY** which has only one pyrene group tethered with monomethyl hexaethylene glycol chain. On the other hand we have designed two amphiphilic naphthalene diimide derivatives **NDI-Cat** and **NDI-Amph,** as acceptor molecules. **NDI-Cat**, is designed with an unsymmetrical amphiphilic structure with a trimethyl ammonium group at one end, which can form a non-covalent amphiphilic pair with **DIPY**, possibly through synergistic CT and ammonium–glycol interaction mediated folding of the donor. This novel non-covalent amphiphilic foldamers can subsequently co-stack with additional **NDI-Cat** or **NDI-Amph** molecules to form an extended alternate D–A stack in polar solvents (Figure 3.2b).

3.3. Synthetic Scheme for Donors and Acceptors

The donors **DIPY**, **MonoPY** and acceptor **NDI-Cat** were synthesised according to the Scheme 3.1, Scheme 3.2 and Scheme 3.3, respectively.
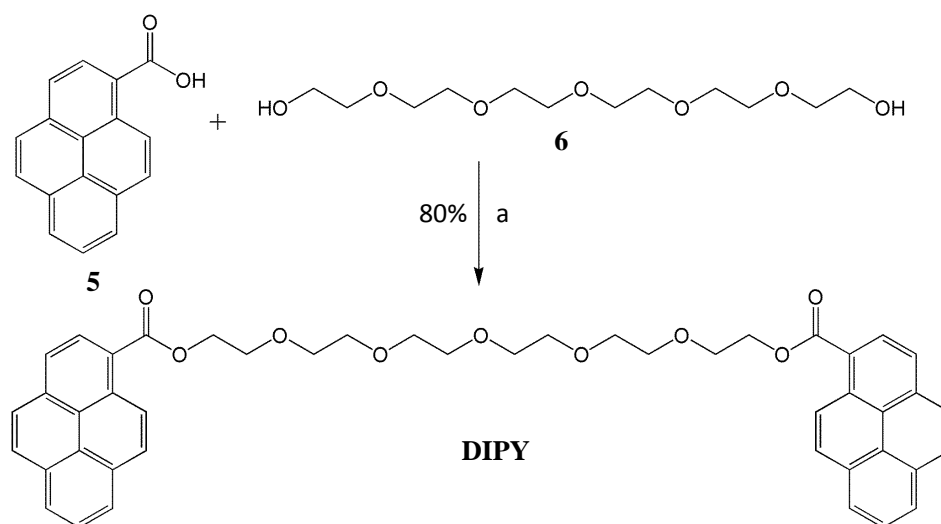
Scheme 3.1: *Synthetic Scheme for **DIPY**. (a) Dry dichloromethane (CH$_2$Cl$_2$), 1-Ethyl-3-(3-dimethylaminopropyl)carbodiimide (EDC), 4-dimethylaminopyridine (DMAP), 0 °C, 24 h.*
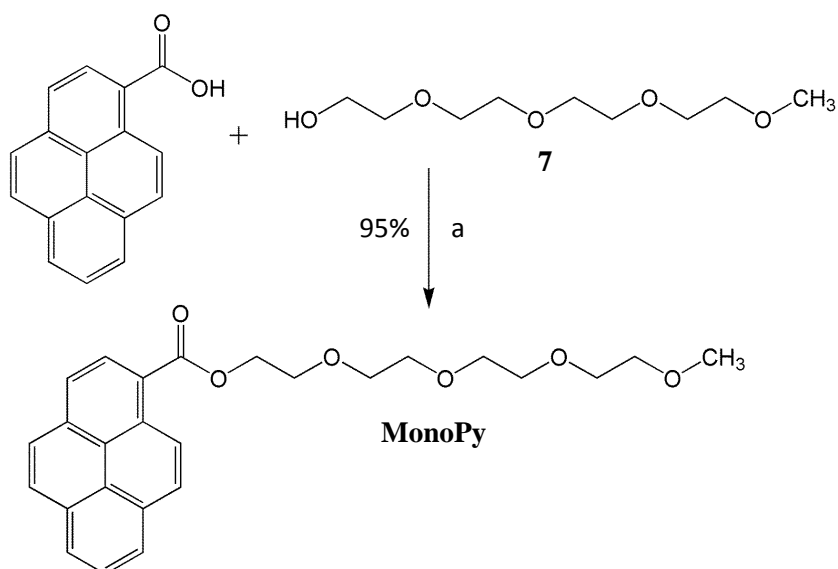
Scheme 3.2: *Synthetic scheme for* **MonoPy.** *(a) Dry dichloromethane (CH₂Cl₂), 1-Ethyl-3-(3-dimethylaminopropyl)carbodiimide (EDC), 4-dimethylaminopyridine (DMAP), 12 h.*
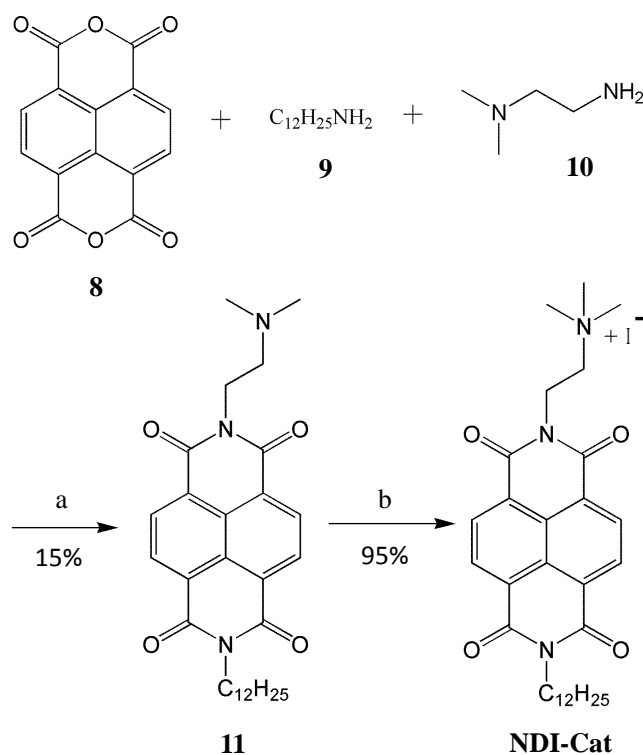
Scheme 3.3: *Synthetic Scheme for* **NDI-Cat.** *(a) Dry DMF, 100 °C, Ar, 24 h; b) CH₃I, 80 °C, 4h.*

The acceptor **NDI-Amph** was synthesised according to the literature procedure. [13]

3.4. Folding of DIPY

The conformation of the **DIPY** foldamer depends on the methanol–water solvent composition, which can be probed by the pyrene excimer resulting from a folded conformation. In 100% methanol, it exists in a molecularly dispersed state with both open and folded conformations as indicated by the characteristic pyrene absorption (λ_{max} = 349 nm) and bimodal emission features ($\lambda_{max(monomer)}$ = 413 nm and $\lambda_{max(excimer)}$ = 519 nm) (Figure 3.3). On the other hand, with increasing percentages of water, hydrophobic interaction forces lead to an increase in folded conformation of **DIPY** as marked by the rise in the ratio of excimer to monomer emission (Figure 3.3a). Whereas, its absorption maximum exhibited a significant red-shift (45 nm) upon increasing the water composition, with the reversal of relative intensity of the vibronic bands compared to that in methanol, characteristic of strong chromophoric interactions in the ground state (Figure 3.3b).[14] In addition, concentration dependent studies (5×10^{-5} M to 5×10^{-6} M) of **DIPY** in 100% methanol (Figure 3.3c) or in a methanol–water solvent mixture (30:70, v/v) (Figure 3.4) did not show any change in their absorption and emission spectra, providing definitive proof for the intramolecular (foldameric) origin of the excimer emission. The role of intermolecular interaction forces for the formation of excimer emission is further ruled out by the concentration dependent emission spectra of glycol appended mono-functional pyrene derivative (**MonoPY**), which showed only monomer emission (Figure 3.3d).
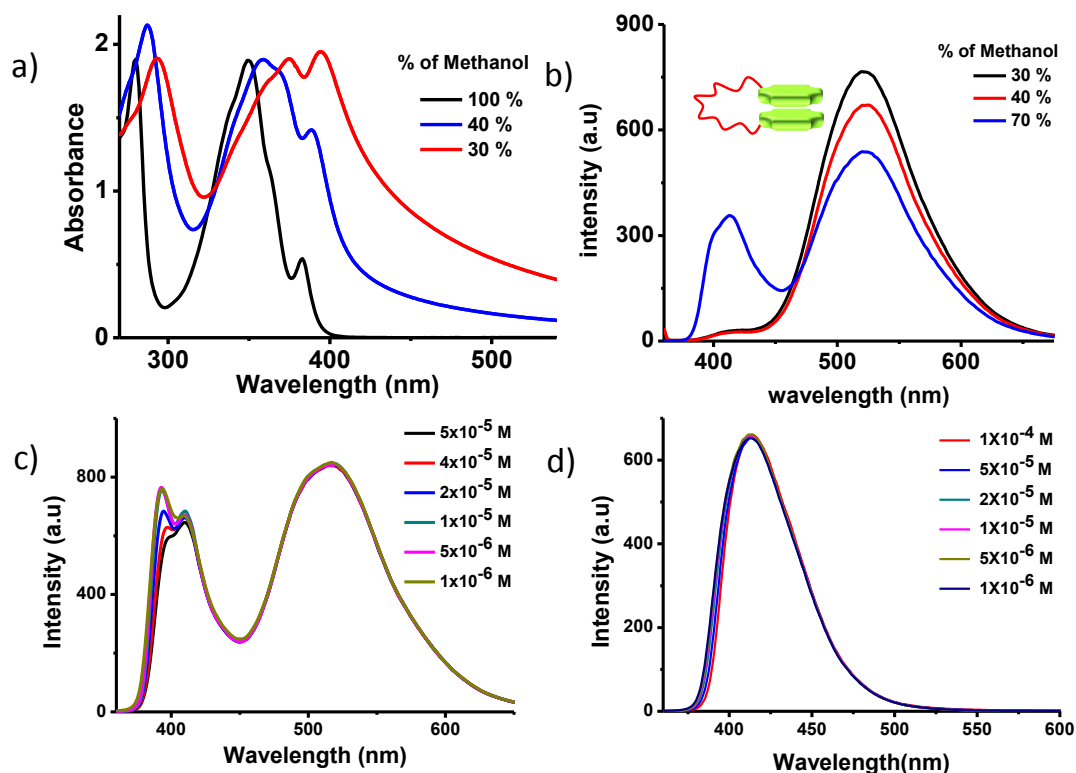
Figure 3.3: *a) Normalized absorption and (b) emission (λ_{exc} = 340 nm) of **DIPY** (c = 4 x 10^{-5} M) in a water–methanol solvent mixture. (λ_{exc} = 340 nm). c) Concentration dependent emission spectra of c) **DIPY** in100% MeOH and d) **MonoPY** in 30% methanol in water solvent mixture.*

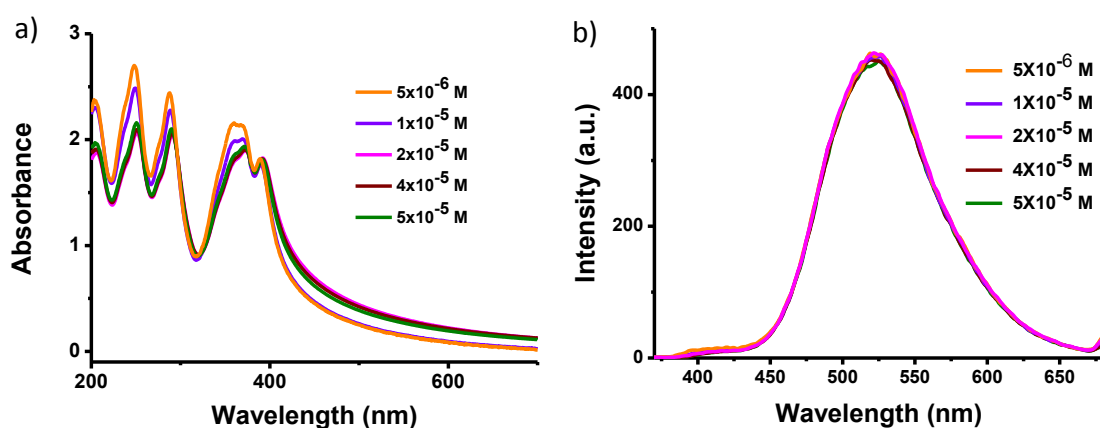**Figure 3.4:** *Concentration dependent (normalized) a) absorption and b) emission spectra (λ_{exc} = 340 nm) of **DIPY** in methanol/water solvent mixture (30:70, v/v). Normalized spectra show that the excimer formation is independent of concentration, confirming intramolecular folded conformation.*

To further prove the folded conformation of **DIPY**, fluorescence lifetime measurements of **DIPY** was done in 30% MeOH in water and 100% MeOH ($\lambda_{exc} = 405$ nm) while collecting emission at monomer (430 nm) and excimer maxima (520 nm) (Figure 3.5). Here the fluorescence life time decay profile of **DIPY** in only MeOH collected at 430 nm shows the major contribution from a very fast decay (1.02 ns) characteristic of monomeric form. On the other hand, in 100% MeOH, the collected emission at 520 nm for **DIPY**, shows a significant contribution from higher lifetime decay (25.03 ns) which could be because of the formation of dynamic excimer in the system. This is because of the presence of both monomer and excimer in 100% MeOH. **DIPY** in 30 % MeOH in water shows a very high lifetime of 40.17 ns indicating the formation of pre-associated excimer.[15] Excitation spectra can also be used to probe the nature of excimers. As we know that the excitation spectra recorded while monitoring the monomer and excimer separately are exactly identical, then the excimer is a dynamic excimer which formed in the excited state without any ground state interaction. In this case, the recorded excitation spectra of **DIPY** collected at excimer emission shows a 50 nm redshift ($\lambda_{max} = 350$ nm to $\lambda_{max} = 400$ nm) in the λ_{max} compared to monomeric absorption spectrum, is clearly an indication of the static excimer formation with inter chromophoric interactions in the ground state. These all experiments unambiguously prove that **DIPY** exist as a folded conformer in the ground state. The folded **DIPY** forms higher order aggregates in water–methanol mixtures as evident from the scattering in their absorption spectra, which is further confirmed by the Transmission Electron Microscopy (TEM) studies (vide infra).
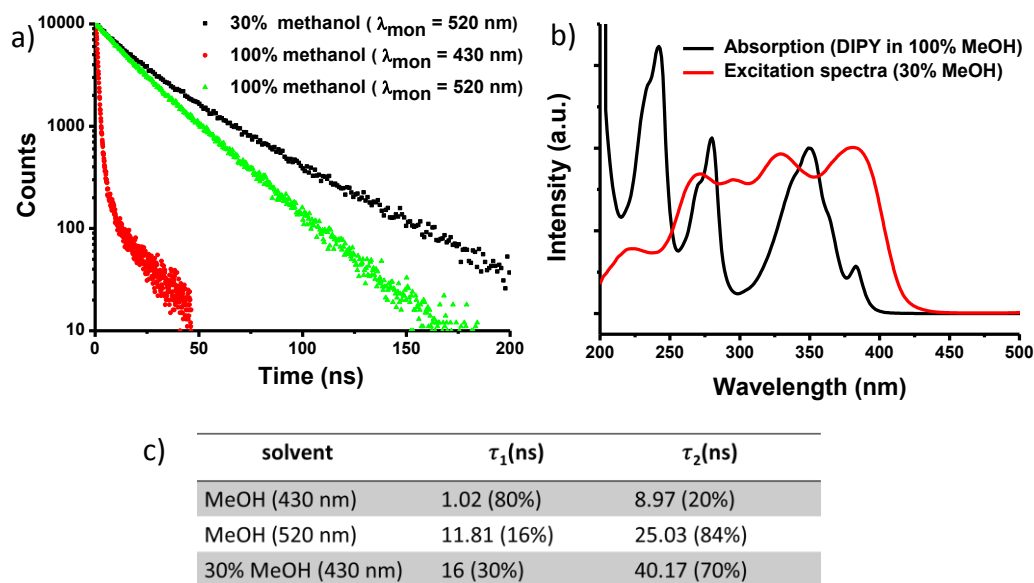
solvent	τ_1(ns)	τ_2(ns)
MeOH (430 nm)	1.02 (80%)	8.97 (20%)
MeOH (520 nm)	11.81 (16%)	25.03 (84%)
30% MeOH (430 nm)	16 (30%)	40.17 (70%)

Figure 3.5: *a) Fluorescence lifetime decay profiles of **DIPY** in 30 % methanol in water and in 100 % methanol (λ_{exc} = 405 nm) while collecting at monomer (430 nm) and excimer emission (λ_{exc} = 520 nm). b) Normalized absorption spectrum (black) of **DIPY** in 100 % methanol compared with that of excitation spectrum (red) in 30 % methanol in water, collected at excimer emission (520 nm). c) Table for the fluorescence life-time values corresponding to figure (a). The percentage number in the bracket shows the population of the corresponding species.*

3.5. Formation of Non-Covalent CT-foldamer

To investigate the CT co-assembly, spectroscopic properties of **DIPY** (c = 4 x 10^{-5} M) were probed in the presence of varying amounts of **NDI-Cat** in methanol–water solvent mixture (30:70, v/v). Figure 3.4, shows the evolution of a broad absorption band with a maximum at 493 nm and gradual quenching of the excimer emission, upon addition of **NDI-Cat**, characteristic of the CT interaction between pyrene and NDI chromophores.[16] Titration curves obtained by probing the CT band at 493 nm and the excimer band at 545 nm against the molar concentration of NDI revealed a two-step co-assembly, as evident from the change in the slope along the curve (Figure 3.6c and d). Initial addition of **NDI-Cat** up to 1 equivalent resulted in a very sharp decrease in the

emission ($I_0/I_{1.0}$ = 13) with the corresponding enhancement of the CT band, indicating the quantitative formation of the non-covalent D–A foldamer. Increasing the NDI concentration beyond 1 equivalent resulted in further gradual increase of the CT band and quenching of fluorescence, suggesting a higher order D–A assembly.
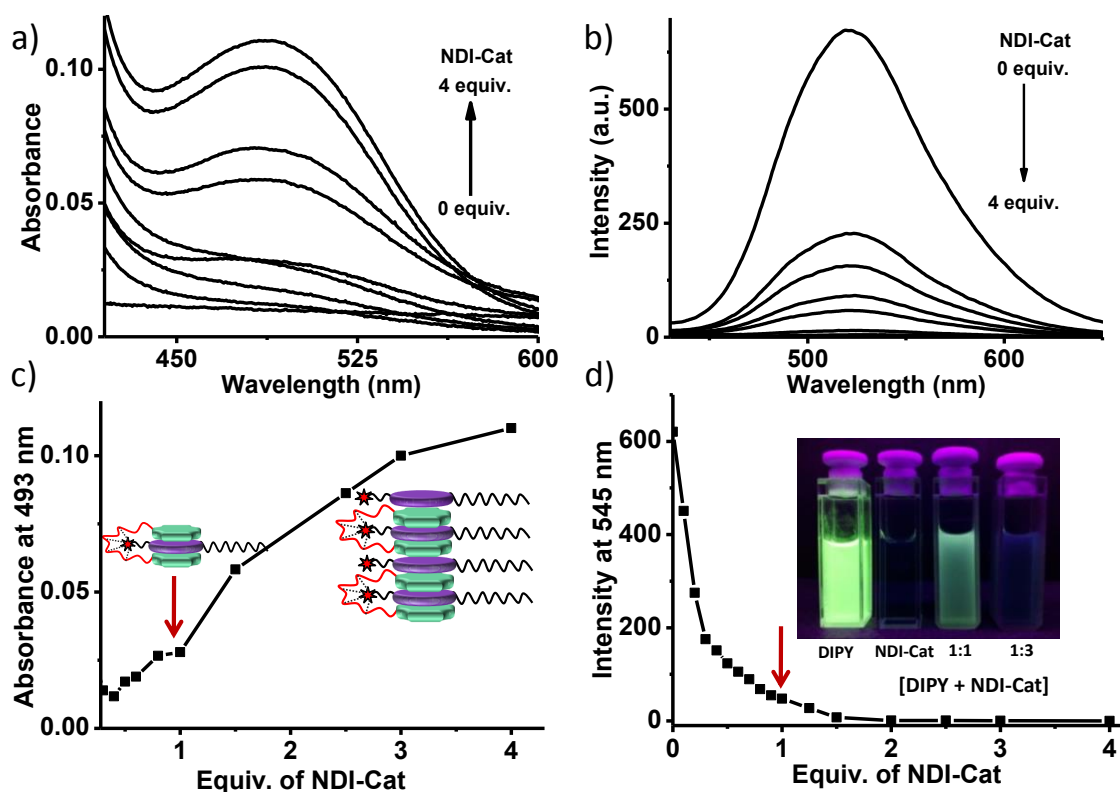
Figure 3.6: *Spectroscopic changes during the titration of **DIPY** (c = 4 x 10^{-5} M) with **NDI-Cat** in methanol–water solvent mixture (30:70, v/v). (a) Evolution of the CT band (the titration curves at lower equivalents of **NDI-Cat** (till 0.4 eq.) is not shown due to high scattering of pre-associated **DIPY** aggregates. (b) quenching of excimer emission (λ_{exc} = 340 nm) upon formation of the **DIPY**+**NDI-Cat** complex. (c) and (d) show the corresponding titration curves obtained by plotting the absorption and fluorescence changes monitored at 489 and 519 nm, respectively. Red arrows mark the change in the slope of these curves. The inset of (d) shows the photographs of solutions under 365 nm UV illumination.*

These results suggest that first **NDI-Cat** molecules bind very efficiently to the pre-associated pyrene foldamers through CT and strong electrostatic interactions with the

glycol units whereas the subsequent **NDI-cat** molecules bridge the foldamers through weak hydrophobic and CT stacking interactions to extend the alternate D–A co-assembly, as shown in the scheme (Figure 3.2b). This hierarchically co-facial CT assembly was later proved by NMR and mass spectroscopic studies.

3.6. Face-to-face D-A Organisation

NMR measurements performed on 1:1 CT complexes (c = 1.2 x 10^{-4} M, 35% D_2O in CD_3OD) shows an upfield shift of the aromatic proton of **NDI-Cat** ($\Delta\delta$ = 0.35 ppm) as well as that of **DIPY** ($\Delta\delta$ = 0.14 ppm), confirming the face to face organization of the chromophores. On the other hand, a strong upfield shift was observed for the $-CH_2$ proton next to the quaternary nitrogen, reiterating the role of strong interactions between electron rich ethylene glycols and electron deficient nitrogen substituents.
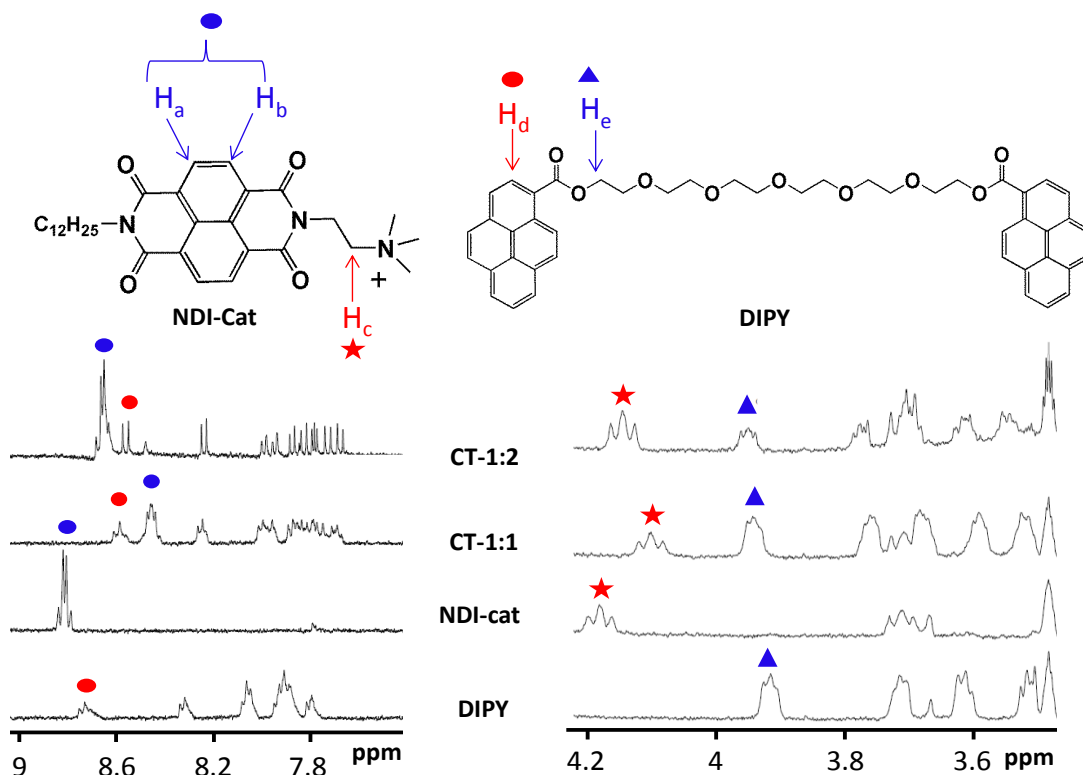

Figure 3.7: *Variation in the ^1H NMR spectra of **DIPY** and **NDI-Cat** upon CT complex formation (35 % D_2O in CD_3OD at 1.2 X 10^{-4} M). Protons of interest are colour coded to guide the eye.*

Interestingly, 1:2 complex show sharpening of **DIPY** and **NDI** peaks along with slight downfield shift. Sharpening of peak could be due to the improved ordering of CT complex in the extended organization leading to 1-D nanostructures (undefined). Downfield shift of protons in the 1:2 complex could be due to the time average signal of two types of NDI involved in two step processes. High concentration and lower D_2O composition (compared to optical studies) was required to get significant NMR signal in the aggregated state.

3.7. Mass Spectrometric Evidence for the Hierarchical Self-assembly

To probe into the two-step CT co-assembly process and its relative stability, high resolution electrospray ionization mass spectrometry HR-ESI-MS was performed in the positive ion mode. Interestingly, the ESI-MS spectra of the CT co-assembly solution of **DIPY** and **NDI-Cat** containing stoichiometric amounts of both components showed a **DIPY**+**NDI-Cat** complex peak at 1258.59 m/z, along with those of **DIPY** (761.27, $[M+Na]^+$) and **NDI-Cat** (521.34, $[M]^+$) molecules, suggesting the formation of a CT pair (Figure 3.8a). Simulated isotopic abundance for 1:1 CT complex ion shows good agreement with the experimentally obtained isotopic abundance which further confirms the CT complex formation (Figure 8c-d). Furthermore, addition of more equivalents of **NDI-Cat** did not result in the formation of higher order complexes, suggesting that the 1:1 complex is the most stable in the gas phase, consistent with the foldamer design. This further justifies the quantitative CT formation till 1 equivalent of NDI and weaker association at higher equivalents, as observed from the optical studies (vide supra) thereby supporting its two step co-assembly. Tandem mass spectroscopy (MS/MS) experiments on the complex ion peak further showed its dissociation into individual components with an increase in accelerating voltage (Figure 3.8b). At low voltage (0 V),

no fragmentation was observed, whereas on increasing voltage (50 V), we see the appearance of peak at 520.31 (m/z) corresponding to **NDI-Cat** with gradual disappearance of CT complex signal. Appearance of another peak at 461.33 (m/z) at 50 V is due to fragmentation of **NDI-Cat** with loss of $N(CH_3)_3$ group. **DIPY** (761.26 m/z) is hardly detected in MS/MS experiments, probably due to lack of inherent charge in the molecule and its inability to gain charge inside collision cell under solvent-free conditions.
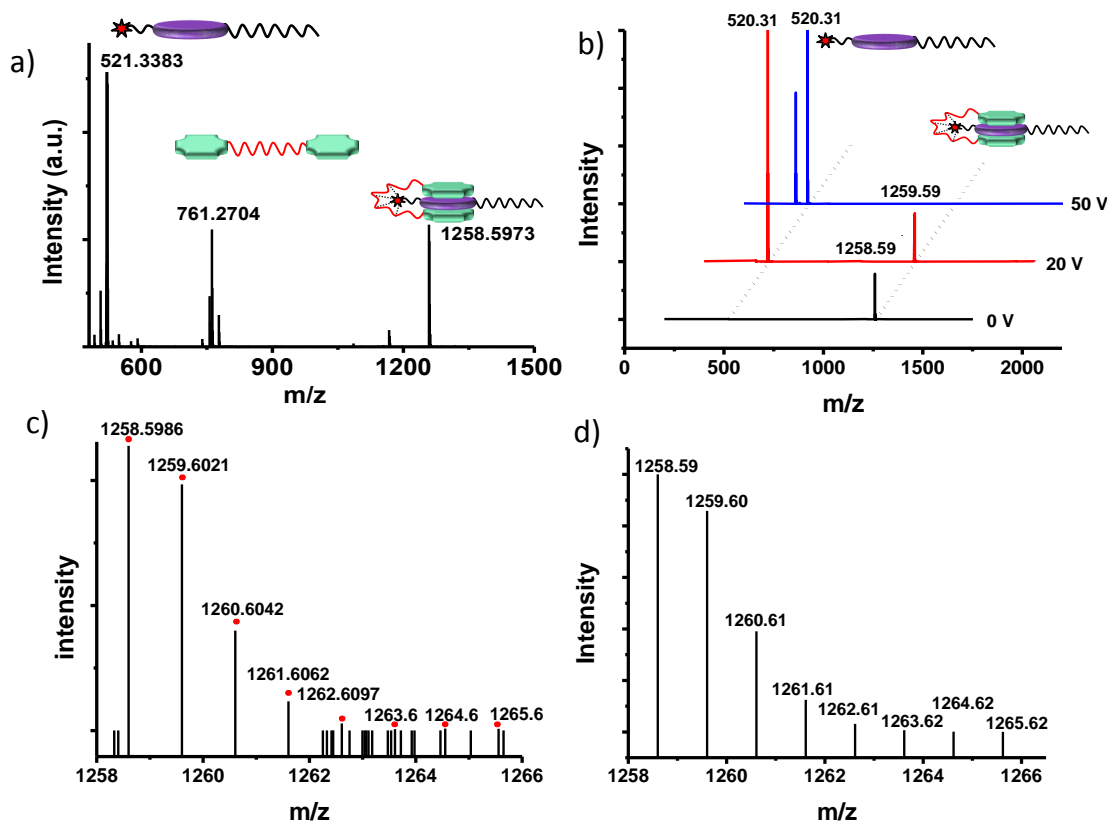
Figure 3.8: *a) High resolution ESI-MS spectra of **DIPY+NDI-Cat** (1:1) complex. b) ESI tandem MS/MS pattern of 1:1 CT complex between **DIPY** and **NDI-Cat** (1258.59 m/z) upon varying accelerating voltage. ESI HRMS spectra of c) obtained and d) simulated isotopic abundance for 1:1 CT complex ion, which is in good agreement with each other confirming CT complex formation. Extra lines in a) is due to background noise interfering with weak isotopic peaks.*

3.8. Formation of CT-hetero structure

Motivated by the two-state assembly mechanism, we have further explored the possibility for the formation of CT haterostructure where we can add a structurally different acceptor to the 1:1 CT complex of **DIPY** and **NDI-Cat** which would give a different CT band compared to the preformed CT pair.

Here we have chosen a structurally different, non-cationic NDI amphiphile acceptor (**NDI-Amph**) which also forms CT complex with **DIPY**. Absorption and emission spectra of **DIPY** and **NDI-Amph** 1:1 CT complex at 4 x 10^{-5} M concentration in 2 % THF, 28 % methanol in water solvent, shows a CT band at λ_{max} = 490 nm (Figure 3.9a) and quenching of **DIPY** emission (Figure 3.9b). Although absorption and fluorescence measurements show the formation of CT complex but the absence of any mass (m/z) corresponding to CT complex indicates that they are much weaker compared to that of **NDI-Cat- DIPY** pair (Figure 3.9c). This also proves the interaction of HEG chain and quaternary nitrogen in stabilizing the D-A pair.

After adding one equivalent of **NDI**-**Amph** to the pre-formed 1:1 complex of **DIPY** and **NDI-Cat**, resulted in the formation of co-assembly as evident from the further increase in CT absorption and quenching of **DIPY** emission (Figure 3.10). This provides an attractive strategy to build hetero CT nanostructures. The two step process of CT complex formation is shown in the schematic (Figure 3.10).
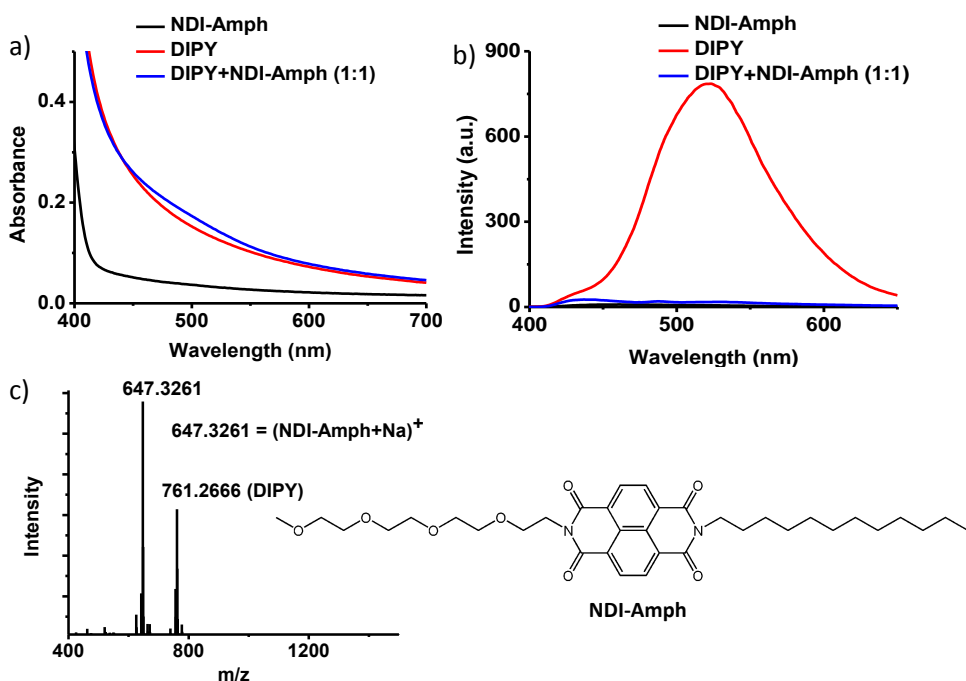
Figure 3.9: *Molecular structure of **NDI-Amph** and steady state a) absorption and b) emission spectra of individual **DIPY** and **NDI-Amph** as well as its 1:1 CT complex (4 x 10^{-5} M, 2% THF, 28% MeOH in water) c) Shows the HRMS of **DIPY** + **NDI-Amph** (1:1) CT complex.*

Figure 3.10: *Steady state a) absorption and b) emission spectra showing two step processes leading to the formation of heterostructure. Schematic illustration of the two-step self-assembly process is also shown.*

3.9. Morphology Study

Figure 3.11: *a) TEM images of 4* x *10^{-5} M solution (30% methanol in water) of* **DIPY**. *b) 1:1 CT complex having nanofibers width of 5nm. Whereas c-d) are nanofibers formed by 1:2 charge transfer complex of* **DIPY** *and* **NDI-Ca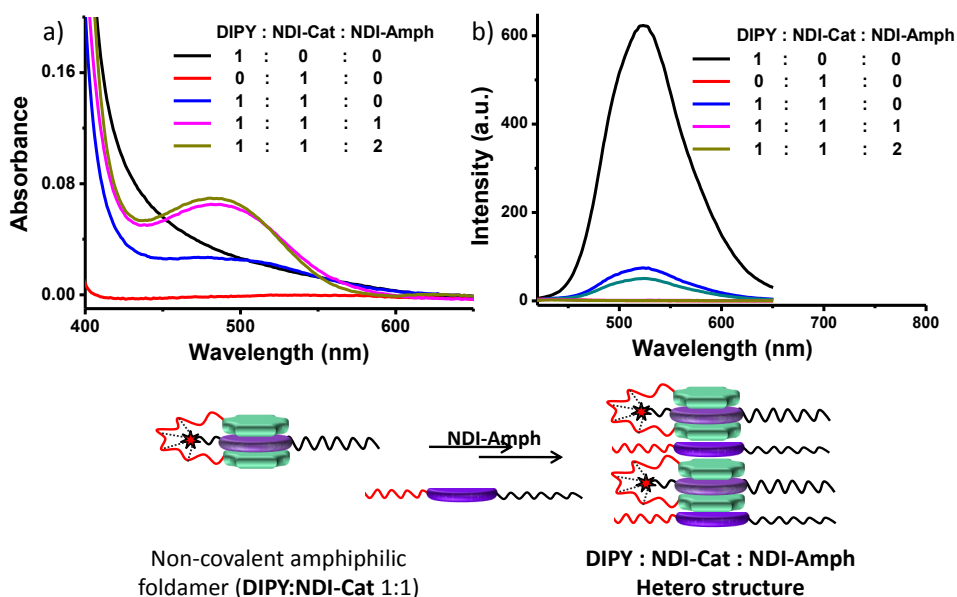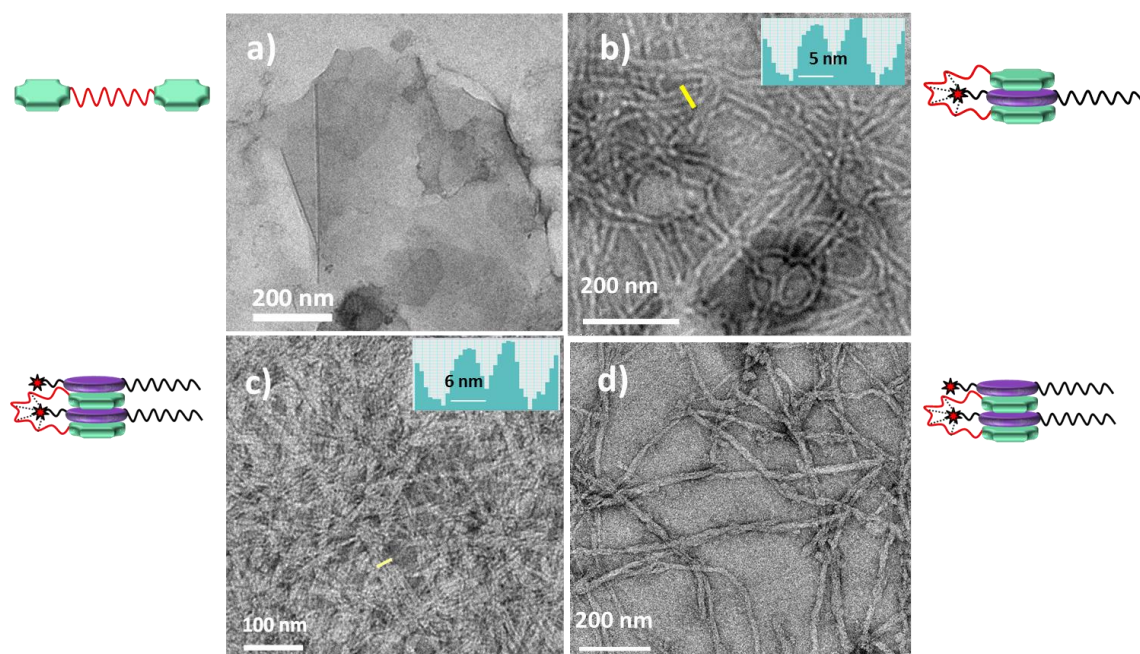t** *in 4* x *10^{-5} M (30% methanol in water) with the inset showing the electron density profile along the yellow line.*

Self-assembled structures of **DIPY** and **NDI-Cat** (methanol–water, 30:70, v/v) drop-casted onto copper grids were visualized using TEM. TEM imaging revealed a two-dimensional (2D) self-assembly of **DIPY** amphiphiles into sheets (Figure 3.11b). NDI-Cat self-assembles into fibre at higher concentration (Figure 2.2.23b). However, the co-assembled **DIPY+NDI-Cat CT** complexes in a 1:2 ratio showed a morphology transition from 2-D sheets to 1-D nanofibers of 100 nm to 1 mm length, confirming the formation of extended D–A 1-D stacks (Figure 3.11c-d). Remarkably, individual fibers of nearly 6 nm width could be identified using TEM, which is in agreement with the bilayer formation of the non-covalent CT amphiphile (CPK modelling showed that the length of the CT amphiphile with extended alkyl chains is 2.5 nm). The self-assembled amphiphilic

CT foldamer in a 1:1 ratio also showed the presence of 1-D nanostructures, suggesting that it can also form aggregated structures because of its amphiphilic nature; however, without a perfect alternate D–A arrangement.

The formation of higher order CT assemblies in solution is also evident from the DLS measurements performed in a methanol–water mixture (30:70, v/v). **DIPY** showed a broad size distribution (100–400 nm) consistent with sheet formation (Figure 3.12). On the other hand, the 1:1 CT complex showed decreased hydrodynamic diameter (100–250 nm), whereas the 1:2 CT complex showed increase in size (200–350 nm) along with sharpening of the peak. Although the self-assembled amphiphilic CT foldamer in 1 : 1 ratio also showed 1-D nanofibers, they showed slight variation of width to around 5 nm as compared to 6 nm obtained with 1 : 2 CT complex, which could be due to the differences in the volume fraction of hydrophobic and hydrophilic components in two cases.
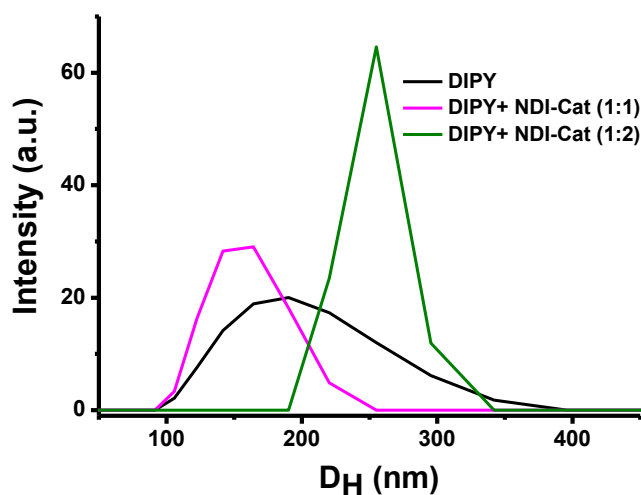
Figure 3.12: *Dynamic light scattering (DLS) measurements showing the hydrodynamic size distribution of **DIPY** and its CT co-assembly with **NDI-Cat** (c = 4 x 10^{-5}M, 30 % Methanol in water). Alone **NDI-Cat** being molecularly dissolved do not scatter.*

3.10. Conclusions

In conclusion, we have shown an efficient non-covalent synthesis of an amphiphilic charge-transfer foldamer for the design of one-dimensional supramolecular

nanostructures with alternate (mixed) donor-acceptor organization. Although, charge-transfer induced folding of polymeric systems has been reported, this is the first time a similar design is exploited for the construction of self-assembled nanostructures. This has been achieved by the clever design of a non-covalent CT foldamer, which structurally resembles an amphiphile, to facilitate its surfactant like self-assembly in polar solvents. We further showed that this donor-acceptor co-assembly occurs through a hierarchical two step process, involving different association abilities, as confirmed by detailed NMR, optical and MS measurements. This hierarchical assembly provides an attractive strategy to construct hetero CT nanostructures with multiple donor or acceptor molecules.

We believe that the findings reported are not only novel, but are also of considerable significance in the emerging and fast expanding field of charge transfer based macromolecular assemblies for nano-sized electronics and organic-ferroelectrics

3.11. Outlook
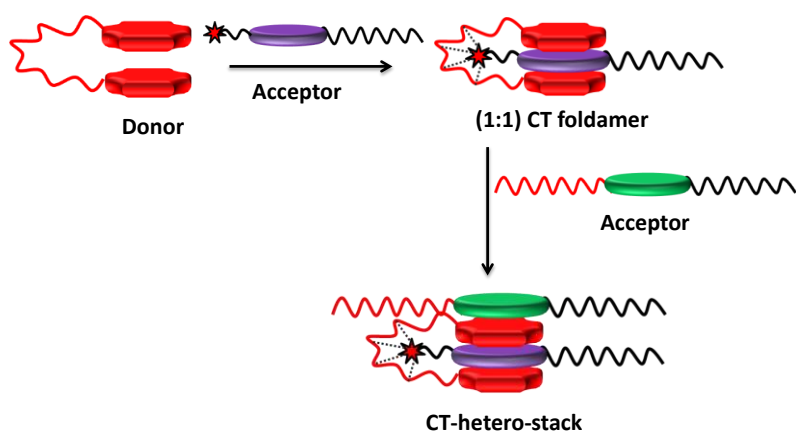
Scheme 3.4: *Formation of CT hetero-stack, using non-covalent amphiphilic foldamer approach.*

Our studies have shown that, this foldamer design is unique with the possibility of increasing acceptor molecules with different association constants. Hence this design can be used to incorporate different acceptor molecules to create a hetero-stack as

demonstrated by the use of **NDI-Cat** and **NDI-Amph**. We have designed **diTTFS** salt similar to **DIPY** where two TTF chromophoric units each bearing two carboxylate functional groups, are connected to each other with flexible hexaethylene glycol chain which would help to fold the two TTF chromophore under suitable solvent condition. As in literature NDI, pyromellitic diimides and viologen chromophores are well-known to form CT complexes with TTF chromophore, we can use various cationic molecules for **diTTFS** donor, such as **NDI-Cat**, **Pym-Cat** and **Bpy-Cat** (shown in Scheme 3.5) as an acceptor counterpart to form 1:1 CT foldamer in the first step. To form CT hetero stack we have designed various non-cationic amphiphilic acceptor molecules, shown in the Scheme 3.6.
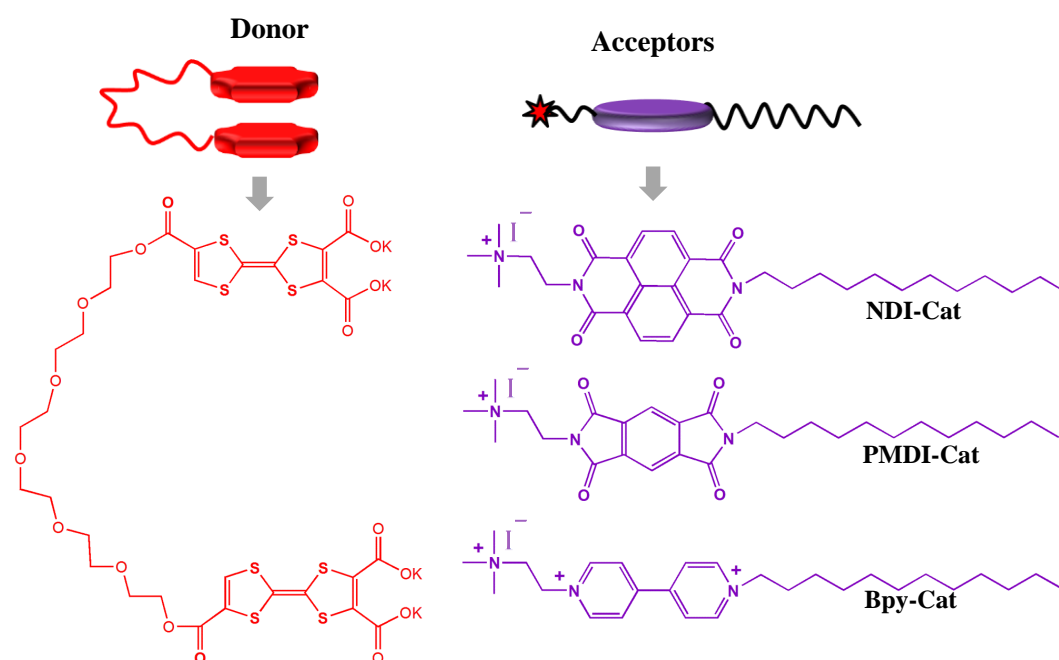
Scheme 3.5 : *Schematic of donor **diTTFS** salt and cationic acceptors to form 1:1 CT foldamer.*
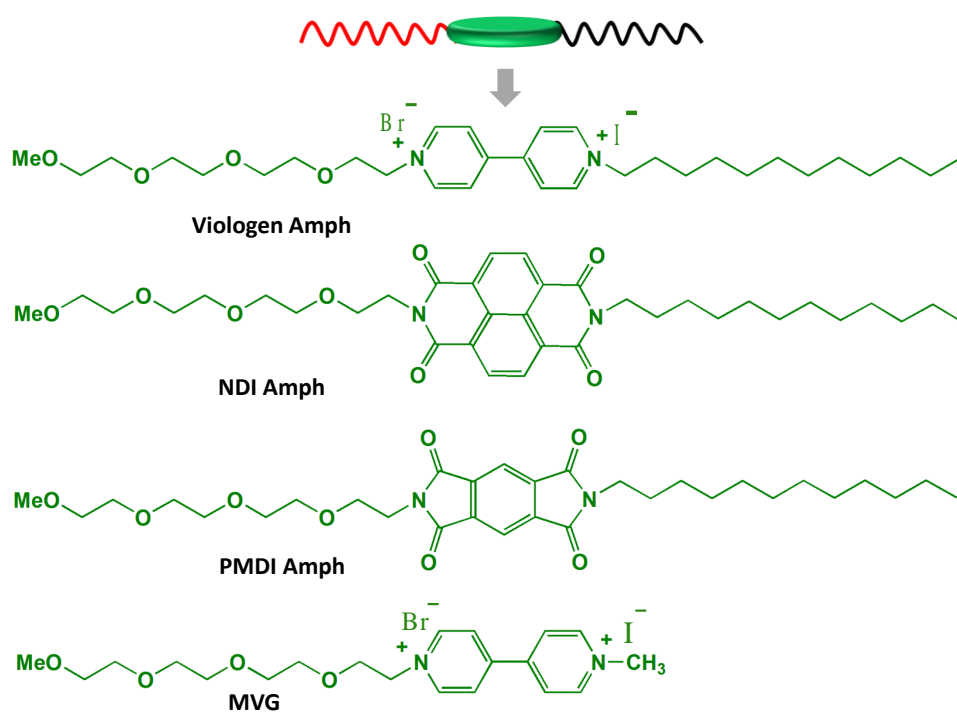
Scheme 3.6: *Molecular structures of various non-cationic amphiphilic acceptor molecules.*

3.11.1. Synthetic Progress of the Work:

Although, we have sarted working towards this outlook, we could not complete the synthesis of **diTTFS** deraivative. We have finished the synthesis of compound **15** in Scheme 3.6. Remaining synthesis will be completed in near future.
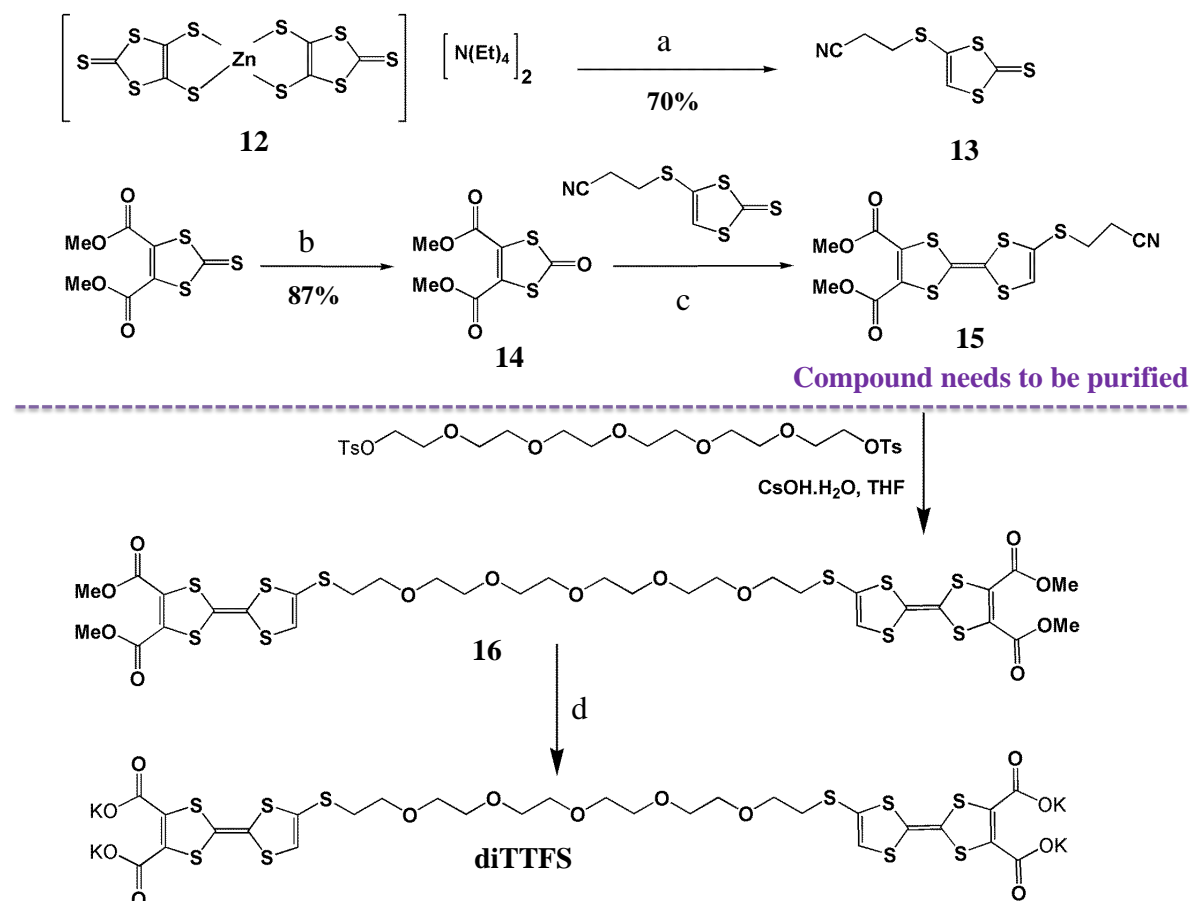
Scheme 3.6: *Synthetic scheme for **diTTFS** molecule. a) 3-bromo propionitrile, Pyridine hydrochloride, CH_3CN, 90 ^{o}C, Ar, reflux. b) $Hg(OAc)_2$, CH_3CO_2H, CH_2Cl_2, RT. c) $P(OEt)_3$, 120 ^{o}C, reflux. d) Hydrolysis, 3.5% KOH in EtOH. The compound (**15**) is under purification.*

The synthesis of acceptor molecules **PMDI-Cat** and **PMDI-Amph** are shown in the Scheme 3.7 and Scheme 3.8 respectively.
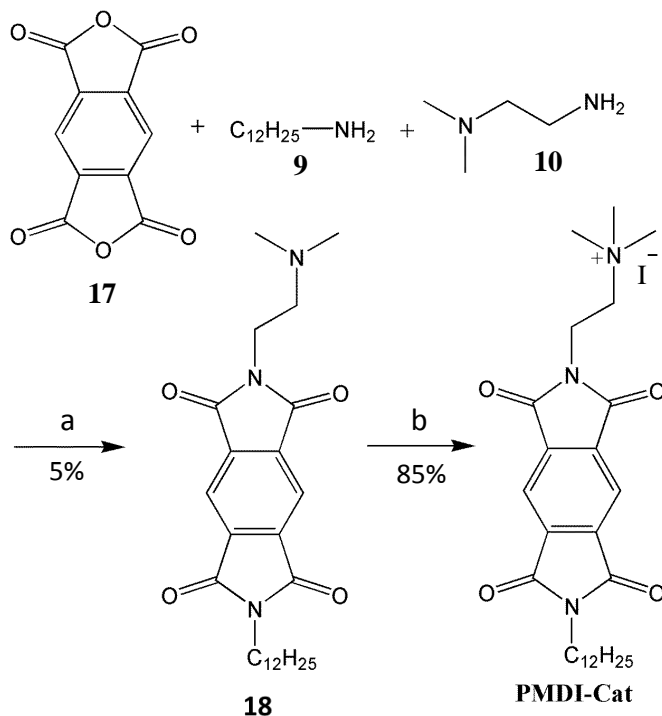
Scheme 3.7: a) *Synthetic Scheme for **PMDI-Cat**. (a) Dry DMF, 100 ^{o}C, Ar, 24 h. b) CH$_3$I, 80 ^{o}C, 4h.*
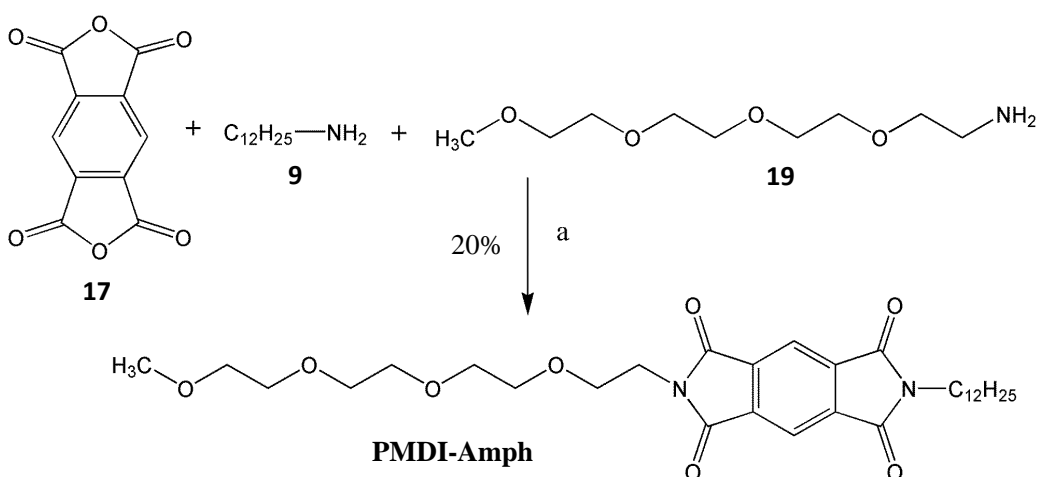
Scheme 3.8: *Synthetic scheme for **PMDI-Amph**. a) Dry DMF, 110 ^{o}C, Ar, 6 h.*

The compound **Viologen Amph** needs to be synthesised and **Bpy-Cat** is under purification.

3.12. Experimental section

General Methods:

Atomic Force Microscopy (AFM): AFM measurements were performed on a Veeco diInnova SPM operating in tapping mode regime. Micro - fabricated silicon cantilever tips doped with phosphorus and with a frequency between 235 and 278 kHz and a spring constant of 20-40 Nm^{-1} were used. The samples were prepared by drop casting 4 x 10^{-5} M solutions of the CT complex or individual molecules on glass substrates and dried in air followed by vacuum drying at room temperature.

Optical Measurements: Electronic absorption spectra were recorded on a Perkin Elmer Lambda 900 UV-Vis-NIR Spectrometer and emission spectra were recorded on Perkin Elmer Ls 55 Luminescence Spectrometer. UV-Vis and emission spectra were recorded in 10 mm path length cuvette. Fluorescence spectra of solutions were recorded with 340 nm excitation wavelength.

NMR Measurements: NMR spectra were obtained with a Bruker AVANCE 400 (400 MHz) Fourier transform NMR spectrometer with chemical shifts reported in parts per million (ppm) with respect to residual solvent peak. Titration measurements were done in 35% D_2O in CD_3OD. The stock solutions were prepared in CD_3OD, which were then injected to appropriate volumes of D_2O and CD_3OD mixture.

High-Resolution Mass-Spectrometry (HRMS): HRMS measurements were performed with Agilent Technologies Q-TOF-LCMS system, 6538 instrument. Measurements were done in ESI mode (positive mode).

Transmission Electron Microscopy (TEM): TEM measurements were performed on a JEOL, JEM 3010 operated at 300 kV. Samples were prepared by placing a drop of the solution on carbon coated copper grids followed by drying at room temperature. The

images were recorded with an operating voltage 300 kV. In order to get a better contrast samples were stained with uranyl acetate (1 wt % in water) before the measurements.

Dynamic light scattering Experiments (DLS):

The measurements were carried out using a NanoZS (Malvern UK) employing a 532 nm laser at a back scattering angle of 173°. 10^{-3} M stock solutions of **NDI-Cat** and **DIPY** were prepared in methanol, which were injected into appropriate volumes of methanol-water solvent mixtures to obtain the required solution.

Sample preparation for optical measurements: Charge-transfer complexes were prepared by injecting pre-mixed **DIPY** and **NDI-Cat** in methanol to appropriate methanol-water solvent mixtures.

3.12.1 Synthetic Procedures

Synthesis of (11):

1,4,5,8-Naphthalenetetracarboxylic dianhydride (2 g, 7.45 mmol) was added to N,N-dimet-hylethylenediamine (0.66 g, 7.45 mmol) and dodecylamine (1.38 g, 7.45 mmol) in 50 ml of dry DMF and the reaction mixture was stirred at 100 °C for 24h under inert atmosphere. DMF was then evaporated under high vacuum. The resulting residue was purified by column chromatography (silica, 100-200 mesh, 100% chloroform to 5/95 v/v methanol/chloroform solvent mixture) followed by size exclusion chromatography (biobeads SX-3, $CHCl_3$) to give 560 mg of **11** in 15% yield. The low yield of the reaction is due to the statistical formation of three possible products. ^{1}H NMR (400 MHz, $CDCl_3$ TMS): δ (ppm) 8.75 (s, 4H), 4.35 (t, J = 6.8 Hz, 2H), 4.18 (t, J = 7.6 Hz, 2H), 2.67 (t, J = 6.8 Hz, 2H), 2.34 (s, 6H), 1.62 (m, 2H), 1.45-1.25 (m, 18H), 0.87 (t, J = 6.8 Hz, 3H); ^{13}C NMR (100 MHz, $CDCl_3$) : δ (ppm) 163.1, 162.9, 131.2, 131.1, 126.9, 126.8, 126.7, 57.1,

45.9, 41.2, 38.8, 32.1, 29.8, 29.77, 29.74, 29.67, 29.5, 28.2, 27.2, 22.8, 14.3. HRMS (ESI): m/z calcd: $C_{30}H_{39}N_3O_4$: 505.2940, found: 506.2994 [M+H]$^+$.

Synthesis of NDI-Cat:

Methyl iodide (0.8 ml, 12.84 mmol) was added to 130 mg (0.26 mmol) of **11** in 20 ml of toluene, and stirred for 4 h at 80 °C under inert atmosphere. The shiny yellow precipitate formed during the reaction was filtered, washed with diethyl ether and dried under vacuum to give 160 mg of pure **NDI-Cat** in 95% yield. ^{1}H NMR (400 MHz, CDCl$_3$, TMS) : δ(ppm) 8.70 (s, 4H), 4.48 (t, J = 7.2 Hz, 2H), 4.05 (t, J = 7.6 Hz, 2H), 3.63 (t, J = 6.8 Hz, 2H), 3.23 (s, 9H), 1.65 (m, 2H), 1.23 (m, 18H), 0.84 (t, J = 6.8 Hz, 3H) ; ^{13}C NMR (100 MHz, CDCl$_3$) : δ (ppm) 162.7, 162.6, 130.5, 126.6, 126.3, 126.2, 61.7, 52.5, 33.9, 31.3, 29.0, 28.7, 27.3, 26.5, 22.1, 13.9; HRMS (ESI): m/z calcd: $C_{31}H_{42}N_3O_4$: 520.3169, found : 520.3279 [M]$^+$.

Synthesis of Dipyrene (DIPY)

Hexaethylene glycol (91 mg, 0.32 mmol) and the pyrene carboxylic acid (200 mg, 0.81 mmol) mixture were added to ice cold dry dichloromethane followed by the addition of 200 mg (1.04 mmol) EDC (200 mg, 1.04 mmol) (N-(3-Dimethylaminopropyl)-N'-ethylcarbodiimide hydrochloride) and DMAP. Whole solution was stirred at room temperature for 2 days. The reaction mixture was then extracted with dichloromethane and water. The organic layer was then concentrated under vacuum and purified by column chromatography (silica gel, 100-200 mesh) with 2 % methanol in chloroform to give 190 mg of the pure product (yield: 80%). ^{1}H NMR (400 MHz, CDCl$_3$, TMS) : δ (ppm) 9.2 (d, J = 9.6 Hz, 2H), 8.6 (d, J = 8.4 Hz, 2H), 8.2 (m, 6H) , 8.1 (m, 4H), 8.0 (t, J = 7.6 Hz, 4H), 3.5-3.8 (m, 22H); ^{13}C NMR (100 MHz, CDCl$_3$): δ (ppm) 168.1, 134.5, 131.3, 131.1, 130.5, 129.7, 129.5, 128.7, 127.3, 126.4, 126.4, 126.3, 125.0, 124.9, 124.30,

124.2, 123.6, 70.86, 70.80, 70.7, 69.5, 64.4; HRMS (ESI) m/z cald: $C_{46}H_{42}O_9Na$: 761.2726, found : 761.2718 [M+Na]$^+$.

Synthesis of TEG appended Monopyrene derivative (MonoPy):

150 mg of pyrenecarboxylic acid (0.61 mmol) and 250 mg of tetraethylene glycol monomethyl ether (1.22 mmol) were mixed with 15 ml of dry dichloromethane and stirred continuously at ice cold temperature. To that, the mixture of 150 mg (0.78 mmol) EDC (N-(3-Dimethylaminopropyl)-N'-ethylcarbodiimide hydrochloride) and 50 mg DMAP (Dimethyl amino pyridine in 15 ml dry dichloromethane was added. The whole solution was stirred at room temperature for 12 h under argon atmosphere. The reaction mixture was then extracted with dichloromethane and water. The organic layer was concentrated under vacuum and purified by column chromatography (silica gel, 100-200 mesh) with 5% methanol in chloroform to give 250 mg of pure product (yield: 94%). ^{1}H NMR (400 MHz, CDCl$_3$, TMS) : δ (ppm) 9.27 (d, J = 9.6 Hz, 1H), 8.66 (d, J = 8 Hz, 1H), 8.25 (m, 3H), 8.18 (d, J = 3.6 Hz, 1H), 8.16 (d, J = 3.6 Hz, 1H), 8.08 (m, 2H), 4.67 (t, J = 4.8 Hz, 2H), 3.97 (t, J = 4.8 Hz, 2H), 3.78 (m, 2H), 3.71 (m, 2H), 3.68 (m, 2H), 3.64 (m, 2H), 3.59 (m, 2H), 3.50 (m, 2H), 3.33 (s, 3H); ^{13}C NMR (100 MHz, CDCl3): δ (ppm) 168.07, 134.46, 131.26, 131.10, 130.48, 129.72, 129.53, 128.65, 127.26, 126.39, 126.37, 126.26, 125.05, 124.91, 124.29, 124.21, 123.63, 72.00, 70.85, 70.80, 70.78, 70.71, 70.59, 69.45, 64.41, 59.00; HRMS (ESI) m/z cald : $C_{26}H_{28}O_6Na$: 459.1783 , found : 459.1780 [M+Na]$^+$.

Synthesis of compound 13: Compound 13 was synthesised according to the literature procedure.[17]

Synthesis of compound 14: Compound 14 was synthesised according to the literature procedure.[18]

Synthesis of compound 15:

1.88 g (8.06 mmol) of compound **3** was mixed with 2.3 g (10.48 mmol) of compound **2** in 10 ml of freshly prepared triethyl phosphate and refluxed at 120 ^{o}C for 5 h under Ar atmosphere. After completion of the reaction the triethyl phosphate was distilled out and the compound mixture was loaded into silica gel column for purification.

Synthesis of compound 18:

Pyromellitic tetracarboxylicacid dianhydride (1 g, 4.58 mmol) was added to N,N-dimet-hylethylenediamine (0.44 g, 5.03 mmol) and dodecylamine (0.93 g, 5.03 mmol) in 40 ml of dry DMF and the reaction mixture was stirred at 100 °C for 16 h under inert atmosphere. DMF was then evaporated under high vacuum. The resulting residue was purified by column chromatography (silica gel, 100-200 mesh) using methanol/chloroform solvent mixture, followed by size exclusion chromatography (biobeads SX-3, CHCl$_3$,) to give 100 mg of **6** in 5% yield. The low yield of the reaction is due to the statistical formation of three possible products.

^{1}H NMR (400 MHz, CDCl$_3$ TMS): δ (ppm) 8.24 (s, 4H), 3.85 (t, J = 6.4 Hz, 2H), 3.72 (t, J = 7.2 Hz, 2H), 2.62 (t, J = 6.8 Hz, 2H), 2.27 (s, 6H), 1.68 (m, 2H), 1.32-1.24 (m, 18H), 0.85 (t, J = 6.8 Hz, 3H); ^{13}C NMR (100 MHz, CDCl$_3$) : δ (ppm) 166.44, 166.31, 137.31, 118.3, 126.9, 57.1, 45.9, 41.2, 38.8, 38.0, 32.1, 29.8, 29.77, 29.74, 29.67, 29.5, 28.2, 27.2, 22.8, 14.3.

Synthesis of PMDI-Cat:

Methyl iodide (1.5 ml, 24 mmol) was added to 90 mg (0.197 mmol) of 1 in 20 ml of toluene, and stirred for 4 h at 80 ^{o}C under inert atmosphere. The shiny yellow precipitate formed during the reaction was filtered, washed with diethyl ether and dried under vacuum to give 100 mg of pure **PMDI-Cat** in 85% yield. ^{1}H NMR (400 MHz, CDCl$_3$,

TMS) : δ(ppm) 8.24 (s, 4H), 3.85 (t, J = 6.4 Hz, 2H), 3.72 (t, J=7.2 Hz, 2H), 2.62 (t, J = 6.8 Hz, 2H), 3.23 (s, 9H), 1.66 (m, 2H), 1.23 (m, 18H), 0.84 (t, J = 6.8 Hz, 3H) ; ^{13}C NMR (100 MHz, CDCl$_3$) : δ (ppm) 166.44, 166.31, 137.31, 118.3, 126.9, 57.1, 45.9, 41.2, 38.8, 38.0, 32.1, 29.8, 29.77, 29.74, 29.67, 29.5, 28.2, 27.2, 22.8, 14.3; HRMS (ESI): m/z calcd: C$_{27}$H$_{40}$N$_3$O$_4$: 470.3013, found : 470.3043[M]$^+$.

Synthesis of PMDI-Amph:

143 mg (0.60 mmol) of pyromellitic tetracarboxilic dianhydride was added to 150 mg of monomethyl tetraethyleneglycol amine (0.72 mmol) and 134 mg of dodecyl amine (0.72 mmol) in 20 ml of dry DMF and stirred for 6 h at 110 ^{o}C. After completion of the reaction, the rection mixture was extracted with chloroform and water followed by the evaporation of the organic layer under high vacuum to remove DMF. The resulting residue was purified by column chromatography (silica gel, 100-200) mesh using methanol/chloroform solvent mixture varying the polarity from 2% MeOH in CHCl$_3$ to 5% MeOH in CHCl$_3$, followed by size exclusion chromatography (biobeads SX-3, CHCl$_3$,) to give 60 mg of **PMDI-Cat** in 20% yield. ^{1}H NMR (400 MHz, CDCl$_3$, TMS) : δ(ppm) 8.26 (s, 2H), 3.94 (t, J = 5.6 Hz, 2H), 3.76 (t, J = 6 Hz, 2H), 3.72 (t, J = 7.6 Hz, 2H), 3.59 (m, 10H), 3.36 (s, 3H), 1.7 (m, 2H), 1.24 (m, 20H), 0.87 (t, J = 6.8 Hz, 3H); ^{13}C NMR (100 MHz, CDCl$_3$) : δ (ppm) 166.44, 166.31, 137.43, 118.30, 72.07, 70.71, 70.63, 70.21, 67.78, 59.15, 38.92, 38.09, 32.04, 29.74, 29.68, 29.60, 29.47, 29.26, 28.58, 26.98, 22.81, 14.24. HRMS (ESI): m/z calcd: C$_{31}$H$_{46}$N$_2$O$_8$: 574.3254, found: 575.3354 [M+H]$^+$.

3.13. References

[1] T. Kitamura, S. Nakaso, N. Mizoshita, Y. Tochigi, T. Shimomura, M. Moriyama and T. Kato, *J. Am. Chem. Soc.,* 2005, **127**, 14769; Y. Tatewaki, T. Hatanaka, R. Tsunashima, T. Nakamura, M. Kimura and H. Shirai, *Chem. Asian J.,* 2009**, 4**, 1474.

[2] G. Kaiser, T. Jarrosson, S. Otto, Y.- F. Ng, A. D. Bond and J. K. M. Sanders, *Angew.Chem. Int. Ed.,* 2004, **43**, 1959; J.-Y. Ortholand, A. M. Z. Slawin, N. Spencer, J. F. Stoddart and D. J. Williams, *Angew. Chem. Int. Ed. Engl.,* 1989, **28**, 1394; G. Koshkakaryan, L. M. Klivansky, D. Cao, M. Snauko, S. J. Teat, J. O. Struppe and Y. Liu, *J. Am. Chem. Soc.*, 2009, **131**, 2078.

[3] J. J. Reczek, K. R. Villazor, V. Lynch, T. M. Swager and B. L. Iverson, *J. Am. Chem. Soc.,* 2006, **128**, 7995; J. Q. Nguyen and B. L. Iverson, *J. Am. Chem. Soc.,* 1999, **121**, 2639; J.-Y. Wang, J. Yan, L. Ding, Y. Ma and J. Pei, *Adv. Funct. Mater.*, 2009, **19**, 1746.

[4] L. Zhu, Y. Yi, Y. Li, E.-G. Kim, V. Coropceanu and J.-L. Brédas, *J. Am. Chem. Soc.,* 2012, **134**, 2340.

[5] J. J. Tan, Z. Ma, W. Xu, G. Zhao, H. Geng, C. Di, W. Hu, Z. Shuai, K. Singh and D. Zhu, *J. Am. Chem. Soc.,* 2013, **135**, 558; J. Zhang, H. Geng, T. S. Virk, Y. Zhao, J. Tan, C.-an Di, W. Xu, K. Singh, W. Hu, Z. Shuai, Y. Liu and D. Zhu, *Adv. Mater.,* 2012, **24**, 2603.

[6] A. S. Tayi, A. K. Shveyd, A. C.-H. Sue, J. M. Szarko, B. S. Rolczynski, D. Cao, T. J. Kennedy, A. Sarjeant, C. L. Stern, W. F. Paxton, W. Wu, S. K. Dey, A. C. Fahrenbach, J. R. Guest, H. Mohseni, L. X. Chen, K. L. Wang, J. F. Stoddart and S. I. Stupp, *Nature,* 2012, **488**, 485; S. Horiuchi and Y. Tokura, *Nature Mater.*, 2008, **7**, 357.

[7] A. Jain, K. V. Rao, U. Mogera, A. A. Sagade and S. J. George, *Chem.-Eur. J.,* 2011, **17**, 12355; A. A. Sagade, K. V. Rao, U. Mogera, S. J. George A. Datta and G. U. Kulkarni, *Adv. Mater.*, 2013, **25,** 559; A. P. H. J. Schenning and E. W. Meijer, *Chem. Commun.*, 2005, 3245; A. Das, M. R. Molla, A. Banerjee, A. Paul and S. Ghosh, *Chem. −Eur. J.,* 2011, **17**, 6061; U. Maitra, P. V. Kumar, N. Chandra, L. J. D'Souza, M. D. Prasanna and A. R. Raju, *Chem. Commun.,* 1999, 595.

[8]   K. V. Rao, K. Jayaramulu, T. K. Maji and S. J. George, *Angew. Chem. Int. Ed.,* 2010, **49**, 4128; K. V. Rao and S. J. George*, Chem. Eur. J.,* 2012, **18**, 14286.

[9]   C. Wang, Z. Wang and X. Zhang, *Acc. Chem. Res.,* 2012, **45**, 608; C. Wang, Y. Guo, Y. Wang, H. Xu, R. Wang and X. Zhang, *Angew. Chem. Int. Ed*., 2009, **48**, 8962.

[10] S. Ghosh and S. Ramakrishnan, *Angew. Chem. Int. Ed.*, 2004, **43**, 3264; S. G. Ramkumar and S. Ramakrishnan, *Macromolecules,* 2010, **43**, 2307; S. Ghosh and S. Ramakrishnan, *Angew. Chem. Int. Ed.*, 2005, **44**, 5441; S. Dey and S. Ramakrishnan, *Chem. Asian J.*, 2011, **6**, 149.

[11]   A. P. de Silva, H. Q. N. Gunaratne, T. Gunnlaugsson, A. J. M. Huxley, C. P. McCoy, J. T. Rademacher and T. E. Rice, *Chem. Rev.,* 1997, **97**, 1515.

[12] A. Ajayaghosh, P. Chithra and R. Varghese, *Angew. Chem. Int. Ed.* 2007, **46**, 230; Y. Zhou, C.-Y. Zhu, X.-S. Gao, X.-Y. You and C. Yao, *Org. Lett.,* 2010, **12**, 2566.

[13] M. Kumar and S. J. George, *Chem.−Eur. J.*, 2011, **17**, 11102.

[14] M. R. Bryce, *Adv. Mater.,* 1999, **11**, 11.

[15]   F. M. Winnik, *Chem. Rev.,*1993, **93**, 587; M. Kumar and S. J. George, *Nanoscale*, 2011, **3**, 2130.

[16] N. S. S. Kumar, M. D. Gujrati and J. N. Wilson, *Chem. Commun.,* 2010, 5464.

[17] C. Jia, D. Zhang, W. Xu, D. Zhu and *Org. Lett.,* 2001, **3**, 1941.

[18] T. L. A. Nguyen, R. D.-Cakan, T. Devic, M. Morcrette, T. Ahnfeldt, P. A. -Senzier, N. Stock, A.-M. Goncalves, Y. Filinchuk, J.-M. Tarascon and G. Férey, *Inorg. Chem.,* 2010, **49**, 7135.